**Sudan University of Science and Technology**

**College of Graduate Studies**

# Removal of Organic Pollutants from Pharmaceutical Plants Waste Water using Polymer Blends Doped with Metal Nanoparticles

# إزالة الملوثات العضوية من مياه صرف المصانع الصيدلانية باستخدام مخاليط البوليمرات المشوبة بالجسيمات النانوية المعدنية

**A Thesis Submitted in Fulfillment of the Requirements for the Degree of Doctor of Philosophy in Chemistry**

**By:**

**Mustafa Elsebty Mohammed Elhassan Ahmed**
**(B. Sc., M. Sc. Chemistry)**

**Supervisor:**

**Dr. Mohammed Adam Abbo**

**Co-Supervisor Dr. Elfatih Ahmed Hassan**

**July 2019**

## Declaration of Original Work

I, Mustafa Elsebty Mohammed Elhassan , the undersigned, a graduate student at Sudan University of Science and Technology and the author of the thesis titled "**Removal of Organic Pollutants from Pharmaceutical plants waste water using Metal Nanoparticles Doped with Polymer Blends**", hereby solemnly declare that this thesis is an original work that has been done and prepared by me under the supervision of Prof.Mohammed Adam Abbo, Co-supervision of Dr. Efatih Ahmad Hassan .This work has not been previously submitted for the award of any degree, or similar title at this or any other university. The materials borrowed from other sources and included in my thesis have been properly cited and acknowledged.

Student's Signature_____ Date_____

# الإستهلال

﴿قَالَ لَهُ مُوسَى هَلْ أَتَّبِعُكَ عَلَى أَنْ تُعَلِّمَنِ مِمَّا عُلِّمْتَ رُشْدًا﴾ صدق الله العظيم

الكهف: ٦٦

# *Dedications*

*To*

The soul of my Father, My mother, My wife Arafa
My brothers Ahmed, Mohand and Azza.

# ***Acknowledgements***

First and foremost, I would like to thank allah to give me power to complete this work. My deepest and sincere appreciations go to my advisors **Prof. Mohammed Adam Abbo** and **Dr. Efatih Ahmad Hassan** who helped me, tremendously, at the initial stages of planning and the preparation of the proposal.

I would like to, gratefully, and sincerely thank **Dr. Ahmed Mohamed Ismiel Eltwab** for his guidance, understanding, patience, and most importantly, his intense knowledge of the subject. His great efforts were paramount in providing a great experience consistent with my research problems. He encouraged me to, not only, grow as an experimentalist and a chemist but also as an independent thinker. I would like to, gratefully sincerely thank all staff work at National Center for Radiation Research and Technology, Cairo.

# Abstract

In this study, polymer blends thin films and polymer blends nano composites, of poly vinyl alcohol, gelatin and copper oxide nanoparticles were prepared in different ratios using casting method. Some of these thin films (polymer blends and polymer blend nanocomposites) were exposed to an irradiation dose of 5KGy of $\gamma$ rays. The irradiated thin films were studied using different techniques such as: FTIR, UV-VIS., XRD, SEM…etc. FTIR results showed no significant difference between unirradiated and irradiated thin films, but swelling degree results showed a significant difference upon irradiation. It is clear that the maximum values of, swelling degree percentages of the studied unirradiated nanocomposite film ratios appeared after 2hr of dipping in de-ionized water. The maximum percentage swelling degree of unirradiated nanocomposite film percentag (PVA/Gelatin/$CuO_{0.01\%, 0.1\%}$) reached 522% after two hours, while it is 220% for irradiated films. SEM images of polymer nanocomposite films of (PVA/Gelatin/CuO) showed that the surface was smooth, continuous and is homogeneous, also, CuO nanoparticles were distributed in the surface of polymer matrix.

XRD showed that the shifts of the characteristic peak in patterns of nanocomposite films of (PVA/Gelatin/CuO) to $2\theta$ values indicate that there is an increase in the interlayer spacing polymer, which is consistent with the presence of the polymeric species in the matrix.

The adsorption behavior of eosin yellow (EY) from aqueous solution onto various ratios of PVA/Gelatin/CuO film in batch technique was studied. The effect of pH, dosage of adsorbent, contact time, and the initial concentration of dye at room temperature were investigated. The maximum amount of dye removal found about 90% at pH 4, the

adsorption dose 0.2mg/L, with an initial dye concentration of 5 mg/L, at 25˚C, with 60 min contact time.

## المستخلص

في هذه الدراسة،تم تحضير أفلام رقيقه لمزيج من بوليمرات الجلاتين ومتعدد فينيل الكحول بنسب مختلفة بطريقة الصب المباشر؛ كما تم أيضاً تحضير مزيج للبوليمرات اعلاه مع اضافة أكسيد النحاسيك النانوي، بعض الافلام المحضره في الحالتين تم تعريضها لجرعة من اشعة جاما المؤينة بمقدار ٥ كيلوجراي والبعض الاخر ترك دون تشعيع. تم دراسة جميع الافلام الرقيقة المحضرة المشعة والغير مشعة باستخدام طرق الطيف المختلفه لتحديد خواصها والتغيرات التي طرأت عليها كتقنية الاشعة تحت الحمراء، الاشعة الفوق بنفسجية،تقنية الاشعة السينية...الخ، دراسات الاشعة تحت الحمراء لم تظهر اختلاف كبير بين الافلام المشعة والغير مشعة إلا أن دراسات خواص الإنتفاخ وإمتصاص السوائل أظهرت ان تشعيع الافلام يقلل من نسبة احتباس السوائل داخل سلسلة البوليمر( النسبة وصلت الي ٥٢٢% للافلام النانوية الغير مشعة بعد الغمر الكامل تحت الماء المقطر لمدة ساعتين بينما كانت٢٢٠% فقط لنفس الافلام بعد التشعيع).

دراسات المجهر الالكتروني الماسح أظهرت ان السطح متجانس واملس تماماً خاصة بعد تشعيع الافلام، كما ان جزيئات النحاسوز النانوية موزعة بصوره متجانسه علي سطح مزيج البوليمر خاصةً بعد إجراء عملية التشعيع.

دراسات حيود الاشعه السينية أظهرت ان هنالك تغير في زاوية الحيود في مصفوفة مزيج البوليمر النانوي.

كتطبيق بيئي، تم دراسة نسبة ازالة مخلوط البوليمرات ومخلوط البوليمر النانوي لصبخة الايوسين الطبية في المحاليل المائية بدرجات وسط هيدروجيني مختلفة في درجة حرارة الغرفة.

مخاليط البوليمر العادية لم تعط اي نتائج في ازالة صبغة الأيوسين بينما كانت نسبة الامتصاص ٩٠% ل(٥ ملجم/لتر) لهذه الصبغة عند استخدام مخلوط الافلام النانوية عند درجة أس هيدروجيني يساوي(٤) عند درجة حرارة الغرفة بعد مرور (٦٠) دقيقة من الغمر الكامل.

# Abbreviations

| | |
|---|---|
| PB | polymer blend |
| NPs | Nanoparticles |
| Tg | glass transition temperature |
| DSC | differential scanning calorimetry |
| FTIR | Fourier Transform Infrared |
| UV–vis | Ultra – violet – Visible Spectrophotometer |
| XRD | X-ray Diffraction Analysis |
| TEM | Transmission electron microscopy |
| SEM | Scanning Electron Microscopy |
| SAED | Selected area electron diffraction |
| PyOx | Pyranose oxidase |
| GCE | Glassy carbon electrode |
| PVA | Poly vinyl alcohol |
| PL | Photoluminescence spectra |
| SERS | The surface-enhanced Raman scattering |
| KGy | Kilogray |
| JAERI | Japanese Atomic Energy Research Institute |
| PhACs | Pharmaceutically-active compounds |
| MBR | Membrane bioreactors |

| | |
|---|---|
| SQUID | superconducting quantum interference device |
| DMFC | Direct-methanol fuel cells |

# Table of Contents

## List of Tables

**List of Figures**

# Chapter One
# Introduction

## 1.1. Nanotechnology:

Nanoparticles are defined as a small object that behaves as a whole unit in terms of its transport and properties. It is further classified according to size in terms of diameter, fine particles cover a range between 100 and 2500 nanometers, while ultrafine particles, on the other hand, are of 1 and 100 nanometers. Similar to ultrafine particles, Nanoparticles are sized between 1 and 100 nanometers.

Nanoparticles may or may not exhibit size related properties that differ significantly from those observed in fine particles or bulk materials [(1)].

Nanoparticles research is currently an area of intense scientific interest due to a wide variety of potential applications in biomedical, optical and electronic fields.

## 1.2. Natural polymers:

The simplest definition of a polymer is something made of many units. The units or "monomers" are small molecules that usually contain ten or less atoms in a row. Carbon and hydrogen are the most common atoms in monomers, but oxygen, nitrogen, chlorine, fluorine, silicon and sulfur may also be present. Think of a polymer as a chain in which the monomers are linked (polymerized) together to make a chain with at least 1000 atoms in a row. It is this feature of large size that gives polymers their special properties. Polymerization can be demonstrated by linking countless strips of construction paper together to make paper garlands or hooking together hundreds of paper clips or gum wrappers together to form extended chains. [(2)]

Wide ranges of naturally occurring polymers derived from renewable resources are available for various materials applications [3, 4].

Some of them, such as starch, cellulose and rubber are actively used in products today, while many others remain underutilized. Natural polymers can sometimes be classified according to their physical character. For example, starch and cellulose are classified into different groups, but they are both polysaccharides according to chemical classification. Nature can provide an impressive array of polymers that have the potential to be used in fibers, adhesives, coating, gels, foams, films, thermoplastics and thermo set resins.

Since the majority of natural polymers are water soluble, water has been used as a solvent, dispersion medium and plasticizer in the processing of many natural polymers blends [5].

## 1.3. Polymer Blends:

Polymer blend (PB) is mixture of at least two polymers or copolymers. Polymer blends are physical mixtures of two or more polymers with/without any chemical bonding between them. [6]

Mixing of two or more polymers together to produce blends or alloys is a well-established strategy for achieving a specified physical and chemical properties, without the need to synthesis specialized polymer systems [7]. The subject is vast and has been the focus of much work, both theoretical and experimental. The manner in which two (or more) polymers are blended is of vital importance in controlling the properties of blends. Moreover, it is becoming apparent that processing can provide a wide range of blend microstructures. From an industrial point of view, polymer blends fill deficiency in price/performance of existing homopolymers with a relatively minor capital investment [8]. A shorter

period of time and effort are required to develop a new product via blending existing materials in comparison with that needed to develop a new polymer. Furthermore, an annual growth rate of around 10% till 1996 has been forecasted for thermoplastic polymer blends.

Recent research and development of polymer material has been directed to blending different polymers to obtain new products having some of the desired properties of each component. Moreover, blending of different existing polymers is of considerable importance as an alternative to graft copolymerization and the very costly development of new homopolymers. There are different reasons for blending two or more polymers together: Firstly, is to improve the polymer process ability. Secondly, is to enhance the physical and mechanical properties of blends making them more desirable than individual polymers. Thirdly, is to meeting the current growing interest in the plastic recycling process where blending technology may be the means of deriving desirable properties from recycled polymers.

The miscibility of polymer- polymer pairs is usually characterized by investigating optical, morphological, glass transition temperature and crystalline melting behavior of the mixture. It is; however, appropriate to mention that a blend of two amorphous polymers with different refractive index of the blend is uniform in all directions. Thus, the sample appears transparent to the incident beam or has domain sizes, which are much smaller than the wavelength of light [9, 10]. An immiscible blend can appear transparent to the light when refractive indices of two polymers are sufficiently close or when blending produces a two-layered film. Miscible blends of an amorphous with a semi-crystalline polymer or two semi-crystalline polymers are transparent when they are quenched. Their

crystalline versions are usually opaque if the refractive indices of amorphous and crystalline regions are different.

The glass transition temperature, (Tg) that marks the characteristic transition of the amorphous region of a polymer or blend from a glassy state to a rubbery state is the most convenient and popular way of investigating the miscibility or immiscibility between two polymers. In a semi-crystalline polymer or a blend, (Tg) is only associated with the amorphous region which is in turn is affected by the presence of crystallinity. The (Tg) is normal by differential scanning calorimetry (DSC), by dynamic mechanical and electrical relaxation methods or other miscellaneous methods [11]. The use of Tg for studying blend immiscibility has its own limitations. For example, if both components have the same or very close Tg(S) or when a small quantity of one polymer is present in the mixture some difficulties may be experienced in resolving the Tg(S) by the above techniques. Furthermore, (Tg) is associated with a domain size of at least $100A^0$. Phase separated domains below this value cannot easily be detected by (Tg) measurements [12].

## 1.3.1. Types of polymer Blends:

### 1.3.1.1. Miscible (Compatible) polymer Blends:

Mixture of two homologous polymers (usually a mixture of narrow molecular weight distribution fractions of the same polymer) [13].

A blend, which consists of two, totally, miscible polymers, can usually be characterized by a single glass transition temperature (Tg) and homogeneous microstructures with phase size down to 5-10 nm as we mentioned before [14]. Favorable physical and mechanical properties can be derived from the blend of two polymers, which are miscible with one

another. The properties of the blend are usually between those of its constituents, with a few exceptions.

An important and determinant aspect of the properties of a blend is the miscibility of its components. **Flory,( 1970)**[15] predicted that the driving force for miscibility is provided by specific interactions between polymeric components, which usually give rise to a negative free energy of mixing in spite of the high molecular weight of polymers. If the specific interactions are strong enough in polymer blends, they would be miscible and possessed special mechanical properties. Polymer blends are a mixture of at least two polymers or copolymers. From an academic point of view, the science associated with polymer blends is a truly multidisciplinary one which spreads over several topics such as chemistry, physics, thermodynamics, interface science, rheology, morphology, and processing**. Utracki,( 1990)**[16] illustrated that the term "compatible" will be used to describe mechanically process able blends, which resist gross phase segregation and / or give desirable properties. A compatible blend may consist of two or more phases. The term "miscible" is also used to describe those blends, which are homogeneous at a molecular level. The compatibility will be also taken to mean the ability of two or more substances to mix with each other to form a homogenous composition with useful properties. This is the sense in which the term is used in the production of plastic materials, and constrains with its use in applications of plastic [14].

### 1.3.1.2. Immiscible (Incompatible) polymer Blends:

The two components are not mutually soluble and two phases are present, will be opaque, no matter in what ratio they have been mixed. Each containing molecules of only one component usually, the major component is a continuous phase, while the minor component is

dispersed as dominos, sometimes large in size. There are two $(Tg)_s$, each characteristic of one component. Such blends normally exhibit relatively poor physical properties, because of poor adhesion between the two phases. Although the immiscibility promotes the desired segregation of phases, it is also responsible for high interfacial tension and poor adhesion between phases. This prevents the achievement of a fine dispersion and promotes a gross segregation during latter processing. The lack of interfacial adhesion is also a barrier to efficient transfer of stress between the phases and explains the disappointing mechanical behavior observed. These problems could be alleviated by the addition of an interfacial agent, just as detergents promote the mixing of oil and water in the colloid filed. This emulsification concept has already been extended to immiscible polymer blends and, of course, block and graft copolymers are quite suitable as potential surface active species [18, 19].

#### 1.3.1.3. Partially Miscible polymer Blends:

Blends those are homogenous at some temperatures and phase separate in other accessible temperature regions are referred to as partially or nearly miscible blends. That is, a part of each component dissolves in the other. Although there are two (Tgs) for each composition, one is slightly higher and the other slightly lower than those of the components. The dimensions of the dispersed phase depend on the adhesion between phases, the melt viscosity of the phases (related partly to molecular weight), and mixing shear. Many blends that have commercial utility and are said to have "good compatibility" are usually only partially miscible. [20]

## 1.4. Polymer Nanocomposite:

In the last years significant interest has been devoted to the study of nanocomposite materials obtained through the addition of inorganic

fillers with at least one dimension in the scale of nanometer to a polymeric matrix. Indeed, such materials showed important improvements in their properties with just few percent of loading, to be compared with classic composites, where filler content well above 30% are needed to obtain interesting results in properties enhancement [21, 22].

Such improvements concern, among the others, the mechanical behavior, the flame resistance as well as the mass transport properties , and make these materials are very attractive for applications in many different fields. Nanocomposites are composites in which at least one of the phases shows dimensions in the nanometer range (1 nm = $10^{-9}$ m). They are reported to be the materials of 21st century in the view of possessing design uniqueness and property combinations that are not found in conventional composites [23].

## 1.5. Gelatin Nanocomposite:

One of the main disadvantages of biodegradable polymers obtained from renewable sources is their dominant hydrophilic character and fast degradation rate. In principle, the properties of natural polymers can be significantly improved by blending with synthetic polymers. Gelatin is an amphoteric protein with iso-ionic point between 5 and 9 depending on raw material and method of manufacture [24].

Gelatin is a protein derived by a mild partial hydrolysis at relatively low temperature from a protein, collagen. In an aqueous solution it is a hydrophilic colloid. It is almost tasteless, odorless, vitreous, brittle solid and usually faintly yellow in color. Gelatin is a mixture of peptides and proteins. Gelatin when heated and solidifies when cooled again. Together with water, it forms a semi-solid colloid gel.

Gelatin forms a solution of high viscosity in water, which sets to a gel on cooling, and its chemical composition (Figure 1.1.) is closely similar to that of its parent collagen [25].

### 1.5.1. Chemical composition of Gelatin :[26]

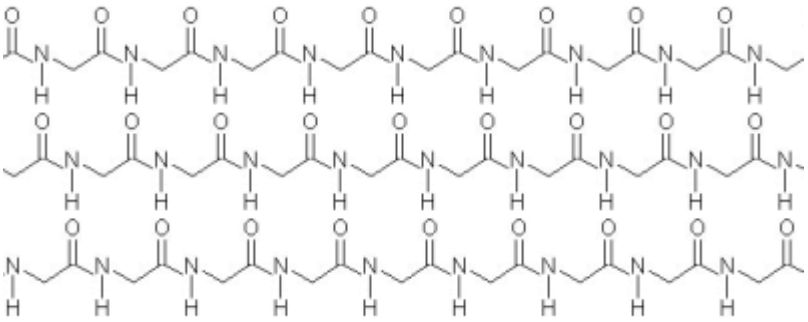

**Figure 1.1.Chemical composition of Gelatin**

Gelatin similar to synthetic polymers shows a rather wide molecular weight distribution [26, 27].

### 1.5.2. Gelatin thin Films:

Gelatin has excellent film-forming and good mechanical properties. In addition, it is unique among hydrocolloids in forming thermo-reversible with a melting point close to body temperature, which is, particularly, significant in edible and pharmaceutical applications [28].

Since the late 1980s, edible films have attracted much attention as food or drudgery packaging. It is because edible films may, partly, substitute traditional plastic films. Edible films can enhance food quality by acting as moisture, gas, aroma and lipid barriers and by providing protection to a food product after the primary package is opened [29]. Edible films can be prepared from proteins, polysaccharides, lipids or the

combination of these components. Among them, protein-based edible films are most attractive. Firstly, they are supposed to provide nutritional value [30].

Due to the hygroscopic character of this material independently of the protein used, the production of edible and biodegradable film requires the use of a plasticizer in order to increase its flexibility and its handling and it may simultaneously induce the reduction of the vitreous transition in an undesirable manner [31].

In structural terms, plasticizers are inserted into the polymeric matrix, increasing the free space between chains, causing a decrease of intermolecular forces along the matrix [32, 33]. The most widely used plasticizers include glycerol [34, 35]. This plasticizer present hydrophilic character, which contribute to the increase of water permeability and susceptibility of the matrix to environmental humidity.

Gelatin films, in particular, have been employed as an adhesive [36], oxygen barrier, mold retardant, antioxidant carrier and frying oil barrier [37] and primary component of certain pharmaceutical capsules and tablet coatings. Gelatin films are successfully used due to their unaffected on environment and easily waste [38].

**Bae et al., (2009)** [39] investigated the effect of clay content, homogenization RPM, and pH on the mechanical and barrier properties of fish gelatin/nanoclay composite films. The addition of 5% nanoclay (w/w) increased the tensile strength from 30.31 - 2.37 MPa to 40.71 -3.30 MPa. The 9 g clay/100 g gelatin film exhibited the largest improvements in oxygen and water barrier properties. Oxygen permeability decreased from 402.8 $X10^{-6}$ - 0.7 $X\ 10^{-6}$ $gm/m^2$ day atm to 114.4$X\ 10^{-6}$ - 16.2 $X10^{-6}$ $gm/m^2$ day atm and the water vapor permeability decreased from 31.2 $X\ 10^{-3}$ -1.6 $X\ 10^{-3}$ ng $m/m^2$s Pa to 8.1$X\ 10^{-3}$- 0.1$X10^{-3}$ ng m/ $m^2$ s Pa. The

XRD and TEM observation suggested that the ultrasonication treatment (30 min at 40% output) resulted in exfoliation of the silicates.

**Caglar et al., (2010)** [40] has been developed a novel pyranose oxidase (PyOx) biosensor based on gold nanoparticles (AuNPs)–polyaniline(PANI)/AgCl/ gelatin nanocomposite for the glucose detection. PyOx was immobilized on the surface of glassy carbon electrode (GCE) via the nanocomposite matrix. The electrode surface was imaged by scanning electron microscopy (SEM). Amperometric detection of the consumed oxygen during the enzymatic reaction was monitored at -0.7 V. After optimization studies, analytical characterization of the biosensor was carried out. The linear response of the AuNPs–AgCl/PANI/gelatin modified PyOx biosensor is found to be from 0.05 to 0.75 mM glucose with the equation of $y = 2.043x + 0.253$; $R2 = 0.993$. Finally, proposed biosensor was used to analyze glucose content in real samples. Obtained data from the biosensing system was compared with a commercial enzyme assay kit based on spectrophotometric Trinder reactionas a reference method.

**Roberta et al., (2005)** [41] synthesized, Hybrid, inorganic/organic materials consisting of Au and AuNi nanoparticles and gelatin by soft chemical routes (reduction by $N_2H_4$ aqueous solution at 277 and 373 K). The average particle size, obtained by transmission electron microscopy, ranged between 4 and 20 nm. For Au–gelatin sample, at 277 K, the gelatin 3D network was maintained and Au nanoparticles were close-packed linear assemblies along gelatin filaments forming a spider web-like network. Because of inter-particle coupling and gelatin adsorption, Au arrays exhibit dipolar plasmon resonances that shift and broaden by hundreds of nanometers. For the first time, AuNi nanoparticles could also be formed at 373 K. At this temperature gelatin was solubilized but AuNi

particles were still stabilized by the protein chains without array formation. AuNi fcc phases were observed by X-ray diffraction. A blue-shift of the plasmon resonance was observed for AuNi–gelatin nanocomposites when compared to Au–gelatin. SQUID magnetometer measurements indicate that AuNi–gelatin samples are ferromagnetic at low temperature. At 2K hysteresis loops were observed with coercivity ($H_c$) values between 450 and 650 Oe and squareness values between 0.15 and 0.37. These new nanocomposites therefore appear very promising for design of nanodevices.

**Jun et al., (2007)** [42] prepared gelatin/montmorillonite–chitosan (Gel/MMT–CS) nanocomposite scaffold via the intercalation process and freeze-drying technique, using the ice particulates as the porogen materials. Properties including pore structure, water adsorption content, in vitro degradation and tensile strength were investigated. It was demonstrated that the introduced intercalation structure endowed the Gel/MMT–CS scaffold with good mechanical properties and a controllable degradation rate. Scanning of electron microscope images revealed that the scaffold obtained was highly porous and suitable for the implanted cells to adhere and grow. The mitochondrial activity assay provided good evidences of cells viability on the Gel/MMT–CS membranes, indicating of possible application in tissue engineering.

**Smitha et al., (2007)** [43] synthesized Silica–biopolymer hybrid using colloidal silica as the precursor for silica and gelatin as the biopolymer counterpart. The surface modification of the hybrid material has been done with methyl tri-methoxysilane leading to the formation of biocompatible hydrophobic silica–gelatin hybrid.The hybrid gel has been evaluated for chemical modification, thermal degradation, hydrophobicity, particle size, transparency under the UV–visible region

and morphology. FTIR spectroscopy has been used to verify the presence of $CH_3$ groups which introduce hydrophobicity to the $SiO_2$–MTMS–gelatin hybrids. The hydrophobic property has also been tailored by varying the concentration of methyltrimethoxysilane. Contact angle by Wilhelmy plate method of transparent hydrophobic silica–gelatin coatings has been found to be as high as ∼95◦. Oxidation of the organic group which induces the hydrophobic character occurs at 530°C which indicates that the surface hydrophobicity is retained up to that temperature. Optical transmittance of $SiO_2$–MTMS–gelatin hybrid coatings on glass substrates was found to be close to 100% which enables the hybrid for possible optical applications and also for preparation of transparent biocompatible hydrophobic coatings on biological substrates such as leather.

**Babita et al., (2008)** [44] synthesized gelatin coated iron oxide nanocomposite (G/IO) and hydroxyapatite (HAp) crystal nucleation and growth in the nanoparticles was explored. Due to the structural similarity of gelatin (and collagen) linked to a mineral phase based on Ca-phosphates compounds with natural bone and increasing application of magnetic iron oxides in hyperthermia. A series of GIO/HAp nanocomposites with various amount of GIO were synthesized by co-precipitation technique using calcium hydroxide and phosphoric acid as precursors. Various physico-chemical analysis showed that the HAp crystal nucleation and growth occurred at acidic group of gelatin, while magnetic iron oxide nanoparticles (b 8nm) were bound to the amide groups of the gelatin chain. Moreover, the growth of HAp nanocrystals in aq. GIO solution was, highly, influenced by the GIO contents in the solution. The mineralized composite with magnetic properties could have

great scope in biomedical field as a thermoseed to kill cancerous cells in bone, side by side, for the bone reinforcement.

## 1.6. Poly vinyl alcohol (PVA) Nanocomposite:

Polymers are commercially available; many are water soluble, biocompatible and have been widely used in the chemistry of colloids as dispersants, chelates, surfactants, food industry, ligands and so forth. In the realm of water compatible polymers reported in literature, poly vinyl alcohol (PVA) and its related products appear as one very interesting choice for preparing colloidal suspensions, due to their biocompatibility and biodegradability aiming at medicine, biology and pharmaceutics applications [45].

Also Poly vinyl alcohol has a melting point of 230 $^0$C and 180- 190 $^0$C for the fully hydrolyzed and partially hydrolyzed grades, respectively. It decomposes rapidly above 200$^0$C as it can undergo pyrolysis at high temperatures [46].

### 1.6.1. Poly vinyl alcohol (PVA) thin Films:

Poly vinyl alcohol has excellent film forming, emulsifying and adhesive properties. Poly vinyl alcohol is a water soluble synthetic polymer. Due to the characteristic of easy preparation, good biodegradability, excellent chemical resistance and good mechanical properties, Poly vinyl alcohol has been used in many biomaterial applications [47].

In recent years, poly vinyl alcohol which is a cheap and nontoxic synthetic polymer has been used widely for cell immobilization. However, there are some synthetic polymers from nonrenewable sources that are biodegradable, such as Poly vinyl alcohol [48]. Poly vinyl alcohol film used in several studies on biopolymer materials produced by casting or extrusion methods [49].

**Saikia et al., (2011)**[50] investigated CdS/PVA nanocomposite thin film deposited on glass substrates by, in situ ,thermolysis of precursors dispersed in polyvinyl alcohol (PVA). The synthetic technique reported in this study is free from complexing agent and hence no need to control the pH of the solution as in the case of conventional CBD. The as-prepared films were characterized by X-ray diffraction (XRD), scanning electron microscopy (SEM), transmission electron microscopy (TEM), selected area electron diffraction (SAED), UV–vis spectroscopy, and photoluminescence (PL) spectra. The XRD and SAED results indicated the formation of CdS Nanoparticles with hexagonal phase in the PVA matrix. The photoluminescence and UV–VIS spectroscopy revealed that CdS/PVA films showed quantum confinement effect. From the shift in optical band gap, particle sizes were calculated using effective mass approximation (EMA) method and it was found to be in agreement with the results obtained from TEM observations. The SEM results indicated that as grown films were homogeneous with no visible pinholes and cracks. The film prepared at 100 $^{0}$C was found to be suitable for application as a window layer in solar cell.

**Fernandes et al., (2011)** [51] synthesized **(**ZnO) Nanoparticles with average diameter of 25nm by a modified sol–gel method and used in the preparation of (in wt.%) (100−x) poly (vinyl alcohol) (PVA)/x ZnO nanocomposite films, with x = 0, 1, 2, 3, 4, and 5. The PVA/ZnO films

were exposed to UV radiation for 96 h., and their thermal, morphological, and spectroscopic properties were investigated. In inert atmosphere, the nanocomposite films showed lower thermal stability than the pure PVA film, and the calorimetric data suggest an interaction between PVA and ZnO in the nanocomposite films. Some crystalline phases could be seen in the films with ZnO, and a direct dependence on the ZnO concentration was also observed. The original structure of ZnO Nanoparticles remained unaltered in the PVA matrix and they were uniformly distributed on the film surface. The roughness of the PVA film was not modified by the addition of ZnO; however, it increased after 96 h of UV irradiation, more significantly in the nanocomposite films. The films showed an absorption band centered at 370 nm and a broad emission band in the UV–VIS region when excited at 325 nm.

**Guang et al., (2007)**[52] prepared novel silver/ (PVA) nanocomposite films by an in situ reduction method, in which the silver nitrate, sodium poly (glutamic acid) (PGA) and PVA acted as precursor, stabilizer and polyolreducant, respectively. The surface-enhanced Raman scattering (SERS)-activity of as-prepared nanocomposite films was investigated using benzoic acid (BA) as probed molecule. The results showed that these surface plasmon resonance (SPR) absorption band on silver films was more symmetric with stronger intensity than silver colloidal solution, indicating that Ag Nanoparticles distribution on the film substrate was uniform. The fact was further confirmed by X-ray diffraction (XRD), transmission electron microscopy (TEM) and field-emission scanning electron microscope (FE-SEM) measurements. It was found that PGA stabilized silver/PVA nanocomposite film revealed the presence of well-dispersed and spherical silver Nanoparticles with average diameter of 90 nm, while the particle sizes were enlarged as the

PGA concentration increased. The new substrate presented high SERS enhancement and the enhanced factor was estimated to be 106 for the detection of benzoic acid.

**Chun, (2007)** [53] prepared PVA/$TiO_2$ composite polymer membrane by a solution casting method. Glutaraldehyde (GA) was used as a cross-linker for the composite polymer membrane in order to enhance the chemical, thermal and mechanical stabilities. The characteristic properties of the cross-linked PVA/TiO2 composite polymer membranes were examined by thermal gravimetric analysis (TGA), X-ray diffraction (XRD), scanning surface microscopy (SEM), and ac impedance method. The novel DMFC, consisting of an air cathode electrode with $MnO_2$ carbon inks, an anode electrode with Pt Ru black inks on carbon paper and the PVA/$TiO_2$ composite polymer membrane, was assembled and examined. It was found that the DMFC using this novel cheap PVA/$TiO_2$ composite polymer membrane showed good electrochemical performance at ambient temperature and pressure. The maximum peak power density of the alkaline DMFC is about 7.54mWcm$^{-2}$ at 60 $^0$C and 1 atm.

**Hongmei et al., (2007)**[54] prepared a series of CdS/PVA nanocomposite films with different amount of Cd salt by means of the in situ synthesis method via the reaction of $Cd^{2+}$ dispersed poly vinyl-alcohol (PVA) with $H_2S$. The as-prepared films were characterized by X-ray diffraction (XRD), transmission electron microscopy (TEM), ultraviolet-visible (UV–VIS.) absorption, photoluminescence (PL) spectra, Fourier transform infrared spectroscope (FTIR) and thermo gravimetric analysis (TGA). The XRD results indicated the formation of CdS Nanoparticles with hexagonal phase in the PVA matrix. The primary FTIR spectra of CdS/PVA nanocomposite in different processing stages have been discussed. The vibrational absorption peak of Cd–S bond at

405 $cm^{-1}$ was observed, which further testified the generation of CdS Nanoparticles. TGA results showed incorporation of CdS Nanoparticles significantly altered the thermal properties of PVA matrix. photoluminescence and UV–VIS. spectroscopy revealed that the CdS/PVA films showed quantum confinement effect.

**Anurag and Ram, (2011)** [55] prepared polyvinyl alcohol (PVA)/Silver nanocomposite. The silver Nanoparticles were enerated in PVA matrix by the reduction of silver ions with PVA molecule at 60–$70^0$C over magnetic stirrer. UV–VIS. analysis, X-ray diffraction studies, transmission electron microscopy, scanning electron microscopy and current–voltage analysis were used to characterize the nanocomposite films prepared. X-ray diffraction analysis reveals that silver metal is present in face centered cubic (fcc) crystal structure. Average crystallite size of silver nanocrystal is 19 nm, which increases to 22nm on annealing the film at 150 $^0$C in air. This result is in good agreement with the result obtained from TEM. The UV–VIS. spectrum shows a single peak at 433 nm, arising from the surface plasmon absorption of silver nanocolloids. This result clearly indicates that silver Nanoparticles are embedded in PVA. An improvement of mechanical properties (storage modulus) was also noticed due to a modification of PVA up to 0.5 wt% of silver content. The current–voltage (I–V) characteristic of nanocomposite films shows increase in current drawn with increasing Ag-content in the films.

**Aleksandra et al., (2007)**[56] prepared Ag/PVA Nanocomposites with different contents of inorganic phase by reduction of $Ag^+$ ions in aqueous PVA solution by gamma irradiation followed by solvent evaporation. Optical properties of the colloidal solutions and the nanocomposite films were investigated using UV–vis spectroscopy. Structural characterization of Ag Nanoparticles was performed by TEM

and XRD. Interaction of the Ag Nanoparticles with polymer matrix and the heat resistance of the Nanocomposites were followed by IR spectroscopy and DSC analysis. IR spectra indicated that Ag nanofiller interact with PVA chain over OH groups. The changes of heat resistance upon the increase of the content of inorganic phase are correlated to the adsorption of polymer chains on the surface of Ag Nanoparticles.

**Yajuan et al., (2009)** [57] prepared, (PVA)/exfoliated a-zirconium phosphate Nanocomposites of various compositions by a solution casting method. The a-ZrP compound was synthesized by refluxing. The characteristic properties of the PVA/e-a-ZrP composite films were examined by thermal gravimetric analysis (TGA), differential scanning calorimetry (DSC), X-ray diffraction (XRD), scanning electron microscopy (SEM) and tensile tests. Tensile tests indicated that with the loading of e-a-ZrP, the tensile strength and the elongation at break were increased by 17.3% and 26.6%, respectively compared to neat PVA. It is noteworthy that optimum film properties were obtained with 0.8 wt% ea-ZrP, and higher proportions of e-a-ZrP, may be related to the aggregation of e-a-ZrP particles and deterioration of the film properties. On the whole, the nanocomposite PVA/ea- ZrP systems had mechanical and thermal properties which were superior to that of the neat polymer and its conventionally filled composites.

**Kuljanin et al., (2006)** [58] synthesized lead sulfide (PbS) nanoparticles (NPs) with average diameter of 26 °A and polyvinyl alcohol (PVA) using colloidal chemistry methods. The PbS/PVA nanocomposites were characterized using optical, structural, thermal and mechanical techniques. No difference between infrared spectra and no difference between glass transition temperatures after incorporation of the PbS NPs in the PVA matrix indicated weak interaction between nanofiller

and polymer. Due to weak interaction between nanofiller and polymer a slight improvement of the mechanical properties of the PbS/PVA nanocomposite was observed compared to the neat PVA. On the other hand, the presence of the PbS NPs in the PVA matrix induced the increase of the crystallization temperature and enthalpy of crystallization. Also, the thermal decomposition of the PVA shifted towards higher temperature of 15 $^{0}$C in the presence of the PbS (NPs).

**Kunhua et al., (2011)** [59] studied Starch/polyvinyl alcohol (PVA)/nano-silicon dioxide (nano-$SiO_2$) biodegradable hybrid films were prepared via the sol–gel method. Fourier transform infrared spectroscopy, scanning electron microscopy, and X-ray photoelectron spectroscopy were used to evaluate the structure of the films. The aging and biodegradable properties of the films were studied as well. A gel network was formed in the films; this network is responsible for improving the performance of the starch/PVA/nano-$SiO_2$ hybrid films. The crystal structure of the films was increased owing to the addition of nano-SiO2. The addition of nano-$SiO_2$ also delays aging of the films. However, the enzymatic degradation test shows that the addition of nano-$SiO_2$ has no significant influence on the biodegradability of the films.

**Soon et al., (2012)** [60] is aimed to prepare starch/PVA composite films with added nano-sized poly (methyl methacrylate-co-acrylamide) (PMMA-co-AAm) particles and to investigate the mechanical properties, water barrier properties, and soil burial degradation for the films. Composite films were prepared using corn starch, polyvinyl alcohol (PVA), nano-sized PMMA-co-AAm particles, and additives, i.e., glycerol, xylitol , and citric acid. Nano-sized PMMA-co-AAm particles were synthesized by emulsion polymerization. The results indicated that the mechanical properties and water resistance were improved up to 70–

400%, the results of the soil burial biodegradation revealed that films added PMMA-co-AAm particles were degraded by about 45–65% after 165 days.

**Rayna et al., (2010)**[61] synthesized novel hybrid material thin films based on polyvinyl alcohol (PVA)/tetraethyl orthosilicate (TEOS) with embedded silver nanoparticles (AgNps) using sol–gel method. Two different strategies for the synthesis of silver nanoparticles in PVA/TEOS matrix were applied based on reduction of the silver ions by thermal annealing of the films or by preliminary preparation of silver nanoparticles using PVA as a reducing agent. The successful incorporation of silver nanoparticles ranging from 5 to 7 nm in PVA/TEOS matrix was confirmed by TEM and EDX analysis, UV–Vis spectroscopy and XRD analysis. The antibacterial activity of the synthesized hybrid materials against strains of three different groups of bacteria Staphylococcus aureus (gram-positive bacteria), Escherichia coli (gram-negative bacteria), Pseudomonas aeruginosa (non-ferment gram-negative bacteria) .The hybrid materials showed a strong bactericidal effect against E. coli, S. aureus and P. aeruginosa and therefore have potential applications in biotechnology and biomedical science.

**Prashant et al., (2011)** [62] investigated Pervaporative performances for dehydration of water–acetonitrile using nanocomposite metal oxide and Pervap 2202 membranes. Poly (vinyl alcohol) based nanocomposite metaloxide membranes were prepared through co-precipitation of different amounts of Fe (II) and Fe (III). The freestanding nanocomposite metal oxide membranes were characterized by Transmission electron microscopy and X-ray diffraction. Sorption studies evaluated the extent of interaction and degree of swelling of the membranes. Fe containing PVA polymer matrix showed improved flux and selectivity. In order to

observe simultaneous effect of flux and selectivity, pervaporation separation index showed10 wt.% iron oxide containing membrane is the most amongst all tested. Diffusion coefficients were calculated using pervaporation results and sorption kinetics data. An attempt was made to predict sorption selectivity thermodynamically. PV separation factor was observed to be governed by sorption and/or diffusion phenomena and sorption selectivity was found to be higher than PV separation factor. Prediction of concentration profile in the membrane was also attempted and the results showed that water concentration in the membrane decreases with increased membrane thickness.

**Li Mei et al., (2008)** [63] prepared a series of photochromic nanocomposite films were prepared by well-dispersed Keggin type polyoxometalates (POM) in polyvinyl alcohol (PVA). The corresponding structure, photochromic behaviors and mechanism of the films were investigated with transmission electron microscopy (TEM), atomic force microscopy (AFM), Fourier transform infrared spectra (FT-IR), ultraviolet visible absorption spectra (UV/VIS) and electron resonance spectra (ESR). In composite films, the sphere-shaped POM nanoparticles were well dispersed with narrow size distribution. AFM images indicated that the surface topography of polymeric matrix changed after adding POM, and the surface appearance of nanocomposite films was different before and after ultraviolet light irradiation. FT-IR results showed that the Keggin geometry of POM was still preserved inside the composites and a charge-transfer bridge was built between POM and PVA polymeric matrix through hydrogen bonding. Irradiated with ultraviolet light, composite films changed from colorless to blue and showed reversible photochromism. The composite film containing molybdenum exhibited faster photochromic efficiency and slower bleaching reaction than that

containing tungsten. The inferior reversibility of composite films was observed during the coloration–decoloration cycle. The appearance of the characteristic signals of $W^{5+}$ or $Mo^{5+}$ in ESR spectra indicated that PVA was a proton donor and the photochemical process was in accordance with the charge-transfer mechanism.

**Karthikeyan, (2005)** [64] prepared Ag–Polyvinyl alcohol (Ag–PVA) films. The influence of annealing time upon the variation of cluster size has been analyzed using optical absorption, emission and Fourier-transform infrared (FTIR) spectra. Measurements of optical spectra show that the surface Plasmon resonance lies around 420 nm, and confirm the growth of Ag clusters. Measurements of FTIR spectra were carried out to identify the role of chemical interface damping which influenced the broadening of the absorption band. The emission peak was observed at 540nm for clusters which were annealed for 1 and 2 min.

## 1.7. Effect of Radiation on Nanocomposite:

Radiation processing can be defined as the treatment of materials and products with radiation or ionizing energy to change their physical, chemical or biological characteristics, to increase their usefulness and value, or to reduce their impact on the environment. Accelerated electrons, X-rays emitted by energetic electrons, and gamma rays emitted by radioactive nuclides are suitable energy sources. These are all capable of ejecting atomic electrons, which can then ionize other atoms in a cascade of collisions. So they can produce similar molecular effects. The choice of energy source is usually based on practical considerations, such

as absorbed dose, dose uniformity (max/min) ratio, material thickness, density and configuration, processing rate, capital and operating costs.

In the case of electron beam (EB) processing, the incident electron energy determines the maximum material thickness, and the electron beam current and power determine the maximum processing rate. In the case of X-ray processing, the emitted power increases with the electron energy and beam power. For high throughput industrial processes, the capital costs and operating costs of an irradiation facility are competitive with more conventional treatment methods.

Successful irradiation processes provide significant advantages in comparison to typical thermal and chemical processes, such as higher throughput rates, reduced energy consumption, less environmental pollution, more precise control over the process and the production of products with superior qualities. In some applications, radiation processing can produce unique effects that cannot be duplicated by other means.

**Krkljes et al., (2007)** [65] investigated the degradation kinetics of gamma radiolytically synthesized Ag/PVA nanocomposite by thermo-gravimetric method under dynamic conditions (30–600$^0$C) in an inert atmosphere. The results showed that thermal degradation of composites was a two stage process for the lower amount of nano filler and single-stage for the higher amount of nano filler. Vyazovkin model-free kinetics method was applied to calculate the activation energy (*E*a) of the degradation process as a function of conversion and temperature. At a given degradation temperature, PVA as a host in nanocomposite presents lower reaction velocity, while its *E*a is higher than that of pure PVA.

**Wael et al., (2011)** [66] used gamma-irradiation to reduce silver ions to generate silver Nanoparticles in PVA matrix. (PVA/Ag) hybrid

nanocomposite which prepared from PVA polymeric film and silver nitrate (AgNO3). UV–visible spectra showed a single peak at 422 nm, arising from the surface plasmon absorption of silver Nanoparticles. The shifting of surface Plasmon resonance peak after irradiation reveals that gamma irradiation can be used as a size controlling agent for the preparation of silver Nanoparticles embedded in PVA film. This result was in good agreement with the result obtained from TEM images. TEM images showed narrow size distribution of Ag Nanoparticles with an average particle size of 30 nm, which decreased to 17nm with increasing irradiation dose. X-ray diffraction analysis revealed that silver metal was present in a face centered cubic (fcc) crystal structure. These results clearly indicate that monodispersed silver Nanoparticles are embedded homogenously in PVA matrix.

**Manjunatha et al., (2007)** [67] studied the effect of electron irradiation on the optical properties of polyvinyl pyrrolidone (PVP) capped cadmium sulphide (CdS) Nanoparticles embedded in polyvinyl alcohol (PVA) matrix. PVP capped CdS Nanoparticles were prepared by a non-aqueous chemical method with cadmium nitrate as the cadmium source and hydrogen Sulphide as the Sulphur source. Synthesized Nanoparticles are used for X-ray diffraction (XRD) studies that confirmed the formation of cubic CdS Nanoparticles with an average size of 3–5 nm. The synthesized CdS nano-powder is dispersed in PVA matrix and self-standing flexible (PVP-CdS) PVA films of thickness 0.2mm were obtained. The nanocomposite were subjected to optical absorption spectroscopy and photoluminescence (PL) studies. The PL emission spectra of the nanocomposite showed two peaks, at 502 and 636 nm, which are attributed to the band edge and surface defects of CdS Nanoparticles, respectively. The composite films are irradiated with

8MeV electrons from a Microtron and optical absorption and PL studies are carried out on the irradiated samples. Irradiation of the samples leads to the quenching of surface defect related emission.

**Manal et al., (2009)** [68] used electron beam irradiation as crosslinking agent for preparing Copolymer hydro-gels composed of poly vinyl alcohol (PVA) and carboxy-methyl cellulose (CMC). The copolymers were characterized by FTIR and the physical properties such as gelatin. The thermal behavior and swelling properties of the prepared hydro-gels were investigated as a function of PVA/CMC composition. The factors effecting adsorption capacity of acid, reactive and direct dyes onto PVA/CMC hydro-gel, such as CMC content, pH value of the dye solution, initial concentration and adsorption temperature for dyes were investigated. Thermodynamic study indicated that the values the negative values of suggested that the adsorption process is exothermic. The value of H (38.81 kJ/mol) suggested that the electrostatic interaction is the dominant mechanism for the adsorption of dyes on hydro-gel.

**Jen et al., (2009)** [69] used UV radiation and sol–gel process through two steps for modification of polyvinyl alcohol (PVA) to prepare the modified PVA membranes. From the first step modification of PVA by UV radiation with 2-hydroxy ethyl methacrylate (HEMA) monomer, the poly (2-hydroxy ethyl methacrylate) (PHEMA) modified poly vinyl alcoho), PVAHEMA, was obtained and characterized by Fourier transfer infrared spectra (FTIR) and optical polarizing microscopy for the chemical compositions and morphology. With the second step modification of sol–gel process, the organic–inorganic hybrid sol–gel material, PVA/HEMA/$SiO_2$, was prepared. Both of the modified PVA, (PVAHEMA and PVA/HEMA/$SiO_2$), were characterized by X-ray diffraction (XRD), differential scanning calorimetry (DSC), and

Thermogravimetic analysis (TGA). To prepare the alkaline solid polymer electrolyte, the various PVAHEMA and PVA/HEMA–$SiO_2$ membranes were immersed in 40 wt% KOH solution to form the KOH containing polymer electrolyte membranes. And then their performances were conducted with impedance spectroscopy to evaluate the ionic conductivity through the membranes. At room temperature, the ionic conductivity increased from 0.044 to 0.073 S/cm for the PVA/HEMA membrane; whereas the ionic conductivity was about 0.11 S/cm for the PVA/HEMA/$SiO_2$ membranes. Compared to other reports in references, hybrid sol–gel membrane is a highly ionic conducting alkaline solid polymer electrolytes membrane.

## 1. 8. Industrial application of Radiation process:

Radiation processing was introduced more than fifty years ago, and many useful applications have since been developed. The most important commercial applications involve modifying a variety of plastic and rubber products, and sterilizing medical devices and consumer items. Emerging applications are pasteurizing and preserving foods, and reducing environmental pollution [(70)].

### 1.8.1. Modifying polymeric materials:

#### 1.8.1.1. Polymerization:

Low-energy (75 keV to 300 keV) electron accelerators are used to cure (polymerize and crosslink) coatings, adhesives and inks on paper, plastic and metal substrates. Such materials consist of oligomers (polymers with low molecular weights) and monomers to provide fluidity before curing. This technique avoids the use of volatile solvents, thereby helping to reduce air pollution. Acrylated urethane polyesters, acrylated epoxies and polyethers are suitable oligomers, and trimethylolpropane triacrylate (TMPTA) is a suitable monomer. Polymerizations are chain

reactions which produce high relative molecular masses. with comparatively low doses of less than 50 kGy. Line speeds up to 1500 m/minPolymerization can be achieved at 10 kGy [71]. High-energy (up to 10 MeV) accelerators are used to cure fiber-reinforced composite materials. In comparison to heat curing, the processing time and cost can be reduced with electron beam or X-ray curing. Acrylated epoxies with carbon fibers are suitable materials. Higher doses (150 kGy to 250 kGy) are needed to obtain a combination of polymerization and crosslinking [72, 73]. This is an emerging application for electron beam and X-ray processing. Composite parts now being used in automobiles and aircraft are mainly cured with heat, but radiation curing offers several advantages [74].

### 1.8.1.2. Grafting:

Graft copolymerization of monomers with preformed polymers can be used to modify the properties of their surfaces [75] . This can be done with common polymers such as polyethylene, polypropylene and some fluoropolymers. Plastic films, membranes, fibers and textiles are suitable products. Styrene, acrylic acid, 4-vinylpyridine and N-vinylpyrrolidone can be grafted onto polytetrafluoroethylene (Teflon) [76]. Other combinations are styrene on cellulose, vinylpyridines on wool and p-nitrostyrene on polyethylene, polyvinyl chloride and polypropylene [77]. Hydrophilic properties can be added to hydrophobic polymers to make permselective membranes [78]. Ion exchange membranes, fuel cell and battery separator films, permeation separation membranes, promotion of surface adhesion, chelating fibers for sea-water treatment and for recovering some precious metals from sea-water are other possibilities [79]. Grafting can also improve the biocompatibility of polymers for medical applications [80].

### 1.8.1.3. Cross-linking:

Radiation cross-linking began more than 50 years ago when it was discovered that polyethylene (PE) could be cross-linked in this way [81]. This is still the most important irradiated material because it is used in many products and it is relatively inexpensive. Cross-linking is the most widely used effect of polymer irradiation because it can improve the mechanical, thermal and chemical qualities of preformed products as well as bulk materials. Both cross-linking and degradation by chain scissoring can occur during polymer irradiation, but one or the other effects may be predominant [82, 83].

Cross-linking doses are usually in the range from 50 to 150 kGy. Multifunctional monomers can be mixed with the polymer to increase the G(X) value and reduce the dose requirement. Antioxidants, UV stabilizers and flame retardant compounds can be added to improve the performance of the material for particular applications. Such additives may inhibit the cross-linking effect, so the properties of commercial materials are usually different from the pure polymers [84].

### 1.8.1.4. Insulated wire and cable:

One of the first commercial applications of radiation cross-linking was the improvement of the insulation of electrical wires and the jackets on multi-conductor cables. Products of this type were introduced during the 1950s by the Raychem Corporation (since acquired by Tyco Electronics), and many wire manufacturers are now using this method to produce high-performance wire for aircraft and automobiles. Polyethylene, polyvinylchloride, ethylene-propylene rubber, polyvinylidene fluoride and ethylene tetra-fluoro ethylene copolymer are some of the materials used in this application. Increased tolerance to overloaded conductors and high temperature environments, fire

retardation, increased abrasion resistance, increased tensile strength, reduction in cold flow and increased resistance to solvents and corrosive chemicals are product improvements obtainable by this method [85, 86, 87].

### 1.8.1.5. Heat-shrinkable plastic tubing and film:

Radiation cross-linking stabilizes the initial dimensions of products and imparts the so-called "memory" effect. Cross-linking occurs mainly in the amorphous zones of polyethylene, but the crystalline zones determine the stiffness of the material. The cross-linked material becomes elastic when heated above the melting temperature of the crystalline zones, which is approximately 100 ºC. The product can then be expanded or stretched to several times its original size. It maintains the larger dimension when cooled, but it contracts to its original size when heated again. Examples of commercial products using this effect are encapsulations for electronic components, jackets for multi conductor cables, exterior telephone cable connectors and food packaging films [88, 89].

### 1.8.1.6. Automobile tires:

Several components of an automobile tire, such as the inner liner, the chafer strip, the sidewall, the body and tread plies, and the fabric or steel-reinforced belt, may be given a low dose of electron beam radiation before the tire is assembled. This partial radiation cross-linking stabilizes their thicknesses when the final chemical curing is done in a heated mold. Procuring also avoids migration of the steel belt through its supporting material. This dimensional stabilization produces a higher quality tire with more uniform thickness and better balance. Therefore, the tire can be made thinner to save material, reduce cost and reduce frictional heating at high speed. Materials are usually isoprene and diene elastomers with doses in the range of 30 to 50 kGy [90, 91].

#### 1.8.1.7. Plastic pipe:

Concrete floors can be heated by circulating hot water through cross-linked polyethylene pipe embedded in the concrete. Such plastic pipe also has other applications. A composite pipe is made with a middle layer of thin aluminum, which withstands the water pressure, an inner plastic layer to avoid contact with the aluminum layer, and an outer plastic layer for abrasion resistance. The inner and outer layers are irradiated, simultaneously, with high-energy electrons [92].

#### 1.8.1.8. Plastic foam:

Plastic foam can be made by mixing a thermally unstable substance with a polymer and then heating the mixture to melt the polymer and decompose the additive. The evolved gas forms bubbles in the polymer. A zodi carbon amide can be used as the foaming additive. Polyethylene, ethylene vinyl acetate copolymer and polypropylene can be used as the polymeric material. The expansion process is more easily controlled with cross-linked material. Foamed gaskets, coaxial cable insulation, coated tapes, helmet liners, athletic safety pads, bra cups, floor backing and automobile seat padding are typical applications [93, 94].

### 1.8.2. Biological applications:

#### 1.8.2.1. Sterilizing medical products:

The first industrial facility for sterilizing medical products with accelerated electrons was built by Johnson at their Ethicon factory in Somerville, New Jersey, USA in 1956. That facility was equipped with a 2 MeV Van de Graff accelerator and a 5 MeV, 5 kW microwave linear accelerator (linac) made by the High Voltage Engineering Corporation in Cambridge, Massachusetts. The next research accelerator facility to be used part time for sterilizing medical products was built at the RISOE National Laboratory in Roskilde, Denmark in 1960. The first linac

installed at that facility was a 10 MeV, 5 kW machine made by Varian Associates in Palo Alto, California. The third industrial accelerator facility for medical device sterilization was built by SRTI/CARIC in Corbeville, Orsay, France in 1967. That facility was equipped with a 6 MeV, 7 kW linac made by CGR-MeV in Corbeville, Orsay, France. The first gamma-ray sterilization facilities with cobalt-60 sources were also built in 1960 in the United Kingdom, France and Australia [95].

Since that time, many industrial facilities equipped with microwave linacs, direct current electron accelerators, radio frequency accelerators, and also with large cobalt-60 sources, have been built and are operating routinely for sterilizing large quantities of medical products [96, 97, 98]. X-ray processing is also finding its place in this field [99, 100]. Dose requirements are in the range of 10 to 30 kGy, depending on the bioburden of the products. The International Organization for Standardization (ISO) has published guidelines for the proper application of electron beam, X-ray and gamma-ray sterilization processes [101].

**1.8.2.2. Preserving food:**

Several experiments on food irradiation were done during the first half of the 20th century, but serious investigations of this treatment process were delayed until the late 1940s when more powerful radiation sources became available. The U.S. Government began to support these activities in the early 1950s. Since then, many studies have been done all over the world and many papers and books have been published on this topic [102, 103]. The recent status of the regulatory and commercial aspects has been reviewed in Reference [104]. A variety of beneficial effects can be obtained by irradiating fresh foods. Low doses in the range of 0.1 to 1.0 KGy can inhibit the sprouting of potatoes, onions, garlic, roots and nuts; insects can be disinfested in cereals and legumes, fresh and dried

fruits, dried fish and meat; parasites can be disinfected in fresh pork, freshwater fish and fresh fruits; and the ripening of some fruits can be delayed. Medium doses of 1 to 7 KGy can extend the shelf-life of raw fish and seafood as well as fruits and vegetables; pathogenic and spoilage bacteria can be nearly eliminated from raw and frozen seafood, meat and poultry, spices and dried vegetable seasonings; some foods will exhibit improved technical properties, such as increased juice yield in grapes, and reduced cooking time in dehydrated vegetables. High doses of 30 to 50 kGy can sterilize meat, poultry, seafood, sausages, prepared meals, hospital diets, etc.; certain food additives, such as spices, enzyme preparations, natural gums and gels, can be decontaminated [105].

### 1.8.3. Pollution control:

#### 1.8.3.1. Reducing acid rain:

Coal-fired and oil-fired electric power plants produce acid rain by emitting sulfur and nitrogen oxides. These gases are converted to sulfuric and nitric acids in the atmosphere by reactions with water vapor, activated by ultraviolet (UV) radiation from the sun. The amounts of such emissions can be, substantially , reduced by irradiating combustion gases with energetic electrons. This process causes the formation of acid vapors under controlled conditions within the power plant. Then these acidic gases can be neutralized by injecting ammonia vapor to produce fine particles of ammonium sulfate and ammonium nitrate, which can be removed from the combustion gas stream by electrostatic precipitators or bag filters. This process was, originally, investigated by the Japanese Atomic Energy Research Institute (JAERI) in Takasaki, Japan in cooperation with the Ebara Corporation during the early 1970s. Initial reports of this work were published in the proceedings of the first international symposium on the treatment of wastes with ionizing radiation [106].

### 1.8.3.2. Treating municipal and industrial wastes:

Ionizing radiation effects on municipal and industrial wastes have been , extensively, investigated. The objectives include the disinfection of municipal wastewater and sewage sludge and the decomposition of toxic substances in industrial wastewater and contaminated soil [106].

Considerable efforts have been made to characterize and describe the physical and chemical properties of metal oxide nano materials because of their extensive applications in numerous technological and biological fields [107,108]. Oxides of transition metals are an important class of semiconductors that have, wide applications in magnetic storage media, solar energy transformation, electronics, and catalysis [109]. Among various transition metal oxides, copper oxide (CuO) has attracted greater attention due to its fascinating properties such as the basis of high critical temperature superconductors. CuO is a semiconducting compound with a narrow band gap and is used for photoconductive and photo-thermal applications. Copper can also be used as an antimicrobial agent, and CuO nanoparticles have been investigated previously for enhancing antibacterial properties [110]. The bactericidal property of such nanoparticles depends on their size, stability, and concentration , which provides greater retention time for bacterium nanoparticles interaction. In general, bacterial cells are in the micron-sized range. Most bacterial cells have cellular membranes that contain pores in the nanometer range. A unique property of crossing the cell membrane can potentially be attributed to synthesized nanoparticles through such bacterial pores. However, to make this possible, it is important to overcome challenges and prepare/design nanoparticles which are stable enough to significantly restrict bacterial growth while crossing the cell membrane. Furthermore,

the antibacterial activities of CuO nanoparticles against pathogenic Gram-positive bacteria, Gram-negative bacteria and fungi were investigated [110].

### 1.9. Water pollution:

The rapidly increasing population, depleting water resources, and climate change resulting in prolonged droughts and floods have rendered drinking water a competitive resource in many parts of the world. The development of cost-effective and stable materials and methods for providing the fresh water in adequate amounts is the need of the water industry. Traditional water/wastewater treatment technologies remain ineffective for providing adequate safe water due to increasing demand of water coupled with stringent health guidelines and emerging contaminants.

It is estimated that 10–20 million people die every year due to waterborne and nonfatal infection causes death of more than 200 million people every year, it is estimated that more than one billion people in the world lack access to safe water and within couple of decades the current water supply will decrease by one-third[111].

### 1.10. Pharmaceutical Water pollution:

Pharmaceutically-active compounds (PhACs) include any substance or mixture of substances manufactured, sold or represented for use in th diagnosis, treatment, mitigation or prevention of disease, disorder or abnormal physical state, or its symptoms in human beings or animals. PhACs are used, primarily, in human and veterinary applications as either medication or growth enhancing substances. Following excretion, these chemicals or their metabolites may enter the aquatic environment PhACs have been detected in soils, sediments, including sewage sludge, surface and ground water, and aquatic organisms [112].

There are several possible sources and routes for pharmaceuticals to reach the
Environment, but wastewater treatment plants have been identified as the main
Point of their collection and subsequent release into the environment, via both
effluent wastewater and sludge. Conventional systems that use an activated sludge
Process are still widely employed for wastewater treatment, mostly because they
Produce effluents that meet required quality standards (suitable for disposal or
Recycling purposes), at reasonable operating and maintenance costs [113].

**1.11. Removal of Pharmaceutical pollutants from Waste Water:**

Most treatment methods of pharmaceuticals wastewater are physicochemical and conventional biological processes. Activated carbon adsorption are frequent examples of physicochemical mechanisms .Currently there are many adsorbents developed and reported for the removal of drugs pollutants from aqueous solutions and industrial effluents .Biological wastewater treatment is one of the main important biotechnological processes in which microorganisms are applied for removal of organic contaminants and of which activated sludge Process and membrane bioreactors are the most frequently used. Most waste water treatment processes use activated sludge processes where in microorganisms are utilized to mineralize the pollutants, or degrade them to acceptable forms. Pollutants can also be eliminated from water by denudation into air or by sorption onto sludge that is regularly discharged. Membrane bioreactors (MBR) combine the biological degradation of

waste products with membrane filtration .The use of (MBR) in wastewater treatment is becoming increasingly important, since their various benefits; high biodegradation efficiency and less sludge production [114].

**(Bartelt-Hunt et al., 2009; Nilsen)**[116] **;( Vazquez-Roig et al., 2010)** [117]**.** Several studies investigated the occurrence and distribution of pharmaceuticals in soil irrigated with reclaimed water.

**(Gielen et al., 2009; Kinney, 2006)**[118]**;** soil that received biosolids from urban sewage treatment plants.

**(Carbonell et al., 2009; Lapen et al., 2008).** These studies indicated that applied wastewater treatments are not efficient enough to remove these micro-pollutants from wastewater and sludge, and as a result they find their way into the environment. Once entered the environment, pharmaceutically active compounds can produce subtle effects on aquatic and terrestrial organisms, especially on the former since they are exposed to long-term continuous influx of wastewater effluents. Several studies investigated and reported on it **(Cleuvers, 2004; Nentwig et al., 2004; Schnell et al., 2009).** [115].

**Table 1.1: Examples of potential applications of nanotechnology in water/wastewater treatment:** [111]

| **Applications** | **Examples of nonmaterial** | **Some of novel properties** |
|---|---|---|
| Adsorption | CNTs/nanoscale metal oxide and Nanofibers | High specific surface area and assessable adsorption sites, selective and more adsorption sites, short intraparticle diffusion distance, tunable surface chemistry, easy reuse, and so forth. |
| Disinfection | Nanosilver/titanium dioxide (Ag/TiO2) and CNTs | Strong antimicrobial activity, low toxicity and cost, high chemical stability ease of use, and so forth. |
| Photocatalysis | Nano-TiO2 and Fullerene derivatives | Photocatalytic activity in solar spectrum, low human toxicity, high stability and selectivity, low cost, and so forth. |
| Membranes | Nano-Ag/TiO2/Zeolites/Magnetite and CNTs | Strong antimicrobial activity, hydrophilicity low toxicity to humans, high mechanical and chemical stability, high permeability and selectivity, photocatalytic activity, and so forth. |

## 1.12. Industrial wastewater:

Many industries, such as Pharmaceutical, textile, paper, plastics and dyestuffs, consume substantial volume of water, and also use chemicals during manufacturing and dyes to color their products. As a result, they generate a considerable amount of polluted wastewater. Colors are visible pollutant and presence of even very minute amount of coloring substance makes it undesirable due to its appearance Generally, dyes are stable to light, heat and oxidizing agents, and are usually biologically non-degradable[119] .

The removal of color arising from the presence of the water-soluble reactive dyes is a major problem due to the difficulty in treating such wastewaters by conventional treatment methods. Dye wastewater is usually treated by physical or chemical treatment processes. These include flocculation combined with flotation, Electroflocculation, membrane filtration, Electrokinetic coagulation, electrochemical destruction, ion-exchange, irradiation, and precipitation, ozonation, and katox treatment method involving the use of activated carbon and air mixtures [119].

## 1.13. Eosin stain:

Eosin dyes(Figure.1.2.), and specifically the one most commonly used to counter stain hem alum is Eosin Y. Eosin Y is a pink water soluble acid dye which also displays yellow-green fluorescence. EosinY, a heterocyclic dye containing bromine atoms [120].

Eosin Y coal tar Xanthene dye, which used extensively in the drugs manufacturing, printing and dyeing industries[119], was chosen as the model anionic dye to avoid environmental hazards during investigation, as this dye is not specifically listed as toxic by different health agencies.

### 1.13.1. Eosin stains structure:

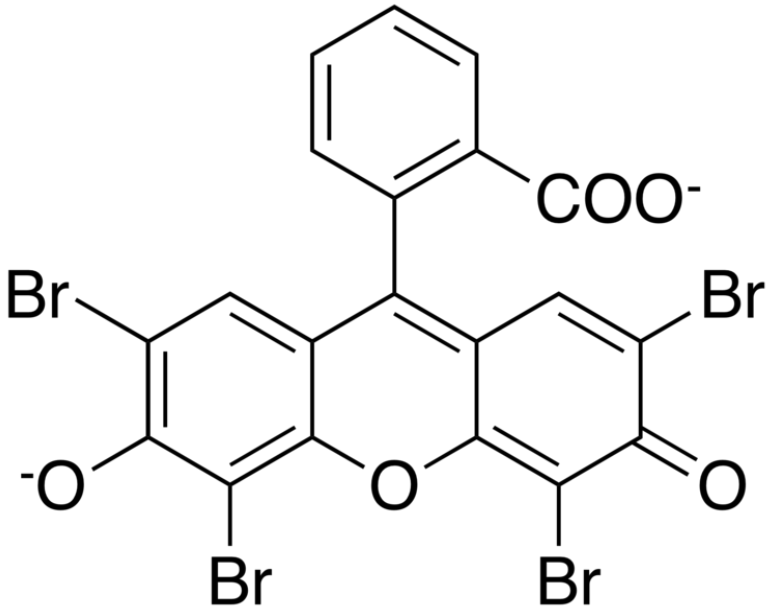


**Figure.1.2. Eosin stains structure**

# Chapter Tow
# Materials and Methods

## 2.1. Materials:

### 2.1.1. Poly (vinyl alcohol), PVA:

Poly (vinyl alcohol), (molecular weight = 450,600g.mol$^{-1}$). With an average degree of polymerization of 1750±50, was obtained from (CRC, Italy). It was in the form of crystalline powder partially hydrolyzed and used without further purification.

### 2.1.2. Gelatin, Gel:

Gelatin type (B) derived from bovine skin, with Bloom number 50-300(from the supplier), were investigated. It presents an iso-electric point between 4.7 and 6. Obtained from Scientific Fischer chemicals Company.

### 2.1.3. Copper Oxide, CuO Nanoparticles:

Copper(II)Oxide (CuO) is black powder, Nanoparticles size is 40nm, with molecular weight of 79.546 g/mol , assay > 99%, melting point 1326°C and density 6.3-6.49g/ml at 20°C obtained from MK Nano (Diven. of M K impex Corp.) Chemical Nano Company, Canada.

### 2.1.4. Citric acid:

Citric acid used in this work, is white powder ($C_6H_8O_7.H_2O$), with molecular weight of 210.14 g/mol, assay 99.5-100.5%, was obtained from PRS Panreac Co. (Spain).

### 2.1.5. Eosin dye:

Eosin yellow, also known as Acid red 87, C.I. 45,380, Bromo fluorescein; Sodium eosin, with Molecular Formula C2OH6Br4Na2O5, and molecular weight equal 691.58 g/mol. were obtained from Scientific Fischer chemicals

Company.

## 2.2. Methods:

### 2.2.1. Preparation of polymer blends of (poly vinyl alcohol)/ Gelatin (PVA/Gel) films:

Films of Poly (vinyl alcohol)/Gelatin (PVA/Gel) blends were prepared by casting solution technique. In all of the prepared samples (PVA/Gel) blends containing different ratios from the two polymers (25/75), (50/50) and (75/25) by weight were prepared as follows:

Accurate weights of PVA powder were prepared by stirring in distilled water for 15 minutes at $95^0$C until completely miscibility of PVA. Then accurate weights of Gelatin were added to PVA solution with stirring at heat temperature $95^0$C for 15minutes until complete miscibility of solution. After cooling solution 0.5ml of citric acid (0.1M) was added to the solution as plasticizer. The produced solution was, subsequently, casted onto plastic dishes to form transparent films. The films were dried under ambient conditions.

### 2.2.2. Preparation of poly (vinyl alcohol)/ Gelatin/Copper Oxide (PVA/Gelatin/CuO) films:

Different weights of Copper Oxide (0.01 and 0.1gm) were dissolved in (0.1N) Hydrochloric acid. These weights were loaded after preparation of PVA/Gelatin powder different ratios (25/75), (50/50) and (75/25) by weight in 20ml of distilled water with spontaneous stirring. The solution of PVA/Gelatin should be cooled during adding citric acid (0.1M) and Copper Oxide. The solution was then subsequently casted onto plastic

dishes to form films. The casted films were dried under ambient conditions. The (PVA/Gelatin/CuO) films have blue-greenish color.

### 2.2.3. Irradiation process:

Electron beam (EB) Irradiation was carried out in atmospheric air at ambient temperature using 1.5 MeV and 25 Kw electron beam accelerator. All specimens were irradiated on one side using a current of 10 mA and scan width variable up to 90 cm. the polymeric samples were exposed to an irradiation dose of about 5 KGY each pass. Several passes under these conditions were required for high irradiation doses. The irradiation doses are ranged throughout this work from 2 to 5 KGY.

### 2.3.1. Measurements and Analysis:

### 2.3.1.1. Swelling Studies:

Swelling study was conducted on (PVA/Gelatin) and synthesis nanocomposite films of (PVA/Gelatin/CuO) as a function of time in which a dry weight of insoluble polymer blend of (PVA/Gelatin) and nanocomposite film of (PVA/Gelatin/CuO) ($W_1$) was immersed in distilled water and different PH values(4-10) , at $25^0$C for different intervals of time durations up to 24h. after each time interval, the sample was withdrawn and blotted on filter paper to remove excess water and weighed ($W_t$), in which the degree of swelling is calculated according to the following equation:

$$\textbf{Degree of swelling (\%)} = [(W_t - W_1)/ W_1] \times 100$$

Where: $W_t$ (is the wet weight after degrading for a predetermined time). $W_0$ (is the original weight of the sample).

### 2.3.1.2. Structure Morphology by SEM:

The scanning electron microscope (SEM) JEOL-JSM-5500 LV (Japan) was employed to examine the structure morphology of (PVA/Gelatin) blend and nanocomposite polymer blend films of (PVA/Gelatin/CuO) before and after irradiation. The blend samples were kept in liquid nitrogen for enough time prior to fracture. A sputter coater was used to pre-coat, conductive, gold onto the fracture surfaces before observing the microstructure.

### 2.3.1.3. Spectroscopic analysis:

#### 2.3.1.3.1. Fourier transform infrared spectrometry, (FTIR):

Fourier transform infrared spectrometry (FTIR-6300)-Japan, was used for scanning and measuring the absorption spectra at resolution 4 $cm^{-1}$, high signal to noise spectra were obtained by collection of one hundred scans for each sample. The spectra of unirradiated and irradiated samples were measured using a designed holder for sample of 2x2 cm dimension, over the range: 400 – 4000 $cm^{-1}$ . From the spectra and the change in absorbance,( peak intensity) at the characteristic peak wave number, ($cm^{-1}$) were recorded.

#### 2.3.1.3.2.Ultravilote/visible spectroscopy,(UV/VIS):

Ultravilote/visible spectroscopy, (UV/VIS) spectrometer (Jasco/v-560 Japan). Was used for scanning the absorption spectra in the range 100 nm to 900 nm and measuring the optical density for unirradiated, irradiated samples.

#### 2.3.1.3.4. X-ray diffraction (XRD):

X-ray diffraction is an important tool used to identify phases by comparison with data from known structures, quantify changes in the cell parameters, orientation, crystallite size and other structural parameters. It is also used to determine the (crystallographic) structure (i.e. cell parameters, space group and atomic coordinates) of novel or unknown crystalline materials. This carried out by using Shimadzu X-ray diffractometer (XRD-6000)-Japan, using Cu-K. The spectra were obtained for structure analysis of the samples.

# Chapter Three
# Results and discussion
# CHARACTERIZATION OF UNIRRADIATED AND IRRADIATED POLYMER BLEND

## 3.1. Swelling degree:

Increasing demand for highly absorbing materials in recent years indicates that this subject will be the topic of extensive research work in future. This because their applications cover a wide range of uses, in particular in the medical and pharmaceutical fields and as diapers or pads for surgical operations [(121)]. Polymer networks are formed through the chemical and/or physical cross-linking of polymer chains. These materials represent an important class of polymer matrices for polymer Nanocomposites since they are used in numerous structural applications due to their long-term resistance to mechanical loads, elasticity, and temperature resistant attributes. The most commonly used polymer networks include epoxies, polyurethanes, and thermoplastic elastomers. In many ways, the presence of Nanoparticles in a polymer matrices. The Nanoparticles can influence the development of local network structure during polymerization and cross-linking reactions, and the excluded volume of the Nanoparticles can impact the local dynamics of chains between cross-links [(122)].

There are many different ways of cross-linking: irradiation using ultraviolet rays, X-ray photons, ions, electron-beam or R-particles, or due to a chemical cross-linker. Irrespective of the method of cross-linking, some fraction of the polymer remains unattached to the network and/or gets detached by the cross-linking process (e.g., chain scission during radiation). The network content of the polymer is called the "gel fraction", and the fraction of loose macromolecules (sol macromolecules)

is called the "sol fraction". In some cases, this sol fraction is large and its influence becomes important [122].

A cross-linked polymer hydrogels swell but not dissolve when water or a solvent enters it. The swelling properties, which usually use degree of swelling to define hydrogels, depend on many factors such as network density, solvent nature, polymer solvent interaction parameter [123].

The swelling degree of the sample was characterized at room temperature $25^0$C for which rounded samples with 1cm diameter were placed in de-ionized water. The swelling character of polymer blend of (PVA/Gelatin) film in different pH was also studied. The experiments were carried out by measuring the weight gain as a function of immersion time in 10 ml water. The swelling degree was calculated by using the following equation:

Water absorption was conducted to characterize the swelling degree state of PVA/Gelatin blend ratios before and after irradiation for different ratios.

### 3.1.1.Swelling of unirradiated polymer blend of (PVA/Gelatin):

The swelling behavior of unirradiated polymer blend of (PVA/Gelatin) film for different ratios were investigated and reported as swelling degree percentage. The observed studied polymer blend ratios were (25/75), (50/50) and (75/25) of PVA/Gelatin. The selected ratio was studied for 24 h., through immersing in de-ionized water and with different solution of pH (4) and pH (10).

Figure(3-1to3-3) showing the swelling degree percentages of unirradiated polymer blend of (PVA/Gelatin) film for different ratios in

de-ionized water and with different solution of pH(4) and pH(10). The obtained results were found that swelling degree percentages were found to be increases gradually by increasing time until to reach saturation level.

It was observed From Figure(3.1), that the unirradiated polymer blend of (PVA/Gelatin) film of the studied ratios (25/75) , (50/50) and (75/25) showed higher swelling degree percentages (%) after different times of immersion in de-ionized water. The higher swelling degree percentage (%)550% was presented after 6h for the studied polymer blend ratio (75/25) while, the unirradiated ratio (50/50) gives 300% at 4h. The highest swelling degree percentage (%) was appeared after 2hrs for the ratio (25/75) was 244%. Then the swelling degree percentages (%) decrease slightly by increasing time of immersion of studied ratio in de-ionized water.

Where after 8h of immersion the swelling degree percentages (%) of unirradiated film ratios (75/25) start to decrease gradually to be (425%). The ability of presented blend ratio(50/50) and (25/75) for swelling degree percentages began to decrease at different values of time respectively after 6 and 4hr of dipping in ionized water. Swelling degree percentages (%) of the obtained ratios (50/50) and (25/75) were 230% and 180% after 6 and 4hr., respectively.

The values of the swelling degree percentages showed that the studied blend film ratio had water retention capability. The reason of higher swelling degree percentages (%) for the unirradiated PVA/Gelatin blend of (75/25) ratio film sample might be due to free amino groups in Gelatin and hydroxyl group which plays an important role in water uptake because of their hydrophilic nature [124]. Also the Polyvinyl alcohol (PVA) is hydrophilic polymer with unique properties leading to

more uptake percentage. It absorbs water, swells easily and it has been used in controlled resale application [125].

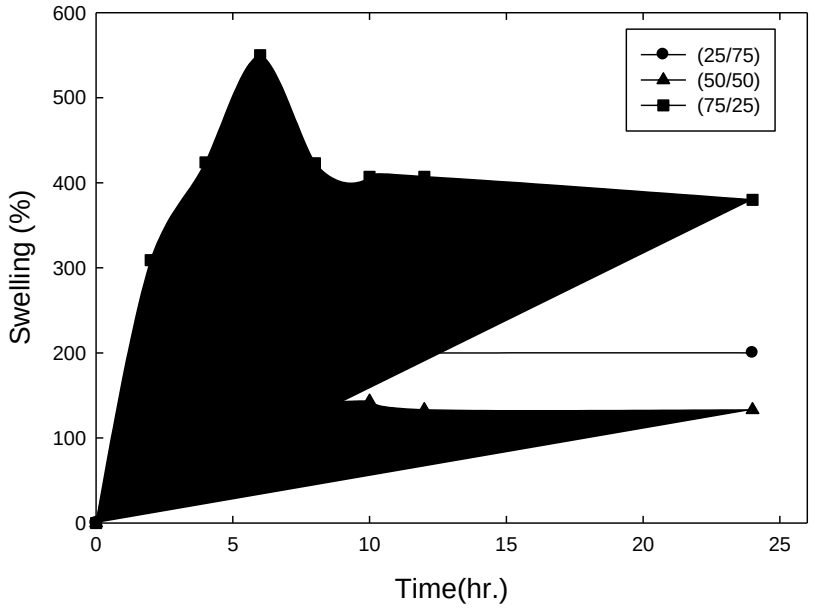


**Figure .3.1.** swelling degree for PVA/ Gelatin polymer blends distilled water.

Figure (3-2) showing the effect of different of pH values (4) and (10) on the swelling degree percentages (%) for unirradiated polymer blend ratios (25/75) , (50/50) and (75/25).

From these Figures, it is clear that the swelling degree percentage (%) gradually increases with increasing pH value and time. At lower pH value (4) different two maximum values of swelling degree percentages (%) were observed for the studied unirradiated ratios (75/25) and (25/75) after 4h., were 500% and 350% respectively. The studied unirradiated ratio (50/50) showed lower swelling degree percentages (%) after 4hr., was 194%. Then swelling degree percentages start to decrease after 8hr., of immersion.

Degradability was found to be absent in case of unirradiated ratio (25/75) , (50/50) and (75/25) which it might be due to the higher

hydrophilic character of PVA and gelatin and also, due to uses of citric acid as cross-linking between the used polymer matrix.

However, under pH 6.4, or in a certain pH range, (4-7) , the majority of the base and acid groups are as $NH^{+3}$ and $COO^{-}$ or $NH_2$ and COOH forms, and therefore ionic interaction of $NH^{+}$ and $COO^{-}$ species (ionic cross-linking) or hydrogen bonding between amine and carboxylic acid (and probably carboxamide groups) may lead to a kind of cross-linking followed by decreased swelling [126].

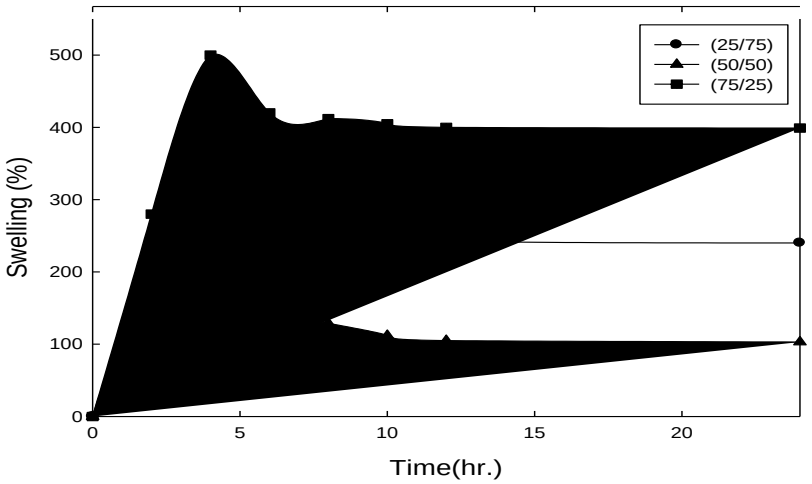


**Figure.3.2.** swelling test of Unirradiated PVA/ Gelatin polymer blends at pH (4).

In presence of higher pH value (10) as shown in Figure (3-3), there are three higher values of swelling degree percentages (%) presented in the following order: (75/25) > (25/75) > (50/50) where, the swelling degree percentages (%) were 700% , 560% and 450% after 6hr for the unirradiated ratios(75/25) , (25/75) and at 4hr for the studied ratio(50/50) respectively. Degradation process has been disappeared for the three studied ratios (25/75) (50/50) and (75/25) at pH value (10).

When the ionic strength of the solution is increased, the deference in osmotic pressure between the polymer blend and the medium is decreased. Thus the swelling capacity of the polymer blend is decreased [126].

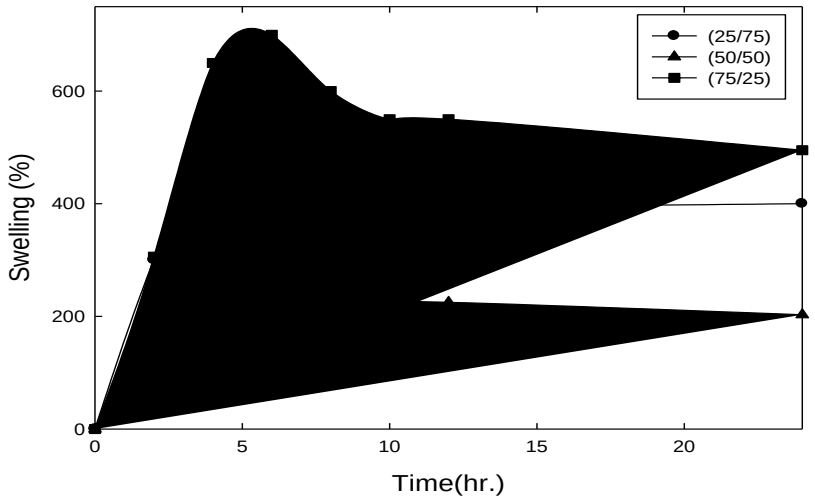


**Figure.3.3.**swelling test for PVA/ Gelatin polymer blends Unirradiated at pH (10)

Swellings of the PVA/Gelatin were dependent on their gelatin proportions. As the proportion of gelatin decreased, there was a significant increase in the swelling ratio. This may be attributed to the higher proportions of gel fraction of gelatin present in the samples. It may be estimated from the swelling studies that the rate of release of the drugs dissolved in the oil phase may be higher for the samples with higher water content. Water content in the gels increases for the samples with high swelling ratio due to the increased amount of gelatin. This may be accounted to the partition coefficient effect, which states that the solute distributes itself amongst the two immiscible liquids in a definite concentration ratio [127,128,129]. The gels were able to maintain their structural integrity even after 8 h of study, though there was some

alteration in their texture. This might facilitate the usage of the emulsion hydrogels (EHs) as implantable delivery devices [130].

The cross-linking yield of unirradiated polymer blends modified by adding citric acid as cross-linker, Citric acid (CA) with one hydroxyl and three carboxyl groups exists widely in citrus fruits and pineapples, where it is the main organic acid. Citric acid was chosen as the additive for the following reasons. First of all, as a result of its multi-carboxylic structure, esterification could take place between the carboxyl groups on citric acid and the hydroxyl groups on the PVA. Such an esterification would improve the water resistibility [131]. Furthermore, because of the multi-carboxyl structure, citric acid may serve as a cross-linking agent. Cross-linking of a blend reinforces the intermolecular binding by introducing covalent bonds that supplement natural intermolecular hydrogen bonds [132] so as to improve the mechanical properties and water resistibility. As compared to the hydroxyl groups on glycerol(in case of using glycerol as cross-linker), the carboxyl groups on citric acid can thus form stronger hydrogen bonds with the hydroxyl groups on PVA/gelatin blends, thus improving the interactions between the molecules [133].

The third point, citric acid is rated as nutritionally harmless since it is a nontoxic metabolic product of the body (Krebs or citric acid cycle).Consequently; it has already been approved by FDA for use in humans [134].

Although Yoon and co-workers also used citric acid as the additive to prepare PS films as the plasticizers [135], they selected 50$^{o}$C as the molding temperature. The esterification will not occur in the blending system under such a low temperature. A series of structural and physical properties changes result from the esterification which need a high

temperature. The water absorption capacity and the degradability are the most important properties for biodegradable materials. It was reported that the water absorption acquired equilibrium in 12 hrs [136] so we selected 24 hrs, which is longer than equilibrium time as the observing time.

### 3.1.2.Swelling of (PVA/Gelatin)irradiated polymer blend:

Swelling behavior of the irradiated polymer blends (PVA/Gelatin) at irradiation dose (5KGy) was investigated to evaluate their capacity to absorb water and simulate their degradation time in the presence of radiation.

Figures (3-4to3-6) shows the effect of irradiated polymer blend ratios (25/75), (50/50) and (75/25) of (PVA/Gelatin) in de-ionized water and in solution of pH (4), pH (10) at the applied dose (5KGy). The same behavior was observed in the studied irradiated polymer blend ratios dipping in de-ionized water and with solution of pH (4).

The swelling degree percentages of irradiated polymer blend ratios (25/75), (50/50) and (75/25) of (PVA/Gelatin) at the applied dose 5KGy of gamma irradiation was found to be gradually increase with increases time until to reach equilibrium time. Also, results show variation of maximum swelling degree percentages of studied ratios.

**Figure.3.4.**shows The maximum values of swelling degree percentages of irradiated polymer blend ratios (25/75), and (75/25) at the applied dose (5KGy) in de-ionized water are (650%, 850%) respectively were presented after 6hrs, while it was (360%) for the ratio (50/50) after 4hrs of dipping, then, the obtained swelling percentages began to decrease after 6hr of dipping.

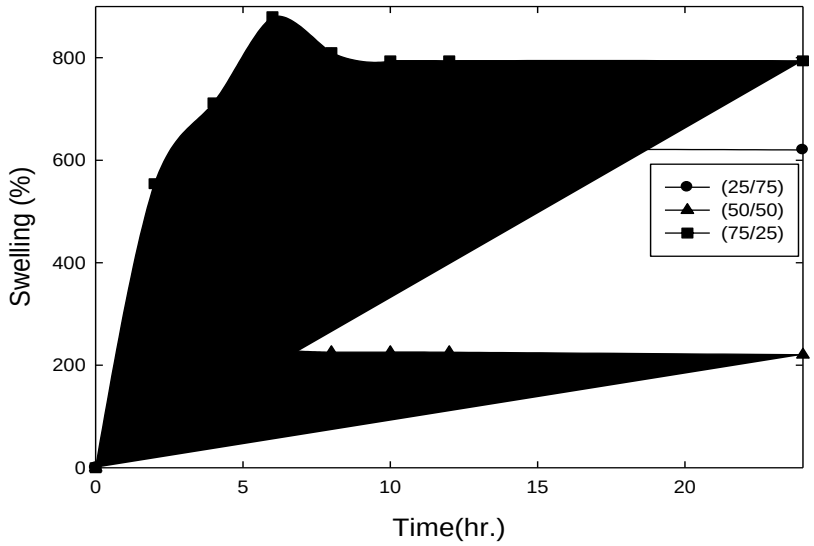


**Figure.3.4.**Swelling test for PVA/ Gelatin irradiated 5kGy in Water

Figure.3.5.shows the swelling behavior at pH(4) for the irradiated polymer blends(PVA/gelatin) different ratios(25/75, 50/50, 75/25) when gamma irradiation dose (5KGy) was applied, the highest values of swelling degree percentages were (350%, 155% and 500%) respectively observed after 4hrs of immersion in pH (4) solution.

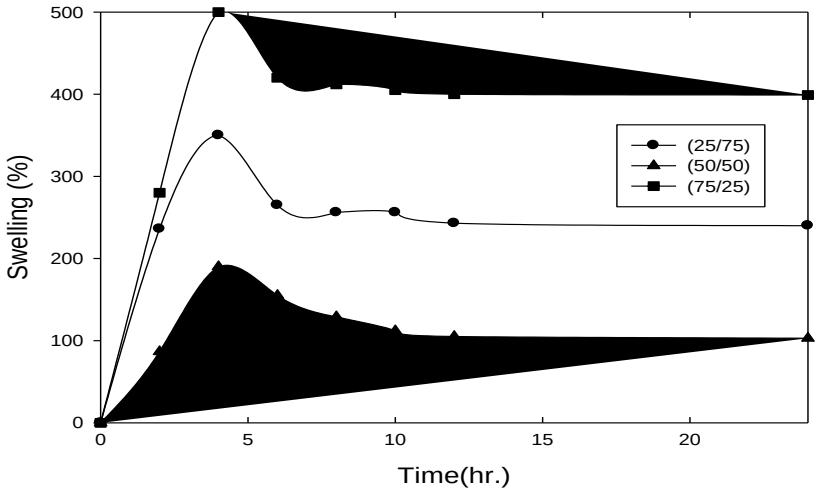


**Figure.3.5.**Swelling test for PVA/ Gelatin irradiated 5kGy in pH (4).

Figure.3.6. illustrated the effect of gamma irradiation dose 5KGy on swelling degree percentages of irradiated polymer blend ratios (25/75), (50/50) and (75/25) of (PVA/Gelatin) when it was dipped in pH (10).

The observed results showed that the irradiated ratio polymer blend ratios (25/75), (50/50) and (75/25) at 5KGy gives a maximum swelling degree after (6hr) of dipping in solution of pH(10) about (460% , 580% and 700%), while, the swelling degree gradually increases with increasing time until the obtained 8hr of saturation level.

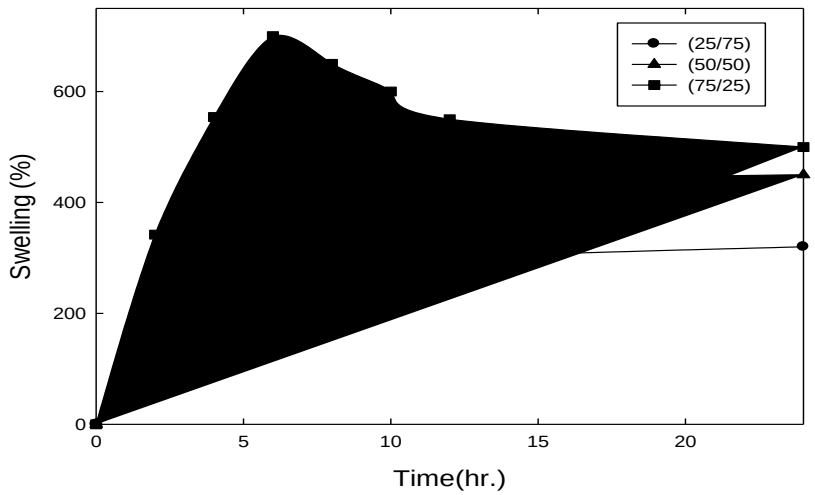


**Figure.3.6.**Swelling test for PVA/ Gelatin irradiated 5kGy in pH (10)

Generally, it was found that the swelling degree decrease as the esterification and crosslink degree increased [131,136].

Cross-linking and chain scission occurred when polymers were exposed to gamma irradiation. Polysaccharides and other natural polymers generally degrade by breaking the glycosidic linkage under gamma radiation [137].

It is reported in the literature that PVA and Gelatin molecules form free radicals when irradiation is caused by a gamma source. Gelatin is a natural biopolymer that consists of protein molecules and can easily

fragment due to gamma irradiation. The exposure of gamma irradiation produces the free radicals due to the chain scission of the gelatin molecules. The generated free radicals may crosslink each other and form more cross-linked sites with the exposure of gamma irradiation; as a result, mechanical properties might be increased [137].

Higher gamma radiation might have caused degradation of the polymer and the film became hard and brittle while at lower doses cross-linking might have dominated over chain seasoning. When the (PVA/ gelatin)film is subjected to the irradiation, the hydroxyl group from PVA and gelatin radicals is initiated to form a cross linked network [137].

## 3.2. FTIR characterization:

Infrared spectra of the polymer blend of (PVA/Gelatin) for different ratios samples were investigated. Infrared spectroscopy has been carried out to further characterize the composition of the polymer blend as-prepared samples. It has also run to study the effect of different doses of gamma radiation on the characteristic functional groups of the prepared film samples.

### 3.2.1. Infrared spectra of unirradiated polymer blend of (PVA/Gelatin) film:

The FTIR spectrum for synthetic unirradiated polymer blends of (PVA/Gelatin) were investigated for different ratios and the frequencies of the absorption bands together with their structural assignments are listed in Figure.3.7. and table .3.1shows The studied of unirradiated ratios of (25/75), (50/50) and (75/25) of (PVA/Gelatin) film. The characteristic absorption peaks in the wavelength ranging 4000-400 $cm^{-1}$ are: The O-H stretching band in the IR spectrum is by far the most characteristic feature

of alcohols and phenols. The unirradiated polymer blend (25/75) of (PVA/Gelatin) film has been showing in( Figure.3.7.A), spectrum gave very broad and strong band centered at 3600cm$^{-1}$ as the stretching vibration of hydroxyl group with strong hydrogen bonding as intra- and/or intertype [126,133,134] this band also indicating the presence of hydroxyl group with polymeric association and a secondary amide. Also this broad band is overlaps the N—H stretching in the same region [135]. A weak band appeared at 2300cm$^{-1}$ is the characteristic bands of symmetric C—H stretching .C, C triple bond band are appeared at 2132.88 cm$^{-1}$. The stretching vibration bands of carboxylate anion $COO^-$ showed at 1708.62 cm$^{-1}$, indicating the esterification of polymer blend of (PVA/Gelatin) film [136].weak band O—H wagging was found at 650cm$^{-1}$ [126].

FTIR spectrum for selected unirradiated polymer blend ratio (50/50) of (PVA/Gelatin) film is shown in (Figure.3.7.B) too. The O–H stretching band in the IR spectrum of unirradiated polymer blend ratio (50/50) of (PVA/Gelatin) film is centered and observed at 3637.94 cm$^{-1}$. The band at 2360.44 cm$^{-1}$ was indicating O—H stretching of hydroxyl group. Symmetric C—H stretching band is present at 2321.87 cm$^{-1}$. A weak band is observed at 2136.74 cm$^{-1}$ and has been assigned to the combination frequency of (CH=+CC) this is identical to study found by **LINGA et al., (2007)** [138]. The peak at 1729.97 cm$^{-1}$ in the unirradiated polymer blend ratio (50/50) of (PVA/Gelatin) film spectrum can be assigned to C=O stretching vibration peak. This band caused by the ester bond and carboxyl group in citric acid as the study produced by **Rui et al., (2008)** [139]. Two peaks are presented at 1655.64-1450.07 cm$^{-1}$ assigned to $NH_2$ bending vibration and Amide (III) respectively which they are the characteristic bands of gelatin [140]. Sharp signal at 1097.18

$cm^{-1}$ is due to C—O—C stretching vibrations were observed. This band is recognized as crystallization sensitive band, [141,142,143].

FTIR spectrum for unirradiated polymer blend ratio (50/50) of (PVA/Gelatin) film is also shown in (Figure.3.7.C) too. From this figure there are different characteristic peaks were observed in the wavelength ranging 4000-400 $cm^{-1}$ such as: 3630$cm^{-1}$ (OH centered stretching broad band), 2370.09 $cm^{-1}$(OH stretching), A weak peak presented at 2324.73 assigned to Symmetric C—H stretching band. A Combination frequency of (CH+CC) observed at 2172.59 $cm^{-1}$ according to study by **LINGA et al., (2007)** [138]. Carbonyl group C=O was present at 1752.65 $cm^{-1}$ as sharp band. C-O-C finger print was appeared at 550$cm^{-1}$ [139].

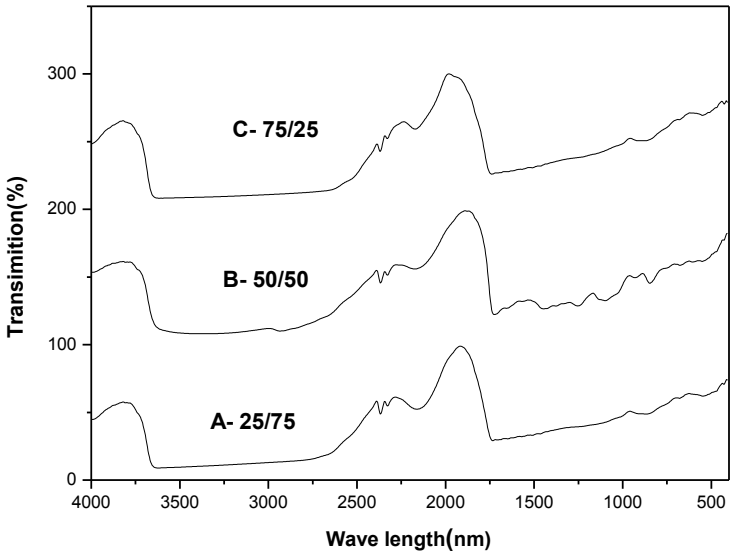


**Figure.3.7.** FTIR of(PVA/gelatin) polymer blend different ratios un irradiated

**Table 3.1.The Assignment of FTIR Spectra of Absorption Bands Polymer blend film of (PVA/Gelatin).**

| **Band position,$Cm^{-1}$** | **Assignment** |
|---|---|
| 3340.1 $cm^{-1}$ | O—H stretching vibration |
| 3340.1 $cm^{-1}$ | N—H stretching |
| 2908.13 $cm^{-1}$ | $CH_2$ symmetric stretching |
| 2321.87 $cm^{-1}$ | C—H symmetric stretching |
| 2149.16 $Cm^{-1}$ | combination frequency of (CH+CC) |
| 2132.88 $cm^{-1}$ | C,C triple bond |
| 2136.74 $cm^{-1}$ | combination frequency of (CH=+CC) |
| 1708.62 $cm^{-1}$ | C=O Stretching |
| 1455.64-1250.07 $cm^{-1}$ | $NH_2$ bending vibration |
| 936.96 $cm^{-1}$ | $CH_2$ rocking |
| 860.88 $cm^{-1}$ | C-C stretching vibration |
| 677.99 $cm^{-1}$ | O—H wagging |
| 541.19 $cm^{-1}$ | C-O-C finger print |

## 3.2.2. Infrared spectra of irradiated polymer blend of (PVA/Gelatin) film:

Infrared spectral analysis monitors the vibrational energy levels in the region of different molecules. The IR spectra for the irradiated polymer blend ratios (25/75), (50/50) and (75/25) of (PVA/Gelatin) through Gamma radiation with (5KGy) dose is shown in Figures (8-3) and Table (1). From the FTIR spectra of irradiated polymer blend ratio (25/75) of (PVA/Gelatin) in Figure.3.8. at 5KGy , we can conclude that the produced film had an ester linkage and secondary alcoholic group. Further, the FTIR results suggest a complete esterification of the of the carboxylic acid of gelatin. This is consistent to study reported by **Dharmendra et al., (2011)** [145].

The FTIR-spectra of irradiated polymer blend ratio (25/75) of (PVA/Gelatin) at (5KGy) in comparison with the FTIR spectrum for unirradiated (25/75) blend of PVA/Gelatin Figure.3.8. shows different remarkable changes were notice .Firstly is the feature in the centered O-H stretching becomes more broad and strong band after radiated at (5KGy) of gamma radiation. Secondly, the intensity of the two bands at 2360.44 and 2321.87 $cm^{-1}$ in unirradiated 25/75 blend of PVA/Gelatin increases at the studied radiation dose (5KGy). It becomes 2370.09 and 2332.05 $cm^{-1}$ which are indicating for O-H stretching and symmetric C-H stretching respectively [126].

Thirdly, the intensity of C,C triple bond stretching band is increasing after radiation and shifted to becomes 2171.83 $cm^{-1}$. Fourthly the peak of stretching vibrational of C=O which appeared at 1708.62 $cm^{-1}$ were found to be positively changed after radiation and it's also shifted to the higher side of the spectrum. This also indicating that all carboxyl groups are esterified [146].

This phenomena demonstrates that the esterification occurred between citric acid and Gelatin as well as between citric acid and polyvinyl

alcohol. Also the esterification occurred more easily between Gelatin and citric acid than that between polyvinyl alcohol and citric acid [139].

The effect of (5KGy) of gamma radiation on the FTIR spectra of the studied irradiated polymer blend ratio (50/50) of (PVA/Gelatin) film is shown in Figure (3-7). As it can be noticed in this figure that O—H stretching centered band becomes more boarders and strong and shifted to be 3345.26 $cm^{-1}$. $CH_2$ symmetric stretching band at 2908.13 $cm^{-1}$ was absent. The band at 2360.44 $cm^{-1}$ after radiation is increase and becomes stronger at 2370.09 $cm^{-1}$ assigned to O–H stretching band.

The symmetric C—H stretching band which present at 2321.87 $cm^{-1}$ were disappeared after radiation. The weak band which observed at 2136.74 $cm^{-1}$ has been increases and shifted to becomes 2171.83 $cm^{-1}$ due to the combination frequency of (CH=+CC) according to **LINGA et al., (2007)** [138].

Strong broad band was present at 1745.34 $cm^{-1}$ reason to carbonyl group C=O. A weak band was appearing at 922.53 $cm^{-1}$ assigned to $CH_2$ rocking,, While C—H stretching was found at 853.56 $cm^{-1}$ . 686.03 $cm^{-1}$ band is observed assigned to O—H wagging [126]. The band at 563.86 $cm^{-1}$ arises from C-O-C finger print [144].

The FTIR spectra of irradiated polymer blend (75/25) of (PVA/Gelatin) at the applied dose (5KGy) shown in Figure.3.8. with comparison of unirradiated polymer blend ratio (75/25) of (PVA/Gelatin) spectra the following data are appeared. There is no change in peaks observed in the wavelength ranging 3330.62 -868.92 $cm^{-1}$. The band at 556.55 $cm^{-1}$ was shifted and decrease to 541.92 $cm^{-1}$ assigned to C-O-C finger print [144].

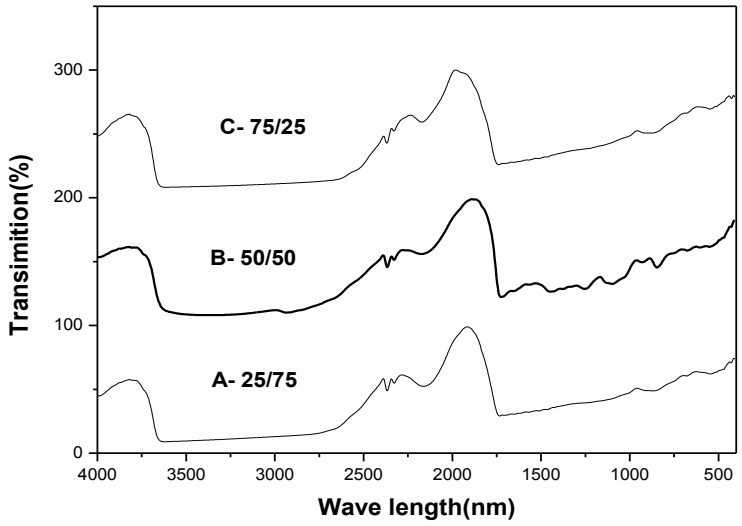


**Figure.3.8.** FTIR PVA/gelatin polymer blend different ratios irradiated 5KGy

# 3.3. Ultraviolet/visible spectroscopy,(UV/VIS):

## 3.3.1. Ultraviolet (visible absorption spectroscopic studies):

Optical properties of materials are very sensitive to the transition from bulk materials to low dimension systems. The good conductor particles are well known to exhibit a strong change of their optical properties. The ultraviolet/visible spectroscopy,(UV/VIS) spectra to different ratio of polymer blend of (PVA/Gelatin) at unirradiated state and with (5KGy) dose of gamma radiation were investigated. The synthesis polymer blend ratios were (25/75),(50/50) and (75/25) of (PVA/Gelatin).

### 3.3.1.1. UV/VIS spectra of unirradiated polymer blend of (PVA/Gelatin) films:

Figure.3.9. displays the UV/VIS spectra of studied unirradiated polymer blend for different ratios of (PVA/Gelatin).

The UV/VIS spectra of unirradiated polymer blend ratio (25/75) of (PVA/Gelatin) an absorption band in the range of 300-320 nm can be seen. Also another band was observed in the range 250-270 nm. The obtained absorption band at (300 nm) can be attributed to the high energy absorption in the UV region and may assigned to II—II* transition which comes from unsaturated bands, mainly C=O and or C—C, which are present in the tail-head of the polymer matrix [147].

The sharp absorption edge around 250 nm indicates the semi-crystalline nature of PVA according to **Elashmawi et al., (2009)** [148]. Also the band observed at 244 nm Can be attributed to amino acids in gelatin which assigned to II—II* transition [149].

The UV/VIS spectra of unirradiated polymer blend ratio(50/50) of (PVA/Gelatin) where, an absorption band in the range 290-300 nm were observed. This band may assigned to II—II* transition due to unsaturated bands, mainly C—O and or C—C, which are present in the tail-head of the polymer matrix [147]. The UV/VIS spectra of unirradiated polymer blend ratio (75/25) of (PVA/Gelatin) were illustrated in Figure.3.9. An absorption band in the range 300-350 nm can be seen. Also another band was observed in the range 240-250 nm. The obtained absorption band at (300 nm) can be attributed to the high energy absorption in the UV region and may assigned to II—II* transition which comes from unsaturated bands, mainly C=O and or C—C, which are present in the tail-head of the polymer matrix [147]. The sharp absorption edge around 244 nm indicates the semi-crystalline nature of PVA according to **Elashmawi et al., (2009)** [148]. Also the band observed at 244 nm Can be attributed to amino acids in gelatin which assigned to II—II* transition [149].

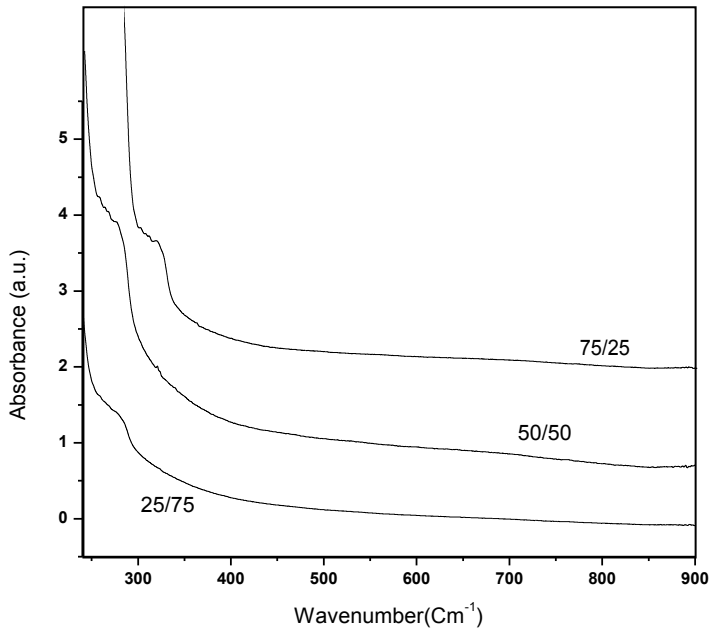


**Figure.3.9.** UV/VIS. for Unirradiated polymer blends different ratios

### 3.3.1.2. UV/VIS spectra of irradiated polymer blend of (PVA/Gelatin) films:

The UV/VIS spectra of irradiated polymer blend different ratios of (PVA/Gelatin) with (5KGy) dose of gamma radiation are observed in Figure.3.10. The UV/VIS spectra of irradiated polymer blend ratio (25/75) of (PVA/Gelatin) at 5KGy dose of gamma radiation illustrated in Figure.3.10. According to this figure, the absorption band presented at (290 nm) increased after radiation and becoming (293 nm)**,** this consistent to **Abd El-kader et al., (2000)** [147]. Also, the intensity of the peak observed at (244 nm) shifted with increasing to becomes (245 nm) according to **Elashmawi et al., (2009)** [148]. Spectra of irradiated polymer blend ratio (50/50) of (PVA/Gelatin) at the selected dose (5KGy) of gamma radiation. The observed band at (290nm) shifted and increasing after radiation to be (293.88nm).

Figure.3.10. also performed the UV/VIS spectra of irradiated polymer blend ratio (75/25) of (PVA/Gelatin) at the selected dose 5KGy of gamma radiation. From this Figure, the absorption band presented at (290 nm) is shifted after radiation and becoming (292 nm). Also, the intensity peak observed at (244 nm) shifted to lower wave length and becomes (238 nm).

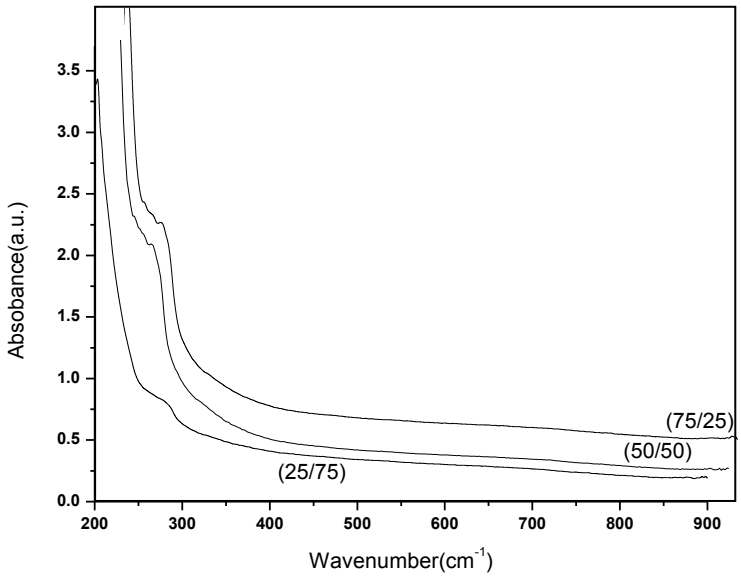


**Figure.3.10.** UV/VIS of polymer blends irradiated (5KGy).

## 3.4. Morphology:

### 3.4.1. Scanning electron microscopy(SEM):

Scanning electron microscope is a type of microscope that uses high-energy beam of electrons instead of light to scan surface of a relatively thick sample. Scanning electron microscope has a resolution of 1 to10 nm. SEM images can be used to study the surface morphology of a

material. A smooth surface can be distinguished from a rough surface by visual inspection. Comparatively larger (~1 µm) aggregates of Nanoparticles at the surface can be observed in the SEM image. SEM images can be used as a quick method to study the formation of polymer blend structure [150].

In order to obtain information about the external shape, microstructure of polymer blend of (PVA/Gelatin) synthesized by casting method, different films ratios of (PVA/Gelatin) were analyzed by Scanning electron microscope (SEM). Also, the effect of (5KGy) doses of gamma irradiation on morphology of the prepared films was studied by using scanning electron microscope (SEM). The scanning electron microscope (SEM) recorded for polymer blend of (PVA/Gelatin) before and after irradiation was displayed in the following data.

### 3.4.1.1. Scanning electron microscopy of unirradiated polymer blend of (PVA/Gelatin) film:

The morphology of the polymer blend film of (PVA/Gelatin) before and after irradiation was investigated by Scanning electron microscope are been shown in Figures (3.11), (3.12), (3.13), (3.14) (3.15) and (3.16).

Figure.3.11. is presents cross-sectional images of studied unirradiated polymer blend film ratio (25/75) of (PVA/Gelatin) before irradiation. It is clear from images that the yield polymer blend film is homogeneous with a regular in the surface. This may be due to the high ratio of gelatin than PVA in polymer matrix of blend, also, homogeneity produced cause of miscibility of polymer blend film of (PVA/Gelatin) through cross-linking by citric acid as plasticizer.

The scanning electron micrographs of unirradiated polymer blend film ratio (50/50) of (PVA/Gelatin) as illustrated in Figure.3.12. From this figure, it was obvious that the upper surface and cross-section of the

studied polymer blend showed homogeneity between the two miscible of PVA and Gelatin phases. The surfaces of the blend films were also rough phase may be due to the two equal percentage of polymer matrix in unirradiated polymer blend film ratio (50/50) of (PVA/Gelatin).

The scanning electron microscope (SEM) images for unirradiated polymer blend film ratio (75/25) of (PVA/Gelatin) are presented in Figure Figure.3.13. The scanning electron micrographs of unirradiated polymer blend film ratio (75/25) of (PVA/Gelatin) shows relatively smooth and homogeneous surface with very sparsely distributed small particles without any phase separation. The homogeneity of the unirradiated polymer blend film ratio (75/25) may be due to the heights ratio of PVA than Gelatin in polymer matrix in presence of citric acid. The regular dots might be due to Gelatin ratio with the heights ratio of PVA in the observed blend. This is consistent to **Mohammad et al., (2012)** [151].

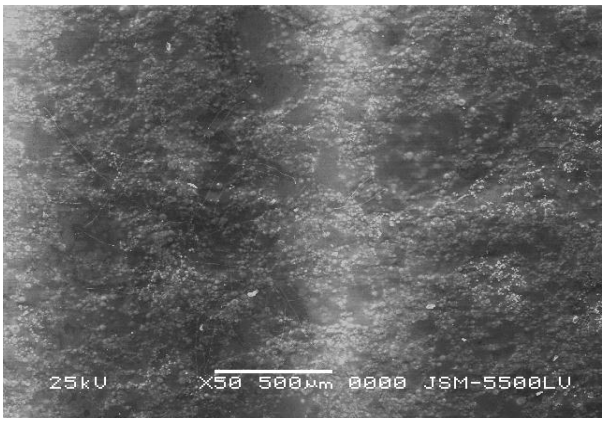


**Fig3.11.**PVA/gelatin Polymer blend 25/75 Unirradiated

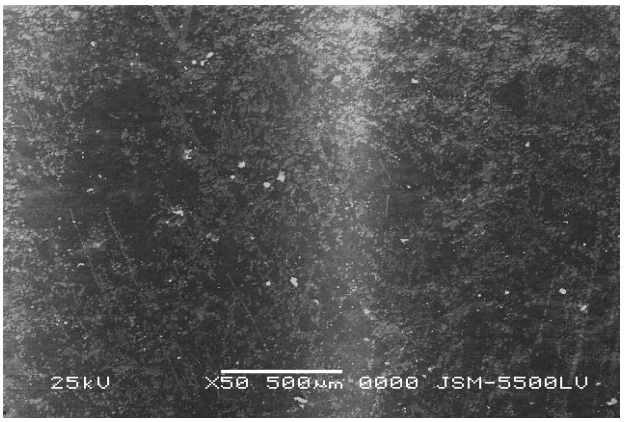


**Fig3.12.**PVA/gelatin Polymer blend 50/50 Unirradiated

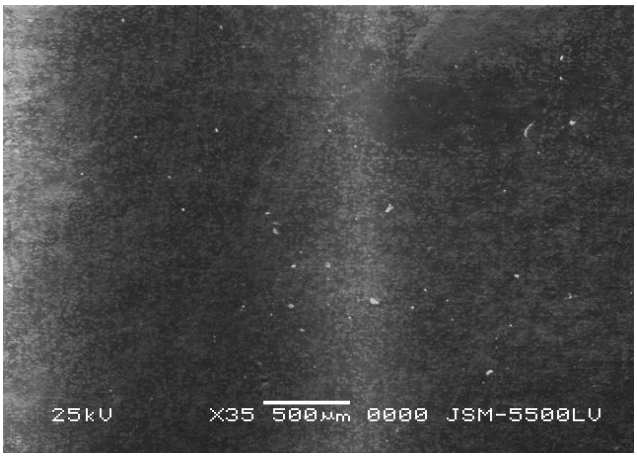


**Fig3.13.**PVA/gelatin Polymer blend
75/25 Unirradiated

### 3.4.1.2. Scanning electron microscopy of irradiated polymer blend of (PVA/Gelatin) film:

The effect of gamma irradiation dose (5KGy) on the selected polymer blend film ratio (25/75) of (PVA/Gelatin) is observed in Figure .3.14.

This Figure shows feature films matrix with smooth surfaces. The observed surface after the irradiation dose (5KGy) becomes more regular and more homogeneity. This indicates that homogeneity and smoothing increases by applying the dose of gamma irradiation. In addition, cross-linking was increasing after irradiation due to presence the binder (citric acid) between the two miscible polymer in the surface of observing irradiation polymer blend ratio (25/75) of (PVA/Gelatin) as seen in Figure .3.14. This is similar to study of (Chitosan/PVA) [152].

The effect of gamma irradiation (5KGy) on the studied polymer blend film ratio of (50/50) of (PVA/Gelatin) has been demonstrated in Figure .3.15. The observed images presented regular and more homogeneous surfaces. Also, images pointed out that the PVA micro

domains were dispersed within the Gelatin matrix in the polymer blend film of (PVA/Gelatin) with relatively good interfacial adhesion between the two components in the selected irradiated polymer blend ratio (50/50) of (PVA/Gelatin). All these characteristic results obtained can be related due to effects of gamma dose irradiation. These data are similar to the study obtained by **Zhuang et al., (2002)** [152].

The last polymer blend film ratio (75/25) of (PVA/Gelatin) was exposed to gamma irradiation (5KGy) as other ratios, It could be notced from scanning electron microscope (SEM) of irradiated polymer blend film ratio (75/25) of (PVA/Gelatin) in Figure.3.16.the surface of the sample observed in smooth phase while, the homogeneity increases after irradiation. Semi regular dots appeared when the film exposed to gamma irradiation.

We can conclude that, played effective role in surface microstructure of irradiated samples. Similar results were obtained by Iuliana **et al., (2012)** [153].

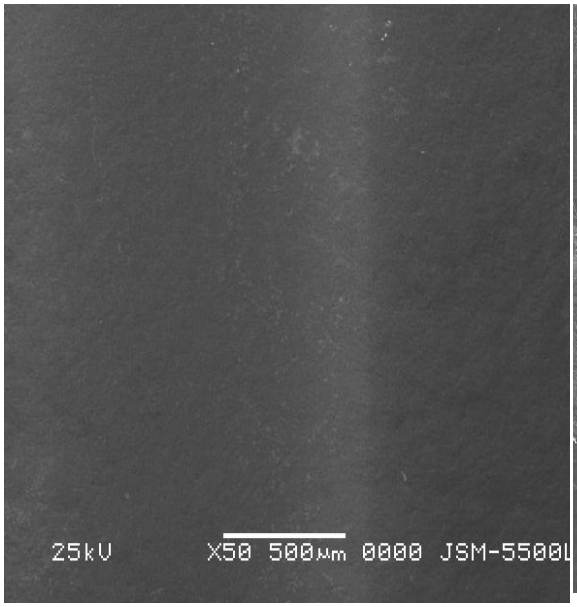


**Figure .3.14.**PVA/gelatin Polymer blend 25/75 irradiated(5KGy)

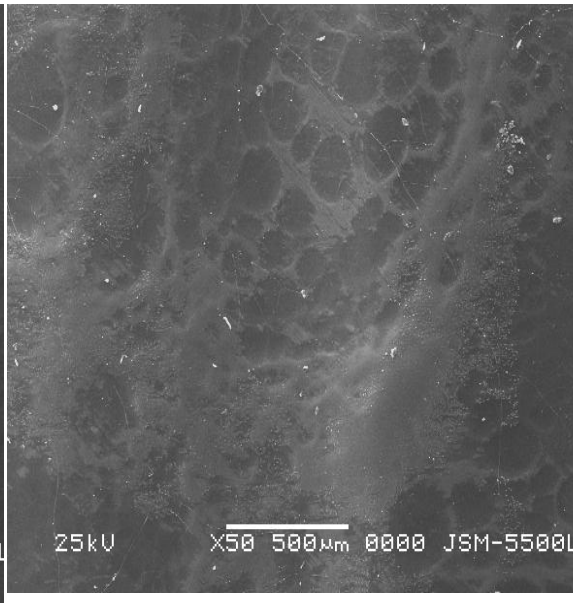


**Figure .3.15.**PVA/gelatin Polymer blend 50/50 irradiated(5KGy)

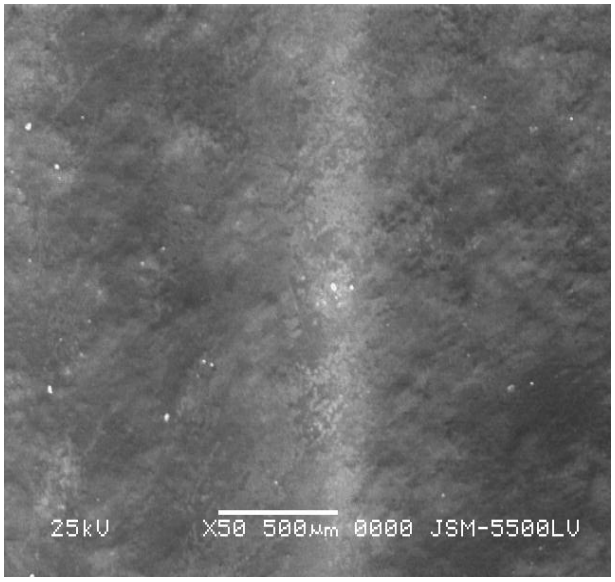


**Figure .3.16.**PVA/gelatin Polymer

Blend 75/25 irradiated (5KGy)

## 3.5. XRD of unirradiated polymer blend of (PVA/Gelatin):

The films based on blends of gelatin and PVA, with fixed concentration of citric acid (0.1N) macromolecule, produced in the present work were subjected to X-ray diffraction (XRD) analysis and the results has been shown in Figures below.

### 3.5.1. XRD of unirradiated pure polymer films of (PVA) and (Gelatin):

Figure .3.17.shows the XRD of pure PVA and Gelatin, from this figure, the diffraction pattern of PVA sample at, 2θ =14°and 19.5° represents the crystalline phase [153], while the shoulder represents the non-crystalline (amorphous) part of PVA sample. The large peak at 2θ = 19.5° corresponds to (110) reflection, a plane which contains the extended planar zig-zag chain direction of the crystallites [154].

The crystalline phase of this polymer may be regarded as an amorphous matrix in which small crystallites are randomly distributed. However, it is

more natural to treat a crystalline region as a certain sufficiently imperfect crystalline lattice in which the free volume is filled with an amorphous phase. Sites saturated with crystal defects, which are due to chain folded crystals, may play the role of an amorphous region [155].

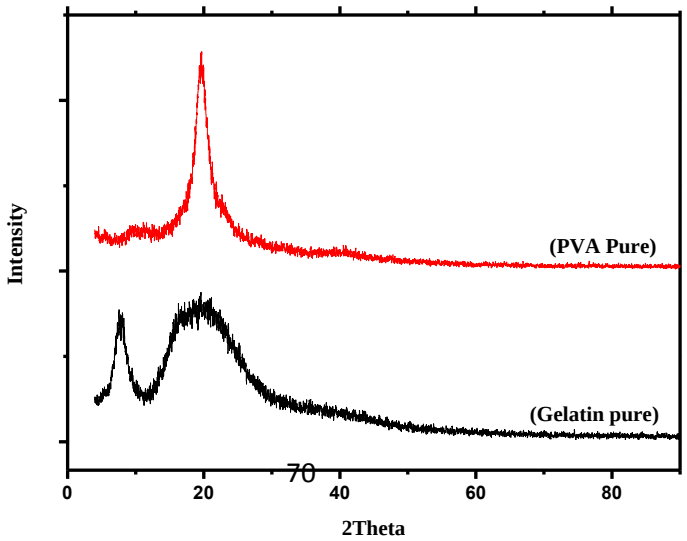

**Figure .3.17.**XRD of pure PVA and Gelatin.

## 3.5.2. XRD of unirradiated polymer blend of (PVA/Gelatin):

The micro structural variations of PVA upon the incorporation of gelatin were investigated with wide-angle X-ray diffraction (WAXD). The observed (WAXD) patterns for (PVA/gelatin) blend films are shown in Figure .3.18.

Irrespective of the ratio and plasticizer, the XRD patterns obtained were typical of partially crystalline materials, with a characteristic peak at $2\theta = 20.22°$, which is agreeing with the results obtained by [221] working with pure PVA films. Similar XRD patterns were observed in previous studies with pure gelatin films and in that for pure PVA films [222] .In a study dealt with the crystallinity of films obtained from blends of gelatin and PVA, observed similar XRD spectra for films based on pure gelatin ($2\theta = 20°$) or pure PVA ($2\theta = 22.5°$), but observed three prominent peaks at $2\theta = 11°$, 17° and 35° for the blended films**.** Similar observations were found with the crystallinity of pure gelatin films, in which they found a characteristic peak at $2\theta = 7°$ to 8°. This peak corresponded to the presence of a small amount of triplehelical structure, characteristic of the rod-like triple helices of collagen[156], intensity of this peak decreases by decreasing the amount of gelatin ratio in the polymer blend matrix as shown in Figure .3.18.These results also show clearly that the gelatin interacts with the polymer chain, mainly with hydroxyl groups, as observed in FTIR spectra and decreases the crystallinity with an increase in its content. The decrease in the crystallinity phase of the

semicrystalline PVA matrix with gelatin is the result of the local ordering in the polymeric structure due to complex formation. These crystalline regions are connected to amorphous regions in which the molecular chains of the polymer are irregularly folded [155].

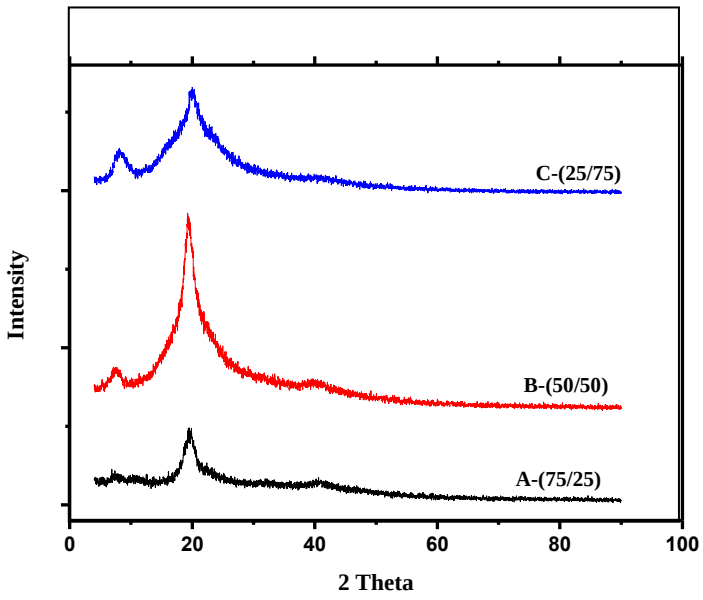


**Figure .3.18.**XRD of unirradiated polymer blend of (PVA/Gelatin)

## 3.5.3. XRD of irradiated polymer blend of (PVA/Gelatin):

XRD pattern of (PVA/gelatin) after exposing to electron beam irradiation of gamma rays has been shown in Figure .3.19.

From this figure, the level of crystallinity percentage decreased after exposed to electron beam irradiation and the ratio of gelatin in the blend composition increased and the interplanar spacing was found to gradually decrease after irradiation [156]. The blends with high gelatin concentration(i.e., less amount of PVA in the blend matrix) showed adecrease in peak intensity and decrease in width at the half maximum of

the peak (2θ = 20°) which may support the participation of gelatin side chains in the PVA crystals in the blends[157].

The decreasing of intterplanar spacing which noticed after the irradiation process of (PVA/gelatin) thin films with different ratios maybe refer to the increasing of the crosslinking induced in the polymer network. PVA has a flexible structure which favors close molecular packing and crystallization and the crystallization of gelatin is due to its tendency to re-naturation.

In general, decreasing in the intensity of the crystallinity peaks (at 2θ = 19.75°) of (PVA/Gelatin) films exposed to electron beam irradiation, has been observed [156].

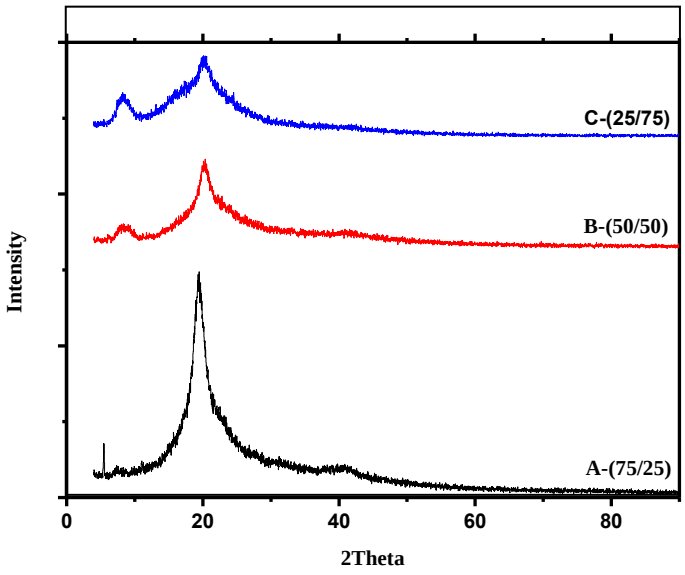

**Figure .3.19.**XRD of irradiated polymer blend of (PVA/Gelatin) at 5Kgy

**Table (3.2). (PVA/gelatin) polymer blends XRD parameters before and after irradiation to a dose of 5 kGy gamma rays:**

| **PVA/gelatin ratio (%)** | **EB dose (kGy)** | **2θ (degrees)** | **Intensity (cps)** |
|---|---|---|---|
| 75/25 | 0 | 20.22 | 118 |
| | 5 | 19.13 | 67 |
| 50/50 | 0 | 19.92 | 26 |
| | 5 | 20.00 | 22 |
| 25/75 | 0 | 20.11 | 79 |
| | 5 | 19.75 | 84 |

## 3.6.Characterization Of Polymer Nanocomposite Before And After Expousing To Ionizing Radiation(γ-Radiation)

### 3.6.1. Swelling degree:

### 3.6.1.1. Swelling of unirradiated nanocomposite films of (PVA/Gelatin/0.01CuO):

The swelling degree of unirradiated nanocomposite blended film ratios (25/75/0.01CuO), (50/50/0.01CuO) and (75/25/0.01CuO) of (PVA/Gelatin/0.01CuO) were performed by dipping the selected ratios samples in de-ionized water and with solutions of pH(4) and pH(10) at different times are mentioned in Figure 3.20, Figure 3.21,and Figure 3.22 Figure 3.20, shows the swelling degree percentages of unirradiated nanocomposite film (25/75/0.01CuO), (50/50/0.01CuO) and (75/25/0.01CuO) of (PVA/Gelatin/0.01CuO) in de-ionized water. From the diagram shown in the figure, it is clear that the maximum values of swelling degree percentages of the studied unirradiated nanocomposite film ratios were appeared after 2hr of dipping in de-ionized water. The maximum values swelling degree percentages were (522%, 300% and 251%) for the unirradiated nanocomposite film ratios (75/25/0.01CuO), (25/75/0.01CuO) and (50/50/0.01CuO) respectively. Then the swelling degree percentages start gradually to decrease until complete saturation occurs after 24hr.

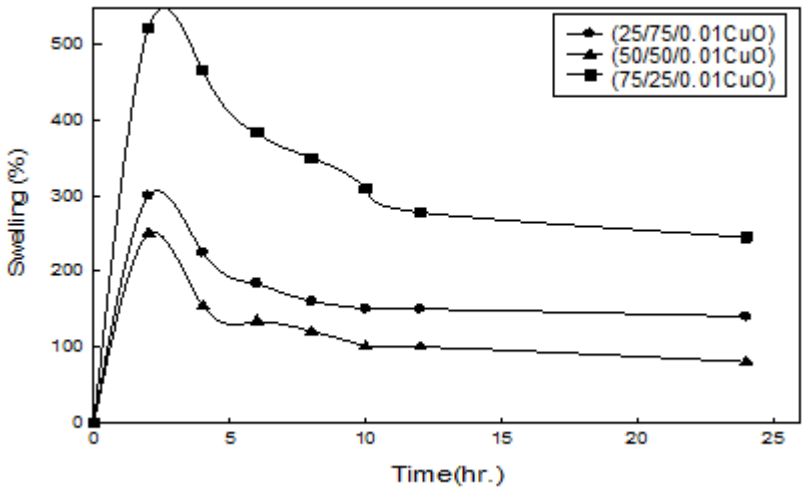


**Figure .3.20.** Swelling degree of unirradiated polymer nanocomposite

(PVA/gelatin/CuO 0.01) in de-ionized water.

Figure 3.21 illustrated the swelling degree of polymer blend nanocomposite with ratios (25/75/0.01CuO), (50/50/0.01CuO) and (75/25/0.01 CuO) of (PVA/Gelatin/0. 1CuO), at pH (4). The results showed high swelling degree percentages were (708%, 503% and 460%) for the unirradiated ratios (25/75/0.1CuO) and (50/50/0.01CuO) (75/25/0.01CuO) then the swelling percentages decreases with increases time.

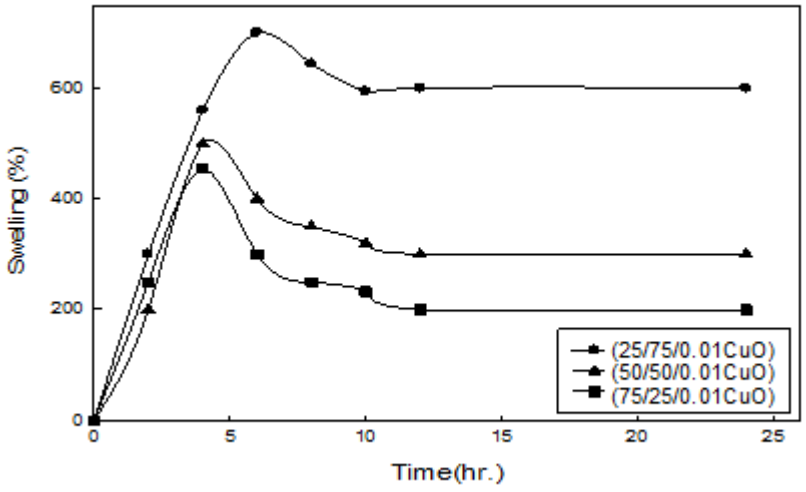

**Figure .3.21.** Swelling degree of unirradiated polymer nanocomposite (PVA/gelatin/CuO 0.01) pH (4).

Figure 3.22.illustrated the effect of pH (10) on the swelling degree percentages of unirradiated nanocomposite ratios (25/75/0.01CuO), (50/50/0.01CuO) and (75/25/0.01CuO) of (PVA/Gelatin/0.01CuO). The swelling degree percentages were found to be decrease with increasing contact time. The higher values of swelling percentages of unirradiated nanocomposite film ratios reaches 700%, 600% and 630% for the selected ratios (25/75/0.01CuO) (50/50/0.01CuO) and (75/25/0.01CuO).

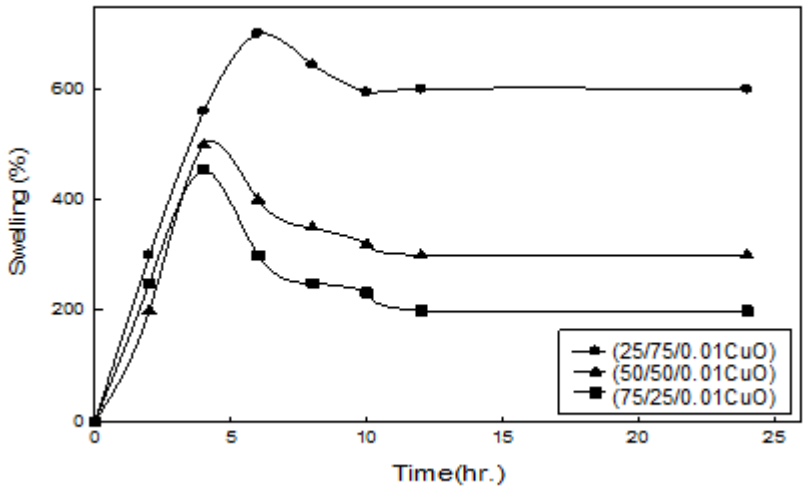


**Figure .3.22.** Swelling degree of unirradiated polymer Nanocomposite (PVA/gelatin/CuO 0.01) pH (10).

## 3.6.1.2.Swelling of irradiated nanocomposite films of (PVA/Gelatin/0.01CuO):

The swelling degree of irradiated nanocomposite film of (PVA/Gelatin/0.01CuO) for different studied ratios (25/75/0.01CuO), (50/50/0.01CuO) and (75/25/0.01CuO), were carried out at dose of gamma radiation has been shown in Figure 3.23.

From this Figure, it is obvious that the rate of swelling degree percentages gradually decreases by increasing dipping time. The

maximum swelling percentages were achieved after 2hr (220%, 270% and 625%) for the irradiated ratios (25/75/0.01CuO), (50/50/0.01CuO) and (75/25/0.01CuO). The obtained data proofed that cross-linking was present between nanocomposite film ratios due to gamma irradiation also, of degradation process not observed even after 24hrs.

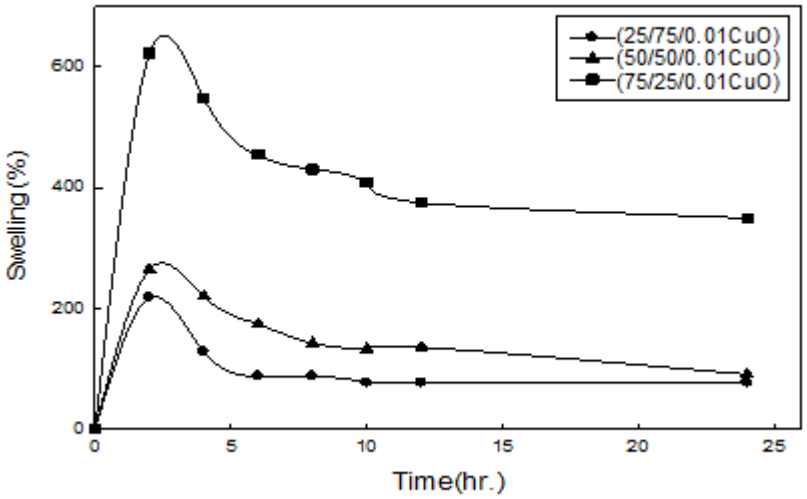


**Figure .3.23.** Swelling degree of irradiated polymer Nanocomposite (PVA/gelatin/CuO 0.01), 5KGy distilled water

The swelling percentages of irradiated nanocomposite film ratios (25/75/0.01CuO), (50/50/0.01CuO) and (75/25/0.01CuO) of (PVA/Gelatin/0.01CuO) at 5KGy was found to be increases at lower pH (4) with contact time as performed in Figure 3.24.However, the time of saturation totally equal with the studied ratios, it was obvious, that the 6hrs is the specific time of saturation. The swelling percentages of the irradiated ratios shows different maximum values were (700%, 604% and 564%) presented after 6hr for the irradiated ratios (75/25/0.01CuO), (25/75/0.01CuO) and (50/50/0.01CuO) respectively.

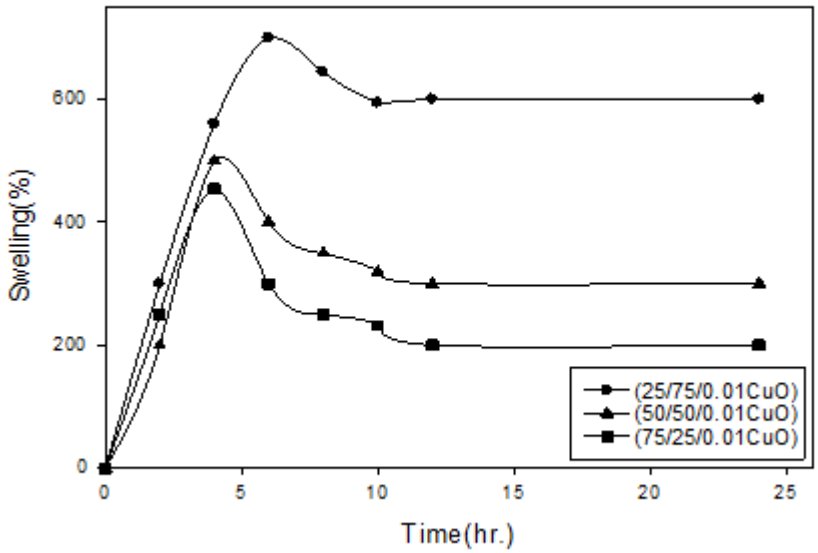


**Figure .3.24.** Swelling degree of irradiated polymer nanocomposite (PVA/gelatin/CuO 0.01) pH (4) 5KGy.

The studied nanocomposite film ratios (25/75/0.01CuO), (50/50/0.01CuO) and (75/25/0.01CuO) of (PVA/Gelatin/0.01CuO) were exposed to the applied doses (5KGy) of gamma irradiation at higher pH(10) values shows the same behavior of pH(4) has been shown in Figure 3.25. The swelling degree of the investigated ratios was observed a maximum swelling percentages after 8hr as the following (636%, 600% and 406%) for nanocomposite film ratios (25/75/0.01CuO), (50/50/0.01CuO) and (75/25/0.01CuO) of (PVA/Gelatin/0.01CuO) in case of applied dose (5KGy). Also, the results indicating that there is no degradation in the observed irradiated nanocomposite ratios.

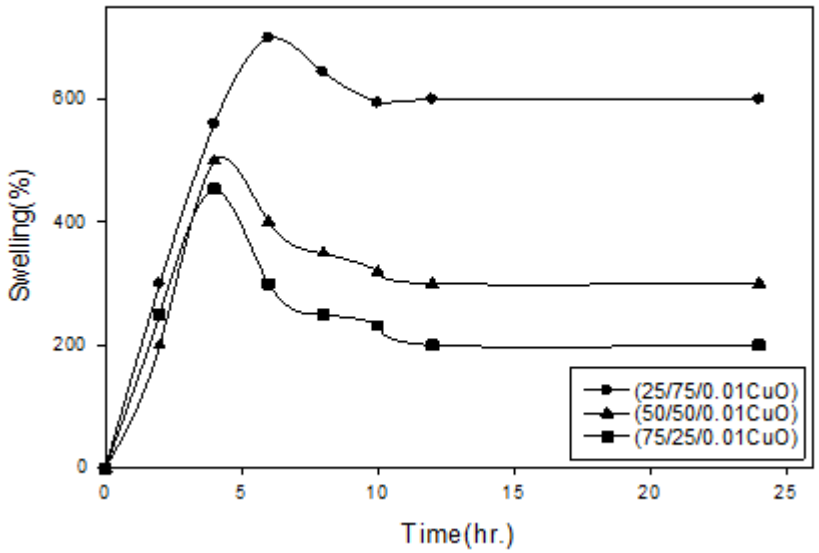


**Figure .3.25.** Swelling degree of irradiated polymer nanocomposite (PVA/gelatin/CuO 0.01) pH (10) 5KGy.

### 3.6.1.3.Swelling of unirradiated (PVA/Gelatin/0.1CuO) nanocomposite films:

The degree of swelling and solubility of unirradiated nanocomposite film ratios (25/75/0.1CuO), (50/50/0.1CuO) and (75/25/0.1CuO) of (PVA/Gelatin/0.1CuO) in de-ionized water and with different values of pH (4, 10) were investigated in presence of higher ratio of Copper oxide Nanoparticles. The performed curves are shown in Figures below.

The observed data of swelling degree percentages of unirradiated nanocomposite film ratios (25/75/0.1CuO), (50/50/0.1CuO) and (75/25/0.1CuO) of (PVA/Gelatin/0.1CuO) in de-ionized water showed that the swelling degree percentages were increase with increasing of dipping time to reach a nearly saturation level of water absorption.

After 6hour of immersing unirradiated ratios (25/75/0.1CuO), (50/50/0.1CuO) and (75/25/0.1CuO) in de-ionized water the higher values of swelling percentages were presented to be (609%, 400% and 800%) respectively. The swelling percentages obtained in lower values

after 8h , which indicting beggaring of saturation and decreases of swelling percentages as shown in Figure 3.26.

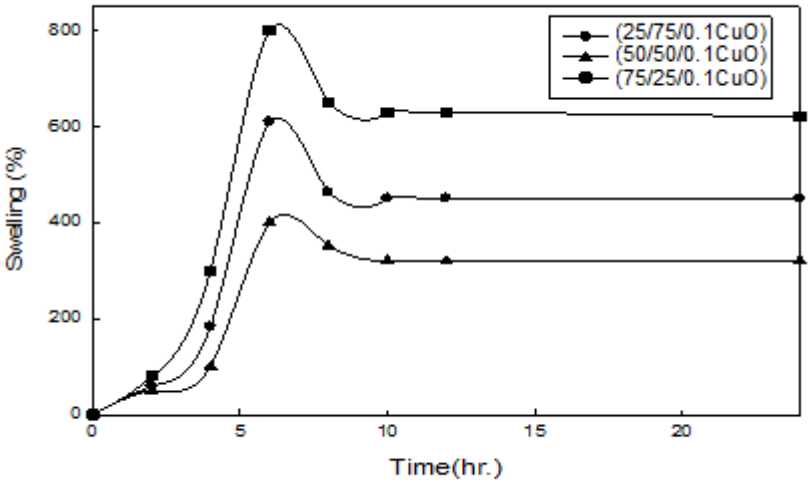


**Figure .3.26.** Swelling degree of unirradiated polymer nanocomposite (PVA/gelatin/CuO 0. 1) in de-ionized water.

The effect of lower pH (4) for unirradiated nanocomposite film ratios (25/75/0.1CuO), (50/50/0.1CuO) and (75/25/0.1CuO) is shown in Figure 3.27., this figure showed similar behavior through ability of swelling reached to 24hr.; it was obvious that 4hr is the specific time of saturation with higher swelling percentage. The maximum observed swelling percentages were (606%, 556% and 653%) respectively for the unirradiated ratios (25/75/0.1CuO), (50/50/0.1CuO) and (75/25/0.1CuO) of (PVA/Gelatin/0.1CuO).

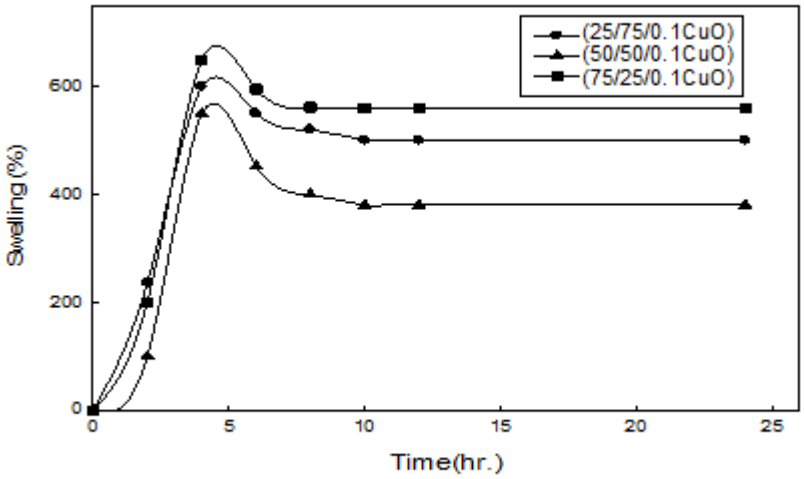


**Figure .3.27.** Swelling degree of unirradiated polymer nanocomposite (PVA/gelatin/CuO 0. 1) in pH (4).

The degree of swelling and solubility of unirradiated nanocomposite film ratios (25/75/0.1CuO), (50/50/0.1CuO) and (75/25/0.1CuO) of (PVA/Gelatin/0.1CuO) at higher value of pH (10) are shown in Figure 4.9.

The obtained results illustrated that 4hr is suitable time of saturation for the unirradiated ratios (25/75/0.1CuO), (50/50/0.1CuO) and (75/25/0.1CuO). It was presented also, that the maximum swelling values are (700%, 600% and 556%) presented after 4hr of dipping the unirradiated ratios (75/25/0.1CuO), (25/75/0.1CuO) and (50/50/0.1CuO) respectively.

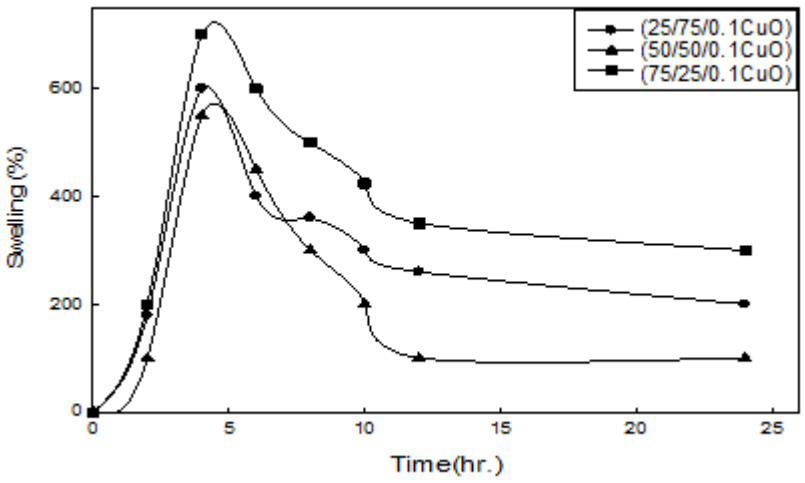


**Figure .3.28.** Swelling degree of unirradiated polymer nanocomposite (PVA/gelatin/CuO 0. 1) in pH (10).

### 3.6.1.4. Swelling of irradiated nanocomposite films of (PVA/Gelatin/0.1CuO):

Figures ("29, 30, 31"-3) depicts the irradiated nanocomposite film ratios (25/75/0.1CuO), (50/50/0.1CuO) and (75/25/0.1CuO) of (PVA/Gelatin/0.1CuO) irradiated with gamma ryes dose (5KGy) in de-ionized water and with different solutions of pH(4) and (10) .

The presented results showed that as Cooper oxide Nanoparticles content increased the swelling degree value ,whereas solubility value of irradiated nanocomposite film ratios (25/75/0.1CuO), (50/50/0.1CuO) and (75/25/0.1CuO) of (PVA/Gelatin/0.1CuO) in de-ionized water and with different solutions of pH(4) and (10) decreased. This result illustrates that inter-intra molecular combination is improved by the presence of interactions between the added nano-size Copper oxide Nanoparticles and the PVA/Gelatin matrix. This is Compatible with study by **Soon et al., (2012)** [158].

Also, the obtained results showed that the studied irradiated nanocomposite film ratios (25/75/0.1CuO), (50/50/0.1CuO) and

(75/25/0.1CuO) of (PVA/Gelatin/0.1CuO) have strong ability tend swelling, due to resistance to soluble in water after immersing for 24 hour. This may be attributed to applied doses of gamma irradiation.

From Figure 3.29.it is clear that the swelling degree of the studied irradiated nanocomposite film ratios in de-ionized water at (5KGy) was increases with increasing dipping time till saturation obtained. The higher values of swelling percentages at (5KGy) are performed after 4hr (640%, ٦٠٠% and 50٠%) respectively for the irradiated nanocomposite film ratios (75/25/0.1CuO), (25/75/0.1CuO) and (50/50/0.1CuO) .

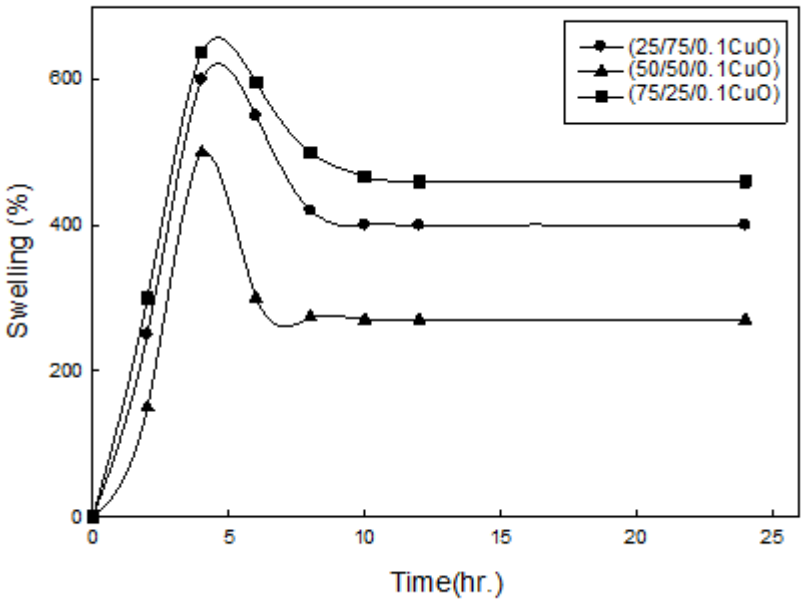


**Figure .3.29.** Swelling degree of irradiated polymer nanocomposite (PVA/gelatin/CuO 0. 1)(5KGy) in de-ionized water.

The maximum swelling degree of irradiated nanocomposite film ratios (25/75/0.1CuO), (50/50/0.1CuO) and (75/25/0.1CuO) of (PVA/Gelatin/0.1CuO) in pH (4) at (5KGy) obtained after (4hrs) around (800%, 600% and 900%) respectively which are listed in Figure 3.30.

Then swelling degree of these studied ratios tends to decrease with less extent, up to 24 hrs.

The measurement of swelling and solubility for the studied films plays a key role in determining the degree of combination between the components of film as well as resistance to water [159,160].

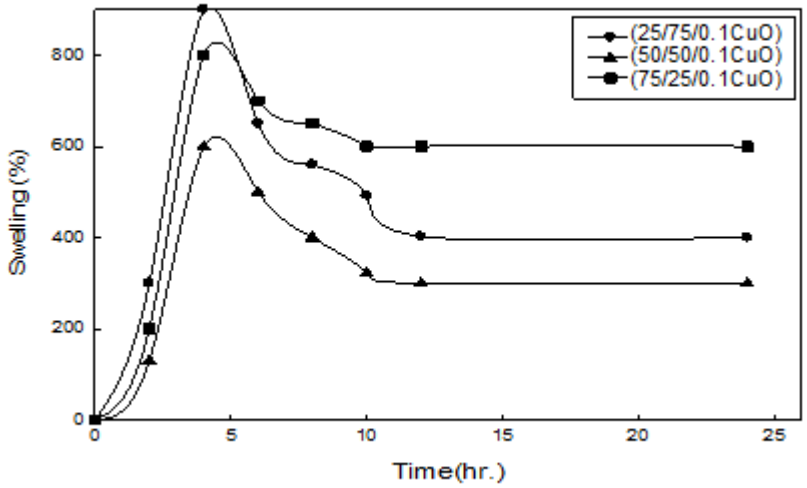


**Figure .3.30.** Swelling degree of irradiated polymer nanocomposite (PVA/gelatin/CuO 0. 1)(5KGy) at pH (4).

The effect of pH (10) on the irradiated nanocomposite film ratios (25/75/0.1CuO), (50/50/0.1CuO) and (75/25/0.1CuO)of (PVA/Gelatin/0.1CuO) was investigated in Figure 3.31. From the obtained curves, it is clear that the swelling degree of the irradiated nanocomposite film ratios increases with increases contact time. The irradiated nanocomposite showed maximum values of swelling degree after 4Hrs were (504%, 402% and 636%) at (5KGy), respectively.

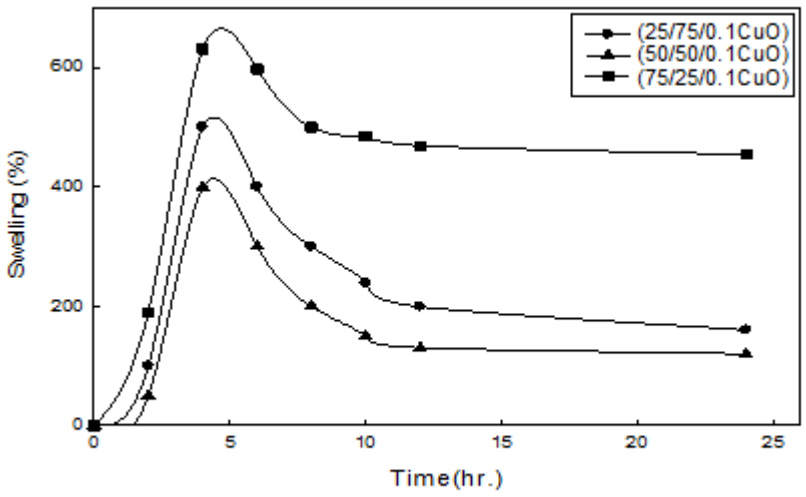


**Figure .3.31.** Swelling degree of irradiated polymer nanocomposite (PVA/gelatin/CuO 0. 1)(5KGy) at pH (10).

## 3.6.2. FTIR characterization:

### 3.6.2.1. Infrared spectra of unirradiated nanocomposite films of (PVA/Gelatin/CuO):

For further confirmation and investigation of the interaction between Copper Oxide nano-rods and nanocomposite film of (polyvinyl

alcohol/Gelatin) matrix, the infrared spectra of nanocomposite films of (polyvinyl alcohol/Gelatin/CuO) were studied by FTIR spectroscopy. Also, the different concentration of Copper Oxide Nanoparticles loaded on (polyvinyl alcohol/Gelatin) matrix was characterized by FTIR spectroscopy.

### 3.6.2.1.1. Infrared spectra of unirradiated nanocomposite film of (PVA/Gelatin/0.01CuO):

Figure.3.32 and Table.3.4. Shows the FT-IR absorption spectra of unirriadiated nanocomposite films ratios of (25/75/0.01CuO), (50/50/0.01CuO) and (75/25/0.01CuO) of (PVA/Gelatin/0.01CuO).

The FT-IR spectra of unirradiated nanocomposite films ratio (25/75/0.01CuO) of (PVA/Gelatin/0.01CuO) showed in (Figure.3.32-A). From this figure different bands were observed. The band at 3600.26 $Cm^{-1}$ is assigned to O—H stretching vibration of hydroxyl groups observed in a strong broad band. Band at 2149.16 $Cm^{-1}$ is generally ascribed to the combination frequency of (CH+CC) according to [138]. Carbonyl group C=O was present at 1745.34 $cm^{-1}$ . The vibrational absorption peaks of all metal oxides (M—O) bands were observed with low intensity. As well as bands in the low frequency range assigned to the loaded CuO Nanoparticles. The intensity bands at 868.92-708.71 $Cm^{-1}$ attributable to Cu—O—Cu in plane vibration according to study **Ali et al., (2009)** [126] and **Zhang et al., (1999)** [161].

The peaks at 556.55 and 434.38 $Cm^{-1}$ are attributed to Cu(II)—O out of plane vibrations [158].

FTIR spectrum for unirradiated nanocomposite film ratio (50/50/0.01CuO) of (PVA/Gelatin/0.01CuO) is shown in (Figure.3.32-B).

The O–H stretching broad band in the IR spectrum is centered and observed at 3345.26 $cm^{-1}$ [126,162,163]. The combination frequency of

(CH+CC) was present at 2171.83 $cm^{-1}$ this is identical to **LINGA et al., (2007)** [138].

The band at 1745.34 $cm^{-1}$ in the unirradiated nanocomposite film ratio (50/50/0.01CuO) of (PVA/Gelatin/0.01CuO) spectrum can be assigned to C=O stretching vibration peak of carbonyl group. This band caused by the ester bond and carboxyl group in citric acid as the study produced by [139].

A weak band is appeared at 936.96 $cm^{-1}$ assigned for $CH_2$ rocking, [119]. The vibrational absorption peaks of all metal oxides (M—O) bands were observed with low intensity. In other words, bands in the low frequency range assigned to the loaded CuO nanoparticles. The intensity bands at 853.92 $Cm^{-1}$ and 708.71 $Cm^{-1}$ are observed due to Cu—O—Cu in plane vibration according to [126,161].

The peak at 647.99 $Cm^{-1}$ indicates the vibration of Cu (I) —O in the studied film [164]. The lower intensity band at 503.15 and 427.06 $Cm^{-1}$ are attributed to Cu(II)—O out of plane vibrations [165].

(Figure.3.32-C) presented FTIR spectra for unirriadiated nanocomposite film ratio of (75/25/0.01CuO) of (PVA/Gelatin/0.01CuO). The FTIR spectrum of unirriadiated nanocomposite film (75/25/0.01CuO) of (PVA/Gelatin/0.01CuO) is shown in (Figure 4.13-C) .This spectrum shows absorption peaks at around 3421.34 $cm^{-1}$ for (OH centered stretching broad band), at around 2171.83 $cm^{-1}$ for combination frequency of (CH=+CC) [138]. Carbonyl group C=O was present at 1745.34 $cm^{-1}$ as broad band. The intensity bands at 853.56 $Cm^{-1}$ referring to Cu—O—Cu in plane vibration [126, 161]. The lower intensity band at 548.50 $Cm^{-1}$ assigned to Cu (II)—O out of plane vibrations [165].

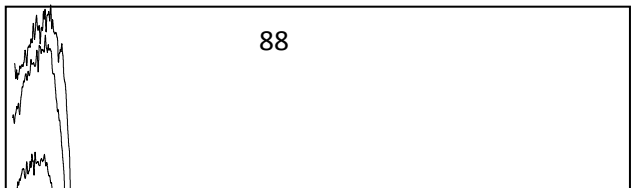

**Figure .3.32.** FTIR spectra of Unirradiatied Nanocomposite film of(PVA/Gelatin/0.01CuO) .

**Table3.4. The Assignment of FTIR Spectra of Absorption Bands Polymer nanocomposite film of (PVA/Gelatin/CuO).**

| **Band position,$Cm^{-1}$** | **Assignment** |
|---|---|
| 3345.26 $Cm^{-1}$ | O—H stretching vibration |
| 2149.16 $Cm^{-1}$ | combination frequency of (CH+CC) |
| 1745.34 $cm^{-1}$ | C=O Stretching |

| | |
|---|---|
| 936.96 $cm^{-1}$ | $CH_2$ rocking |
| 868.92-708.71 $Cm^{-1}$ | Cu—O—Cu in plane vibration |
| 647.99 $Cm^{-1}$ | Cu (I) —O vibration |
| 556.55 and 434.38 $Cm^{-1}$ | Cu(II)—O out of plane vibrations |

### 3.6.2.1.2. Infrared spectra of irradiated nanocomposite film of (PVA/Gelatin/0.01CuO):

The effect of dose of Gamma irradiation on different nanocomposite film ratios of (PVA/Gelatin/0.01CuO) were performed by FT-IR spectroscopy as shown in Figure .3.33 and table 3.4.

The FT-IR spectra of irradiated nanocomposite film ratio (25/75/0.01CuO) of (PVA/Gelatin/0.01CuO) at 5KGy illustrated in (Figure .3.33 -A)

Comparison with unirradiated nanocomposite film ratio of (25/75/0.01CuO) of (PVA/Gelatin/0.01CuO) obtained same characteristic peaks were observed in the wavelength at 3345.26-2149.16 $cm^{-1}$. While the band presented at 1745.34 $cm^{-1}$ which assigned to Carbonyl group was shifted after radiation to lower wave number 1737.29 $cm^{-1}$ due to the stretching C=O [166] may be due to the breaking of hydrogen bonds as a result of irradiation treatment. The bands in the low frequency range which indicating the loaded CuO Nanoparticles to (PVA/Gelatin) film. The intensity bands at 868.92-708.71 $Cm^{-1}$ attributable to Cu—O—Cu in plane vibration according to study [126,161] with no change in their wave number.

The effect of (5KGy) dose of gamma radiation on the FTIR spectra of the studied irradiated nanocomposite film ratio (50/50/0.01CuO) of (PVA/Gelatin/0.01CuO) is shown in (Figure.3.33 -B).As it can be illustrated in (Figure 4.14-B)that O—H stretching centered band becomes more boarder. The intensity band at 2171.83 $cm^{-1}$ after radiation at (5KGy) decrease and becomes 2149.16 $cm^{-1}$ Strong broad band was present at 1745.34 $cm^{-1}$ reason to carbonyl group. Cu—O—Cu stretching band appeared at 853.92 $Cm^{-1}$

The FTIR spectra of irradiated nanocomposite film (75/25/0.01CuO) of (PVA/Gelatin/0.01CuO) at the selected dose 5KGy showed in (Figure .3.33 -C)with comparison this spectrum with unirriadiated nanocomposite film (75/25/0.01CuO) of (PVA/Gelatin/0.01CuO) nanocomposite film spectra, the bands at wave number 3421.34 -2171.83 $cm^{-1}$ are the same after 5KGy dose of gamma radiation. The absorption band observed at 1745.34 $cm^{-1}$ were shifted towards lower wave number to becomes 1729.97 $cm^{-1}$ due to the breaking of hydrogen bonds as a result of irradiation treatment assigned to stretching C=O [166]. $CH_2$ rocking was presented after (5KGy) dose of radiation at 922.33 $cm^{-1}$ [126]. The intensity band at 853.56 $Cm^{-1}$ does not affected by(5KGy) dose of radiation referring to Cu—O—Cu in plane vibration [119,157]. The band at 548.50 $cm^{-1}$ was shifted and increase to 556.55 $cm^{-1}$ assigned to Cu(II)—O out of plane vibrations [165].

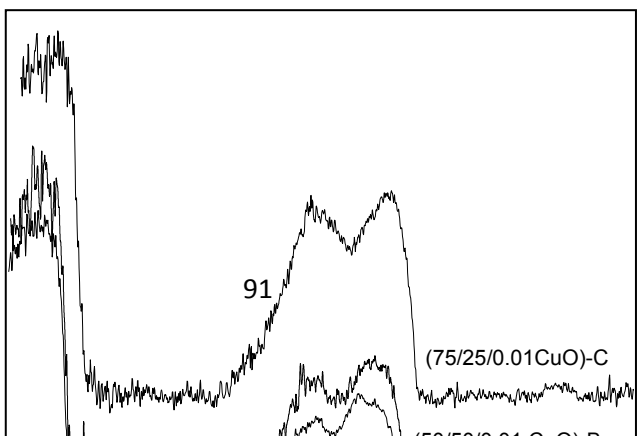

**Figure .3.33.** FTIR spectra of irradiatied5KGy Nanocomposite film of (PVA/Gelatin/0.01CuO)

### 3.6.2.1.3. Infrared spectra of unirradiated nanocomposite film of (PVA/Gelatin/0.1CuO):

The effects of higher concentration of CuO nanoparticles loaded on polyvinyl alcohol/gelatin matrix were investigated by FT-IR analysis. The interaction between higher concentration of CuO nanoparticles and polyvinyl alcohol/gelatin films are displayed in Figure .3.34and table 3.4.

The FT-IR spectra of unirradiated nanocomposite film ratio of (25/75/0.1CuO) of (PVA/Gelatin/0.1CuO) illustrated in Figure (Figure .3.34-A)From this figure it can be seen that the O—H stretching vibration of hydroxyl groups observed in a strong broad band at 3652.06 $Cm^{-1}$ Where the combination frequency of (CH=+CC) band presented at 2171.83 $Cm^{-1}$ [138]. Carbonyl group C=O was present at 1745.34 $cm^{-1}$ . The band at 914.28 $cm^{-1}$ assigned to $CH_2$ rocking [126].

Also Figure (Figure .3.34-B)shows the FTIR spectrum for unirradiated nanocomposite film ratio (50/50/0.1CuO) of (PVA/Gelatin/0.1CuO).

The broad and strong centered band is observed at 3634.95 $cm^{-1}$ corresponding to the O–H stretching frequency [126,162,163]. The

combination frequency of (CH+CC) was appeared at 2171.83 $cm^{-1}$, where this is identical to [138].

The band at 1745.34 $cm^{-1}$ in the IR spectrum of unirradiated nanocomposite film ratio (50/50/0.1CuO) of (PVA/Gelatin/0.1CuO) spectrum can be assigned to C=O stretching vibration peak of carbonyl group. This band caused by the ester bond and carboxyl group in citric acid [139]. The vibrational absorption peaks of all metal oxides (M—O) bands should be observed in low intensity. In other words, bands in the low frequency range assigned to the loaded CuO Nanoparticles in studied produced films. The intensity bands at 853.56 $Cm^{-1}$ and 548.50 $Cm^{-1}$ are observed due to Cu—O—Cu in plane vibration and to Cu(II)—O out of plane vibrations according to [126,161,165].

(Figure.3.34-C) shows the FTIR spectra of unirriadiated nanocomposite film ratio (75/25/0.1CuO) of (PVA/Gelatin/0.1CuO). This figure illustrated the FTIR spectrum of unirriadiated nanocomposite film ratio (75/25/0.1CuO) of (PVA/Gelatin/0.1CuO). This spectrum shows absorption peaks at around 3634.95 $cm^{-1}$ assigned to O—H centered stretching broad band. The combination frequency of (CH=+CC) was not observed. Carbonyl group C=O is presented at 1745.34 $cm^{-1}$. The lower intensity bands at 1517.09 $Cm^{-1}$ and at 1013.78 $Cm^{-1}$ were appeared as a new bands attributed to symmetric stretching modes (Cu—O ) [167].

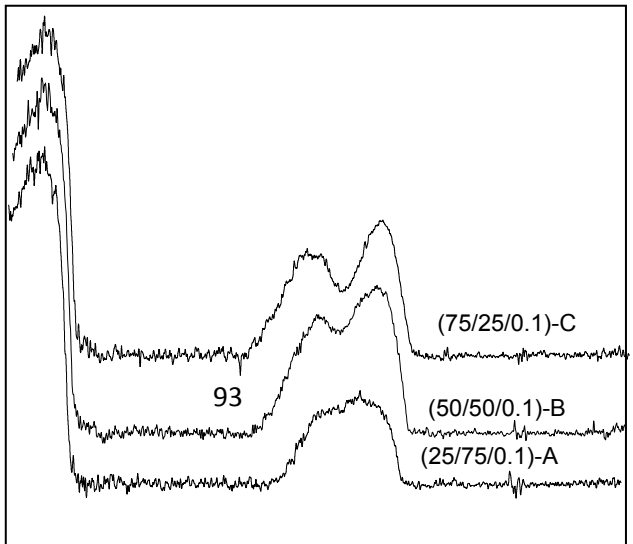

**Figure .3.34.** FTIR spectra of Unirradiatied Nanocomposite film of (PVA/Gelatin/0. 1CuO)

### 3.6.2.1.4.Infrared spectra of irradiated nanocomposite film of (PVA/Gelatin/0.1CuO):

FTIR is of importance to study the molecular structure. The width and intensity of spectral bands as well as position of peaks are all sensitive to environmental changes and to conformations of macromolecule on molecular level. Thus, FTIR spectra have been done for irradiated nanocomposite film of different ratios (PVA/Gelatin/0.1CuO) as shown in Figure .3.35.

The FT-IR spectra of irradiated nanocomposite film ratio (25/75/0.1CuO) of (PVA/Gelatin/0.1CuO) at 5KGy illustrated in (Figure .3.35-A) In case of irradiation at 5KGy as in (Figure .3.35-A) the FTIR spectra of irradiated nanocomposite film ratio (25/75/0.1CuO) of (PVA/Gelatin/0.1CuO) was shifted to the higher side of the spectrum. O—H centered stretching broad band becomes less boarder and sharp also increased to a 3619.59 $cm^{-1}$ after 5KGy dose of irradiation. A new band appeared after 5KGy dose of irradiation at 2346.87 $cm^{-1}$ assigned to symmetric C—H stretching [126]. While the bands at 2171.83 $Cm^{-1}$, 1745.34 $cm^{-1}$ and at 533.14 $Cm^{-1}$ are absent in case of 5KGy dose of gamma irradiation. The new peak presented at 1516.36 $cm^{-1}$ after irradiation may be attributable to symmetric stretching modes (Cu—O) [167].

FTIR spectra for the ratio(50/50/0.1CuO) of (PVA/Gelatin/0.1CuO) at 5KGy ,has been shown in (Figure .3.35-B), from this figure we can observe that O—H band becomes more boarder and strong also shifted to be 3650.91 $cm^{-1}$ after radiation with gamma rays . The intensity band at 2171.83 $cm^{-1}$ after radiation at (5KGy) decrease and becomes 2163.79 $cm^{-1}$, the band appear at 1750.72 $cm^{-1}$ refers to carbonyl group[165].

The FTIR spectra of irradiated nanocomposite film (75/25/0.1CuO) of PVA/Gelatin/0.1CuO) at 5KGy dose of gamma radiation showed (Figure .3.35-C), In case of comparison of this spectrum with unirradiated nanocomposite film (75/25/0.1CuO) of (PVA/Gelatin/0.1CuO) spectra, the peak at wave number 3634.95 $cm^{-1}$ is shifted and decrease after 5KGy dose of gamma radiation to becomes 3626.91 $cm^{-1}$. The absorption band observed at 1745.34 $cm^{-1}$ were shifted towards lower wave number at 1729.97 $cm^{-1}$ due to the breaking of hydrogen bonds as a result of irradiation treatment assigned to acetyl group stretching C=O [166]. The lower intensity bands at 1517.09 $Cm^{-1}$ , 1013.78 $Cm^{-1}$ and 853.56 $Cm^{-1}$ were absent. The band at 541.19 $cm^{-1}$ assigned to Cu(II)—O out of plane vibrations was also absent [165].

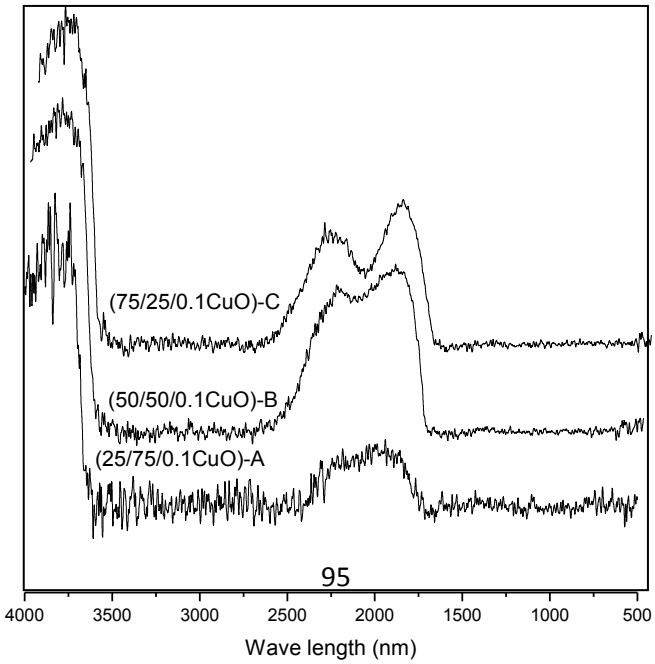

**Figure .3.35.** FTIR spectra of Irradiatied5 KGy Nanocomposite film of (PVA/Gelatin/0. 1CuO)

## 3.6.3.Ultraviolet/visible spectroscopy,(UV/VIS):

### 3.6.3.1.UV/VIS spectra of unirradiated nanocomposite films of (PVA/Gelatin/0.01CuO):

The UV/VIS spectra of unirradiated nanocomposite film of (PVA/Gelatin/0.01CuO) were observed in Figure.3.36. The studied unirradiated nanocomposite films of (PVA/Gelatin/0.01CuO) films are (25/75/0.01CuO), (50/50/0.01CuO) and (75/25/0.01CuO) of (PVA/Gelatin/0.01CuO).

(Figure.3.36-A) shows the absorption spectra of unirradiated nanocomposite film of (25/75/0.01CuO) of (PVA/Gelatin/0.01CuO). From this figure it is clear that, an absorption band was visualized at about (390 nm), which corresponds to II-II$^{*}$ transition of conjugated polymer structure. The obtained absorption band might be occurred in a distorted octahedral environment arising from the intercalation with the

polymer matrix. The interaction of CuO Nannoparticles into the polymer matrix significantly affected (red shift) on the main absorption band (280-390) which gives evidence of strong interaction between the host structure and the organic polymeric matrix [168].

The UV/VIS spectra of unirradiated nanocomposite film ratio (50/50/0.01CuO) of (PVA/Gelatin/0.01CuO) were carried out as been shown (Figure.3.36-B) It can be seen from this figure that, an absorption broad band was presented at about (400-440 nm), which corresponds to II-II* transition. This due to the strong interaction of CuO Nannoparticles into the polymer matrix as (red shift) [168].

The UV/VIS spectra of unirradiated nanocomposite film of (75/25/0.01CuO) of (PVA/Gelatin/0.01CuO) were investigated as been shown (Figure.3.36-C) It can be observed, a strong broad band was mentioned at range (400-440 nm), which corresponds to II-II* transition. This due to interaction of CuO Nannoparticles into the polymer matrix significantly as (red shift) on the appearing ratio [168].

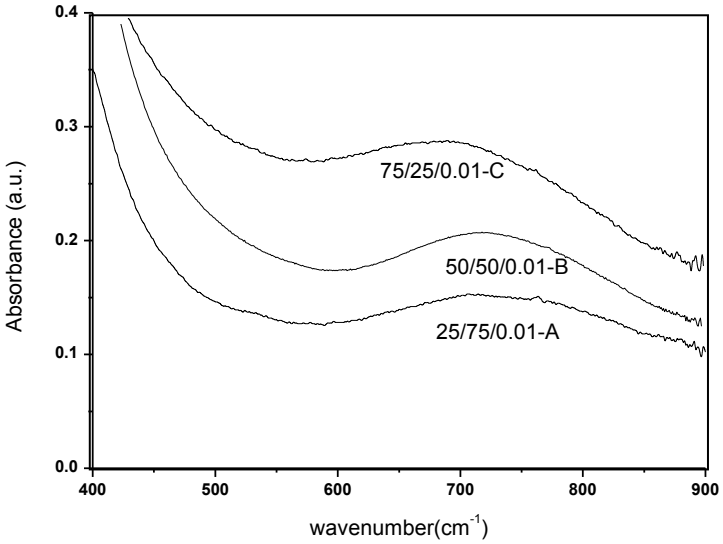

**Figure .3.36.** The UV/VIS spectra of unirradiated nanocomposite film of (PVA/Gelatin/0.01CuO).

### 3.6.3.2.UV/VIS spectra of irradiated nanocomposite films of (PVA/Gelatin/0.01CuO):

The effect of (5 KGy) dose of gamma irradiation on nanocomposite films of different ratios (25/75/0.01CuO), (50/50/0.01CuO) and (75/25/0.1CuO) of (PVA/Gelatin/0.01CuO) were investigated by measurements of the UV/VIS spectra as displayed in Figure.3.37.

The UV/VIS spectra of irradiated nanocomposite film ratio (25/75/0.01CuO) of (PVA/Gelatin/0.01CuO) has been observed at (Figure.3.37-A). The studied irradiated nanocomposite ratio (25/75/0.01CuO) of (PVA/Gelatin/0.01CuO) was affected by radiation dose (5KGy), The absorption band which observed at unirradiated same ratio at (390nm) was shifted to higher wave length after irradiation dose (5KGy), which increasing the absorption intensity of the peak at (450-480nm) of red shift. This also, attributed to CuO in polymeric matrix as study of [168].

The same behavior has been observed in the other irradiated ratios of polymer nanocomposite (50/50/0.01 CuO) and (75/25/0.01 CuO) which has been shown in (Figure.3.37-B), (Figure.3.37-C) respectively.

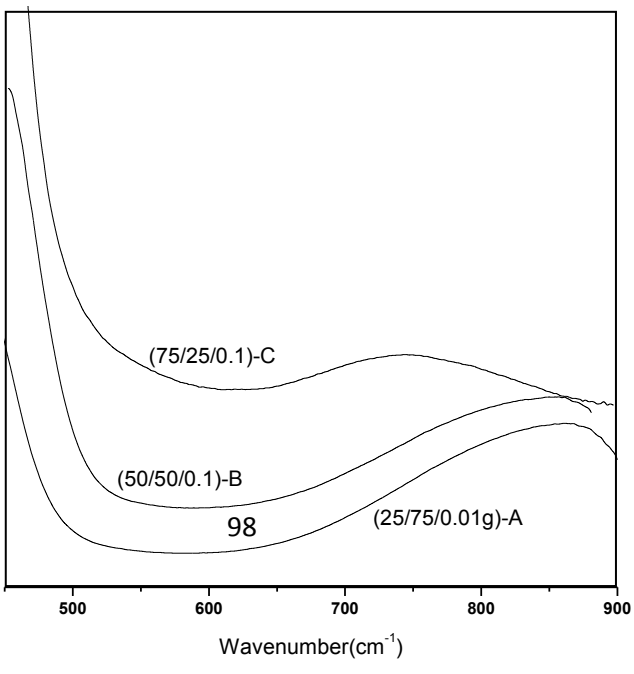

**Figure .3.37.** the UV/VIS spectra of irradiated (5KGy) nanocomposite film of (PVA/Gelatin/0.01CuO).

### 3.6.3.3.UV/VIS spectra of unirradiated Nanocomposite films of (PVA/Gelatin/0.1CuO):

The UV/VIS spectra of unirradiated nanocomposite films of (PVA/Gelatin/0.1CuO) were observed in Figure.3.38, while, the studied unirradiated nanocomposite films ratios of (PVA/Gelatin/0.1CuO) films are (25/75/0.1CuO), (50/50/0.2CuO) and (75/25/0.1CuO) of (PVA/Gelatin/0.1CuO).

(Figure.3.38-A) displays the UV/VIS absorption spectra of unirradiated nanocomposite polymeric film ratio (25/75/0.1CuO) of (PVA/Gelatin/0.1CuO). The UV/VIS absorption spectra of studied unirradiated film ratio show noticeable absorption peak from (400-440nm), which were related to the formation of CuO nanoparticles. The observed peak in this case presented as abroad band, indicating distributed the higher concentration of CuO nanoparticles in PVA/Gelatin film matrix [169].

The optical absorption spectrum of polymeric film of unirradiated nanocomposite films ratio (50/50/0.1CuO) of (PVA/Gelatin/0.1CuO) was recorded in the wavelength region from 200 to 900 nm and is shown in (Figure.3.38-B). The UV absorption edge for the CuO nanoparticles in PVA/Gelatin film matrix was observed to be around 420 nm [163]. The yield absorption intensity band dependence on concentration of CuO and the ratio of PVA to gelatin [170].

(Figure.3.38-C) represents the absorption spectrum of prepared the unirradiated nanocomposite films of (75/25/0.1CuO) ratio of (PVA/Gelatin/0.1CuO). The spectra of the presented ratio exhibit an absorption band at around 480nm, which related to high energy absorption. This band also provides an evidence for the miscibility and complete distribution of CuO nanoparticles on the selected ratio (75/25/0.1CuO) of (PVA/Gelatin/0.1CuO) film matrix in unirradiated case. This similar to studies by [169,170].

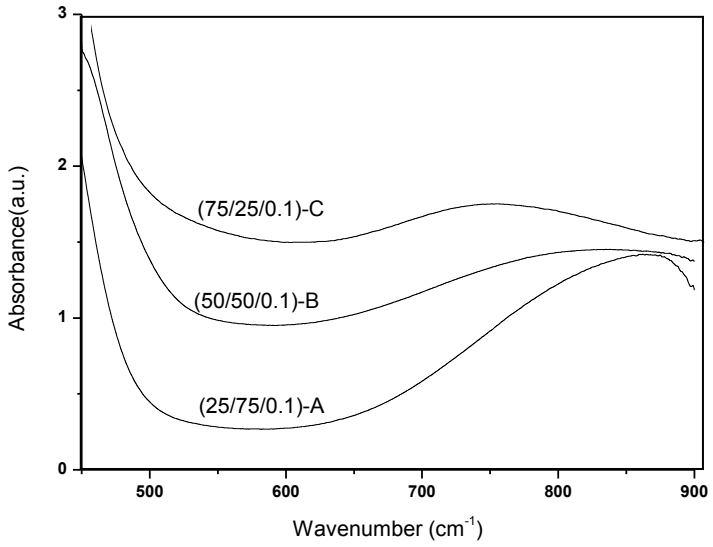


**Figure .3.38.** the UV/VIS spectra of un irradiated nanocomposite film of (PVA/Gelatin/0. 1CuO).

## 3.6.3.4.UV/VIS spectra of irradiated Nanocomposite films of (PVA/Gelatin/0.1CuO):

Figure.4.20 shows the effect of irradiation dose of gamma radiation (5KGy) on the higher concentration of CuO Nanoparticles in polymer matrix of studied ratios.

The UV/VIS spectra of nanocomposite films of (PVA/Gelatin/0.1CuO) were observed in Figure.3.39. The studied nanocomposite films of (PVA/Gelatin/0.1CuO) ratios are (25/75/0.1CuO), (50/50/0.1CuO) and (75/25/0.1CuO). The figures show also the effect of irradiation dose of gamma radiation on the higher concentration of CuO Nanoparticles in polymer matrix of studied ratios.

In order to investigate the effect of the selected dose (5KGy) of gamma irradiation on the presented ratio of (25/75/0.1CuO) of (PVA/Gelatin/0.1CuO), the UV/VIS spectrum was measured as been shown in (Figure.3.39-A). From the observed UV/VIS spectra of related ratio a strong and broad absorption intensity peak at (450nm**).** This indicating, that during irradiated the studied ratio of (25/75/0.1CuO) of (PVA/Gelatin/0.1CuO) by the applied dose (5KGy) the loaded CuO Nanoparticles in prepared sample were speared on texture of polymeric matrix. This is consistent to **Wael et al., (2012)** [169].

(Figure.3.39-B) show the UV/VIS absorption spectra of irradiated nanocomposite polymeric film ratio (50/50/0.1CuO) of (PVA/Gelatin/0.1CuO) ratio at (5KGy). The UV/VIS absorption spectra of studied ratio show a shoulder absorption abroad band at 400nm which were related to the formation of CuO nanoparticles in (PVA/Gelatin) film matrix after radiation. This accordance to [169].

(Figure.3.39-C)illustrated the UV/VIS absorption spectra of irradiated nanocomposite polymeric film ratio (75/25/0.1CuO) of (PVA/Gelatin/0.1CuO) at (5KGy). The UV/VIS absorption spectra of studied ratio show absorption abroad band at 441nm .The corresponding band is also related to the formation of CuO nanoparticles in PVA/Gelatin film matrix after radiation. This accordance to **Wael et al., (2012)** [169].

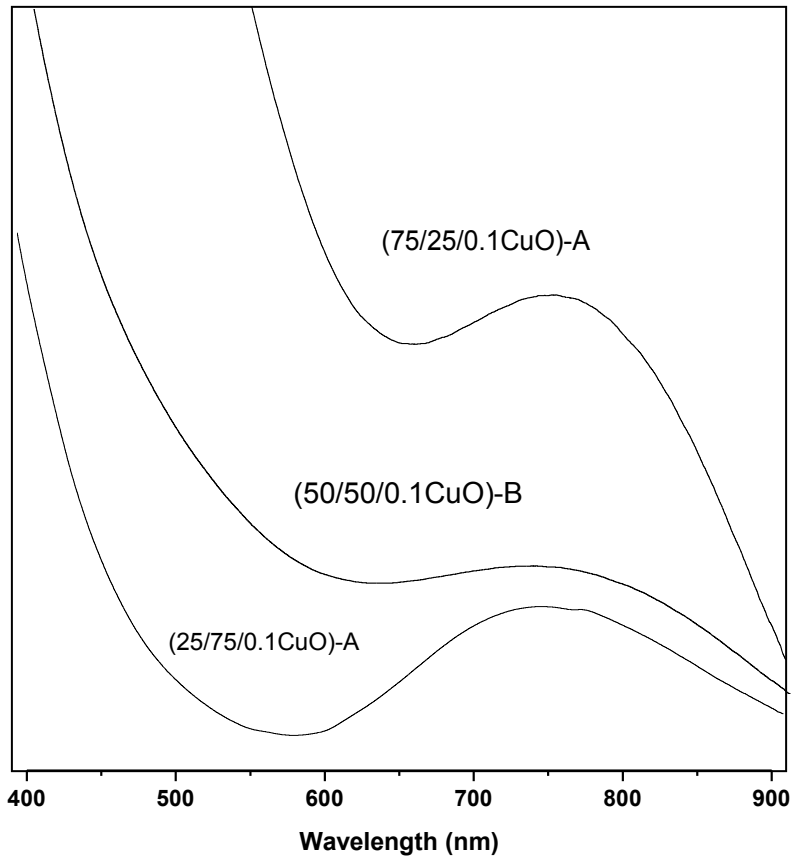


**Figure .3.39.** The UV/VIS spectra of irradiated (5KGy) nanocomposite film of (PVA/Gelatin/0. 1CuO).

## 3.6. 4. <u>Morphology</u>:

## 3.6. 4.1. Scanning electron microscopy:

### 3.6.4.1.1.Scanning electron microscopy of unirradiated nanocomposite films of (PVA/Gelatin/0.01CuO):

The morphology of nanocomposite films of (PVA/Gelatin/0.01CuO) inserts was studied through the analysis of images obtained by scanning electron microscope (SEM) for the nanocomposite films ratios (25/75/0.01CuO), (50/50/0.01CuO) and (25/75/0.01CuO) before irradiation displayed in Figures showed below.

Figure.3.40.represents the scanning electron microscope (SEM) images of studied unirradiated nanocomposite films ratio (25/75/0.01CuO) of (PVA/Gelatin/0.01CuO). The observed image shows smooth surfaces and homogeneous of films samples. The images showed also small particles in surface. These small particles may be due to undistributed CuO nanoparticles on the surface during the preparation of film sample.

The CuO nanocomposite distribution in the surface and cross section of the yielding unirradiated nanocomposite films ratio (50/50/0.01CuO) of (PVA/Gelatin/0.01CuO) was detected by employing scanning electron microscope (SEM) images and presented in Figure.3.41.The observed SEM images of selected ratio shows flat sheet film, while, CuO nanoparticles dispersed uniformly in polymer bulk. Also, the images presented CuO nanoparticles as small white particles.

SEM images of unirradiated nanocomposite films ratio (75/25/0.01CuO) of (PVA/Gelatin/0.01CuO) were depicts in Figure.3.42.These images showed that the surface was smooth, continuous and in homogeneous case. An image shows also regular small pores on the surface, it might be of low concentration of gelatin. Also, the CuO nanoparticles were distributed in the surface of polymer matrix.

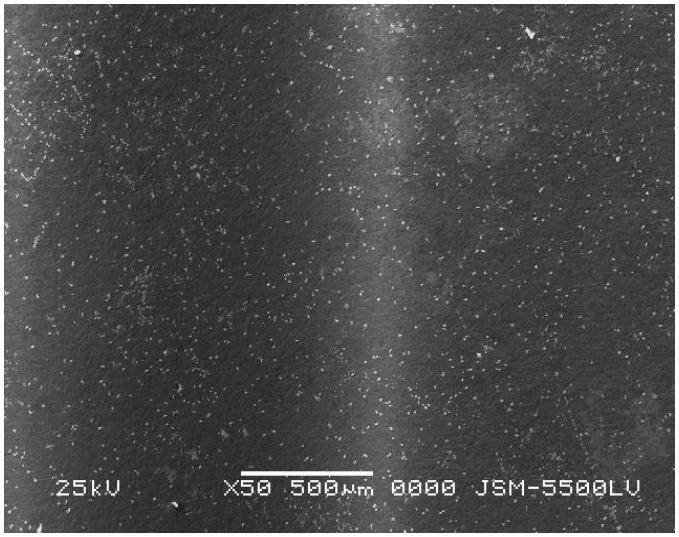


Figure .3.40. SEM(25/75/0.01CuO)

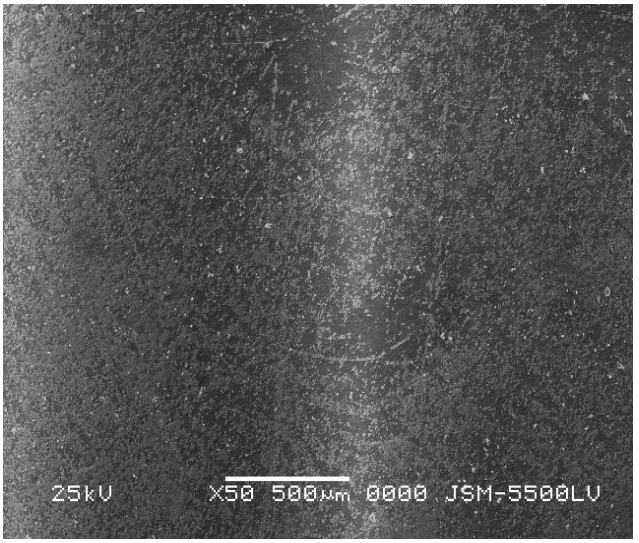


Figure .3.41. SEM(50/50/0.01C

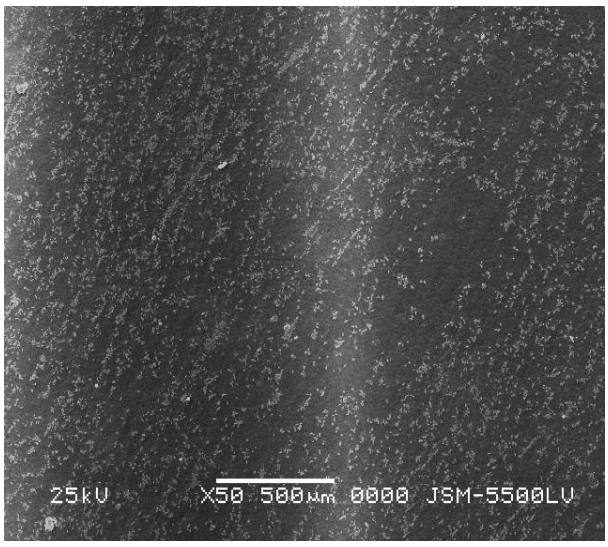


Figure .3.42. SEM (75/25/0.01CuO)

## 3.6.4.1.2.Scanning electron microscopy of irradiated nanocomposite films of (PVA/Gelatin/0.01CuO):

Figures.3.43, 44and 45 performed the effect of gamma irradiation dose on the different ratios of nanocomposite films of (PVA/Gelatin/0.01CuO) with SEM.

To investigate the effect of gamma irradiation dose(5KGy) on observed nanocomposite films ratio (25/75/0.01CuO) of (PVA/Gelatin/0.01CuO), the scanning electron microscope (SEM) was determined as been shown in Figure.3.43

The produced images reveal an unusual microstructure of CuO nanoparticles in low concentration filled polymer matrix composite. In other words, the small particles size of CuO nanoparticles in surface were distributed completely on all of the surfaces in regular behavior due to effective of the used dose of gamma irradiation. This is accordance to study of **Denice et al., (2010)** [152]. The scanning electron microscope (SEM) images in Figure.4.24 showed that inserts surface becomes smooth and more homogeneous.

However, the irradiated nanocomposite films ratio (50/50/0.01CuO) of (PVA/Gelatin/0.01CuO) through gamma irradiation dose (5KGy) was analyzed by using scanning electron microscope (SEM). The results of irradiation are observed in Figure.3.44.SEM images in case of (5KGy) dose irradiation showed more homogeneity and smooth on the surface of irradiated film sample as been shown in Figure.3.45. The images appearance distribution of CuO nanoparticles in upper surface of polymer matrix of studied ratio irradiated nanocomposite films ratio (50/50/0.01CuO) of (PVA/Gelatin/0.01CuO).

No phases separation was observed, indicating good compatibility between insert matrix and CuO nanoparticles [145].

The same irradiated nanocomposite films ratio (75/25/0.01CuO) of (PVA/Gelatin/0.01CuO) was exposed to gamma irradiation dose of (5KGy).

The irradiated film was investigated by scanning electron microscope (SEM) to note any changes on the surface of studied film, this has been shown in Figure.4.26. SEM images of irradiated samples display changes in surface, where the pores are homogeneously disappeared completely and surface becomes more smoothing. Also, images showed complete distribution of CuO nanoparticles on the surface of irradiated nanocomposite films ratio (75/25/0.01CuO) of (PVA/Gelatin/0.01CuO).

These observed results proved that smooth, homogeneity, disappearing of pores and distribution of CuO nanoparticles on the surface increases by exposing the nanocomposite films to the dose of gamma irradiation[145].

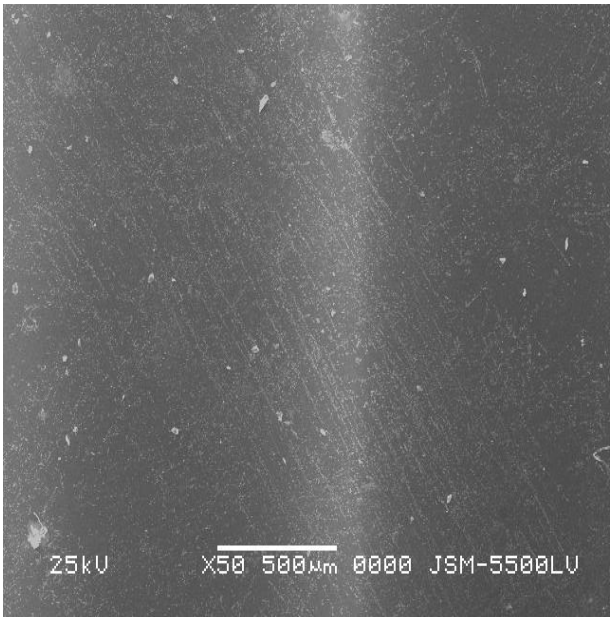


Figure .3.43. SEM(25/75/0.01CuO) Irradiated

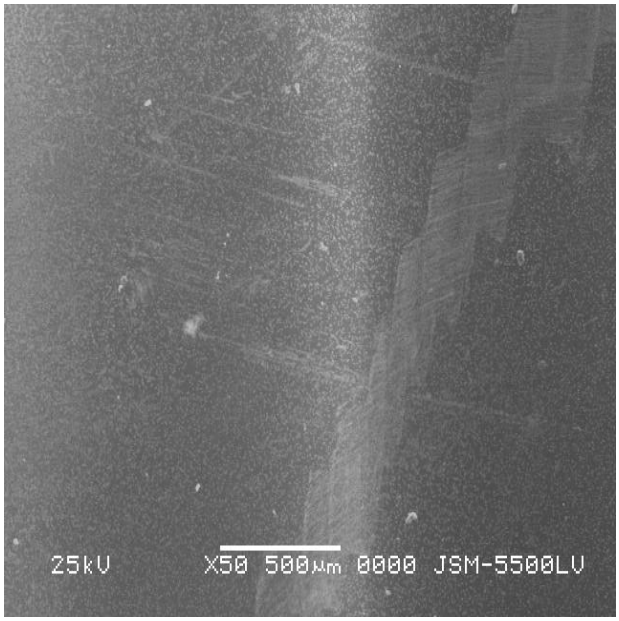


Figure .3.44.SEM(50/50/0.01CuO) Irradiated

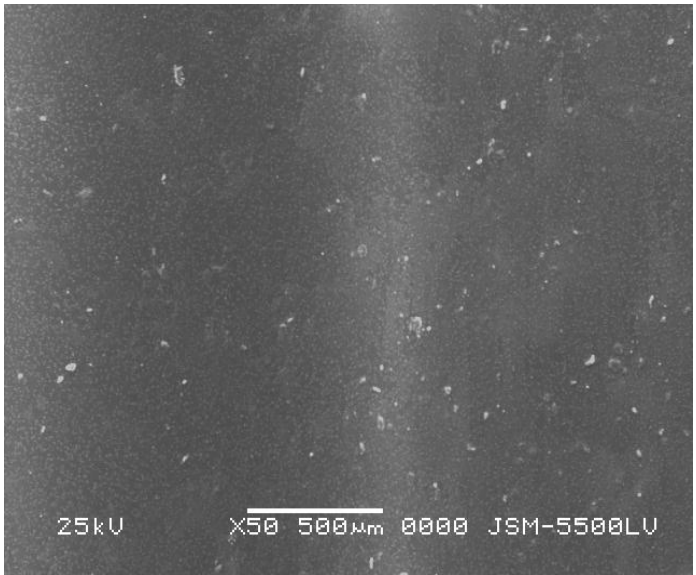

Figure .3.45. SEM(75/25/0.01CuO) Irradiated

### 3.6.4.1.3.Scanning electron microscopy of unirradiated nanocomposite films of (PVA/Gelatin/0.1CuO):

The morphological analysis of unirradiated nanocomposite films of (PVA/Gelatin/0.1CuO) was carried out using a scanning electron microscope (SEM). SEM was carried out to investigate different factors such as distribution, the higher concentration of CuO Nanoparticles behavior, homogeneity, smooth and continuous on the surface films. The

studied unirradiated nanocomposite films ratio was (25/75/0.1CuO), (50/50/0.1CuO) and (75/25/0.1CuO) of (PVA/Gelatin/0.1CuO).

Scanning electron microscope (SEM) images of unirradiated nanocomposite films ratio (25/75/0.1CuO) are presented in Figure.3.46. The photomicrographs of the films obtained by SEM for the upper surface and cross-section showed homogeneity between CuO nanoparticles and (PVA/Gelatin) phases with pores observation. A similar effect observed in study **Denice et al., (2010)** [152]. Also, the surface becomes smooth and continuous.

Scanning electron microscope (SEM) images in Figure.3.47. Was recorded for unirradiated nanocomposite films ratio (50/50/0.1CuO) of (PVA/Gelatin/0.2CuO). It could be seen from the observed images that the surface characterizes by smooth homogeneity with regular pores. Homogeneity indicated the miscibility of CuO nanoparticles with (PVA/Gelatin) matrix.

The SEM images of unirradiated nanocomposite films ratio (75/25/0.1CuO) of (PVA/Gelatin/0.1CuO) were observed in Figure.3.48. SEM images showed that the surface was rough, continuous and in homogeneous phase. The rough phase might be due to low concentration of gelatin. Images shows also an regular distribution of CuO nanoparticles in the surface of polymer matrix.

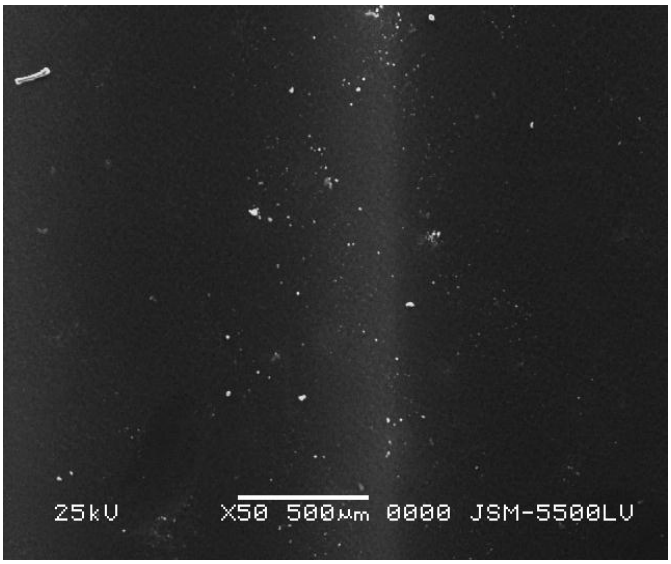


Figure .3.46. SEM(25/75/0. 1CuO)Unirradiated 1CuO)Unirradiated

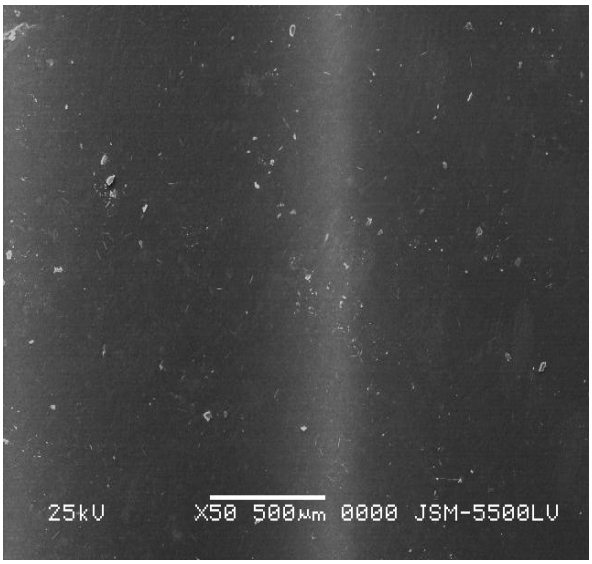


Figure.3.47.SEM(50/50/0.

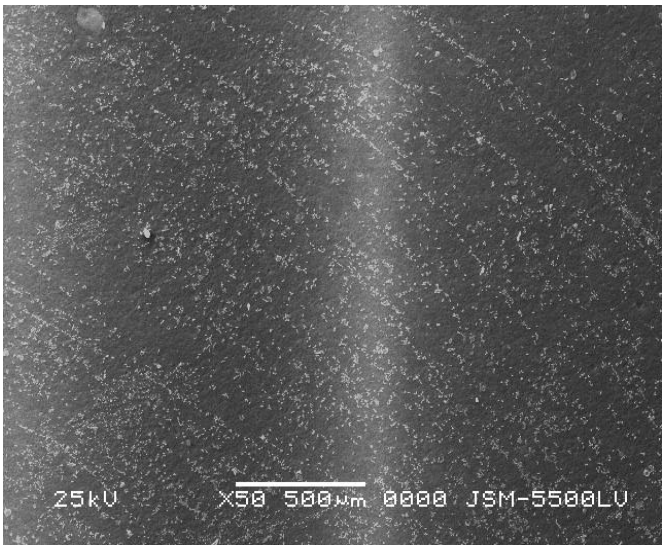


Figure.3.48.SEM(75/25/0. 1CuO)Unirradiated

### 3.6.4.1.4.Scanning electron microscope of irradiated nanocomposite films of (PVA/Gelatin/0.1CuO):

Figure.3.49 show the cross-section view of the irradiated nanocomposite films ratio (25/75/0.1CuO) of (PVA/Gelatin/0.1CuO) when it is exposed to dose of gamma irradiation (5KGy). The cross-

section structure clearly indicates the role of the gamma irradiation. At (5KGy) dose the observed surface was more homogeneity, smooth and absence of pores. Agumirlation of nano copper particles has been noted as white particles.

Gamma irradiation dose effect applied to the selected irradiated nanocomposite films ratio (50/50/0.1CuO) of (PVA/Gelatin/0.1CuO) were carried out through Scanning electron microscope (SEM) and illustrated Figure.3.50. The SEM images at (5KGy) shows homogeneity surface with distribution of CuO nanoparticles on the surface. The yield surface has smooth phase as in Figure.3.50.

The selected irradiated nanocomposite films ratio (75/25/0.1CuO) of (PVA/Gelatin/0.1CuO) was exposed to gamma irradiation dose of (5KGy).

The irradiated nanocomposite thin film at (5KGy) was followed by scanning electron microscope (SEM) to determine any changes on the surface of studied film, this has been shown in Figure.3.51.SEM images of irradiated samples display changes in surface, where the surface becomes homogeneously, smoothing in case of (5KGy), While CuO nanoparticles were distributed completely in shape of regular groups of white tall thin sticks on the surface presented in Figure.3.51.

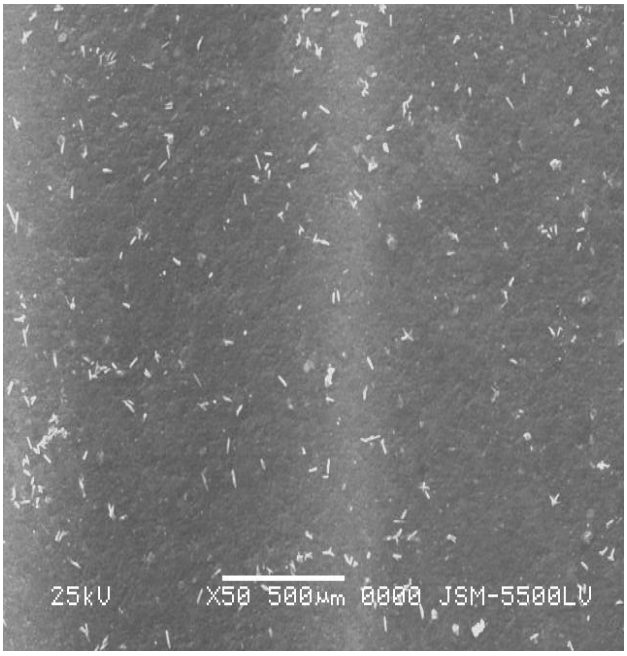


Figure.3.49.SEM (25/75/0. 1CuO) Irradiated

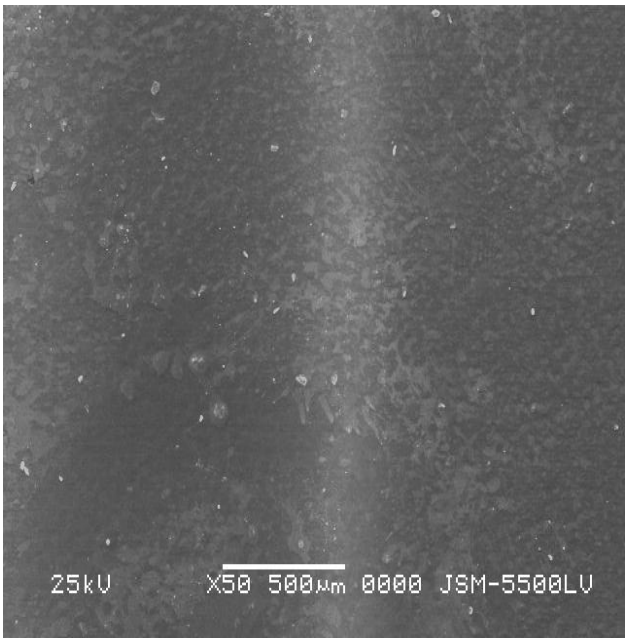


Figure.3.50.SEM(50/50/0. 1CuO) Irradiated

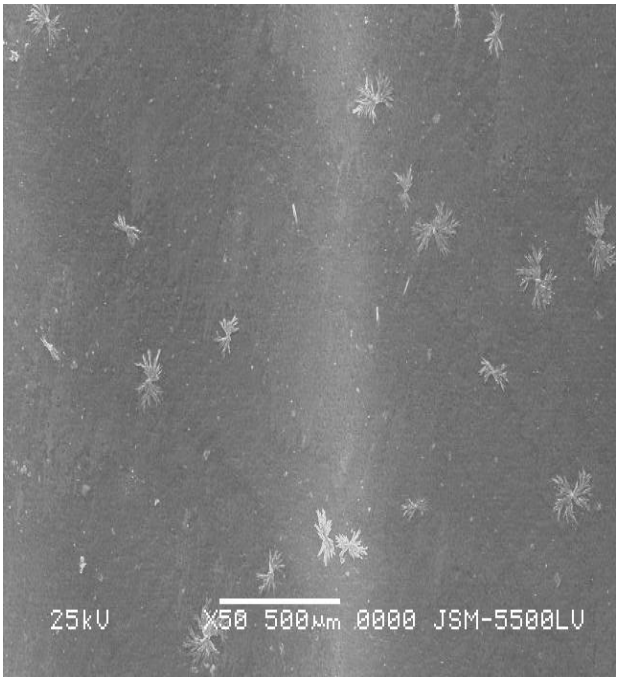


Figure.3.51SEM (75/25/0. 1CuO) Irradiated

## 3.6.4.2.X-ray diffraction:

The X-ray diffraction characterization of CuO nanoparticles, unirradiated nanocomposite films of (PVA/Gelatin/CuO) for the studied ratios (25/75/0.01CuO), (50/50/0.01CuO) and (75/25/0.01CuO) and with higher concentration of CuO nanoparticles of nanocomposite ratios (25/75/0.1CuO), (50/50/0.1CuO) and (75/25/0.1CuO) were carried out to

determine the variation in structure and crystallinty percent as a result of irradiation, polymer content and CuO Nanoparticles dose content.

## 3.6. 4.2.1. X-ray diffraction of CuO nanoparticles:

Figure.3.52.represents the XRD pattern of the typical sample of CuO nanoparticles. All the peaks on the XRD pattern can be indexed to that of monoclinic CuO according to the literature [171]. The detailed analysis of the XRD and the assignments of various reflections are given in the Table (3-5).

X-ray diffraction graph Figure.3.52 indicated that all the CuO nanoparticle samples had strong crystalline structure. Intensity of the XRD peak at 2353K was higher than 2214K and 697K. It was suggestive that at higher reactor temperature, stronger crystalline structures were obtained. Also, the XRD pattern of the CuO nanoparticle shows stronger three peaks observed at 2θ= (35.45, 38.67 and 48.69). This study is identical with **Hua et al, (2002)** [172].

**Table 3.5.The strongest peaks observed in XRD Pattern of CuO nanoparticle:**

| NO. | Peak no. | 2θ(deg) | d ($A^0$) | FWHM(deg) | Intensity (count) |
|---|---|---|---|---|---|
| **1** | 2 | 35.45 | 2.53 | 0.245 | 1448 |
| **2** | 3 | 38.67 | 2.32 | 0.238 | 1405 |
| **3** | 4 | 48.69 | 1.8 | 0.225 | 410 |

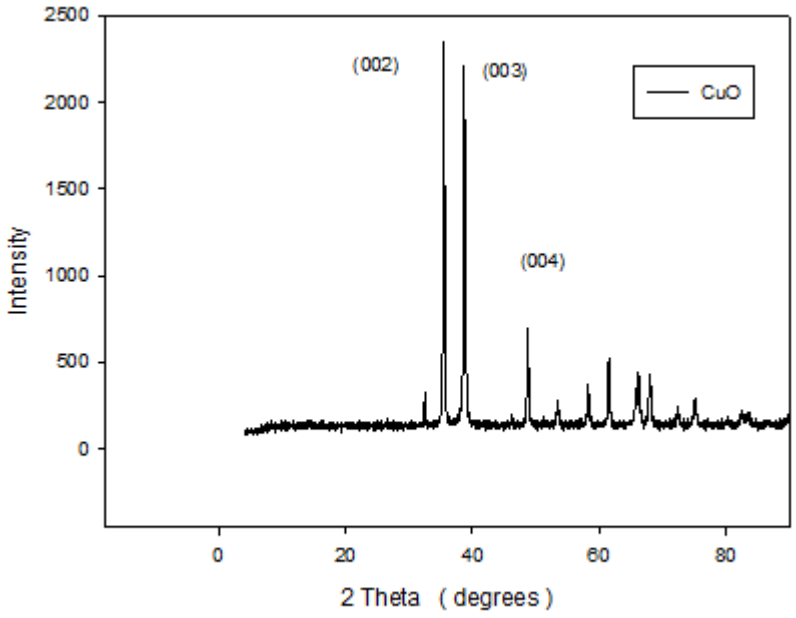


Figure.3.52. XRD pattern of CuO Nanoparticles powder.

### 3.6.4.2.2. X-ray diffraction of unirradiated Nanocomposite films of (PVA/Gelatin /0.01CuO):

The X-ray diffraction characterization of unirradiated nanocomposite films ratios (25/75/0.01CuO), (50/50/0.01CuO) and (75/25/0.01CuO) of (PVA/Gelatin/0.01CuO) were carried out as been shown in Figure.3.53.and Table.3.6.

(Figure.3.53-A) shows the X-ray diffraction patterns of unirradiated nanocomposite film ratio (25/75/0.01CuO) of (PVA/Gelatin/0.01CuO). From this Figure, the observed peak at 2θ= (20°) represent the crystalline phase. The main peak at about at 2θ= (20°) corresponds to the 110 reflection; a plane which contains the extended planner-zigzag chain direction of the crystallinites these peaks have resulted from the part crystallinity in polymer chain molecule. This crystallinity is a result of strong intermolecular and intra-molecular hydrogen bonding between the polymer molecular chains [173,174].

It is well known that the sharpness of the main peak in the XRD patterns reflects the higher crystallinity (i.e. lower amorphous content) for the sample [175].

Also, the observed peak X-ray diffraction of unirradiated nanocomposite film ratio (25/75/0.01CuO) of (PVA/Gelatin/0.01CuO), indicating a large distance between CuO nanoparticles layer in polymer matrix. This behavior corresponds to the intercalation of large size of PVA/Gelatin molecular material [176]. Also, this shift corresponds to an expansion of the layer spacing which indicate some reorganization of PVA/Gelatin in the intercalate [176]. Peak appear at 2Theta 12 need comment which represent peak of glatin.(mustafa)

The X-ray diffraction of unirradiated nanocomposite film ratio (50/50/0.01CuO) of (PVA/Gelatin/0.01CuO) is shown in (Figure.3.53-B) The peak of XRD pattern of unirradiated nanocomposite film ratio was observed at 2θ =20.25° represent the crystalline phase. crystallinity is evidence of strong intermolecular and intra-molecular hydrogen bonding between the polymer molecular chain [168,169]. From a general point of view the diffraction patterns of unirradiated hybrid composite film ratio (50/50/0.01CuO) of (PVA/Gelatin/0.01CuO) show the presence of broad

peak at 2θ =20.00°. This value of the peak and Intensity peak are lower. The reason of that is due to the interaction of CuO nanoparticles hybrid with PVA/Gelatin matrix [176]. Peak of gelatin at 2 theta =12 disappeared, this may be due to equal amounts of gelatin an PVA (mustafa).

(Figure.3.53-C) illustrated the XRD pattern of unirradiated nanocomposite film of (PVA/Gelatin/0.01CuO) for the appearance ratio (75/25/0.01CuO). From the observed curve of the diffraction patterns of unirradiated nanocomposite film (75/25/0.01CuO), it is clear that presence of broad lower peak at 2θ =20.50°. The reason of lower values of peak and Intensity is due to the interaction of CuO nanoparticles hybrid with PVA/Gelatin matrix [176]. The 2θ peaks and their intensities were shown in table (3). Peak appear at 2Theta 12 need comment which represent peak of glatin.(mustafa)

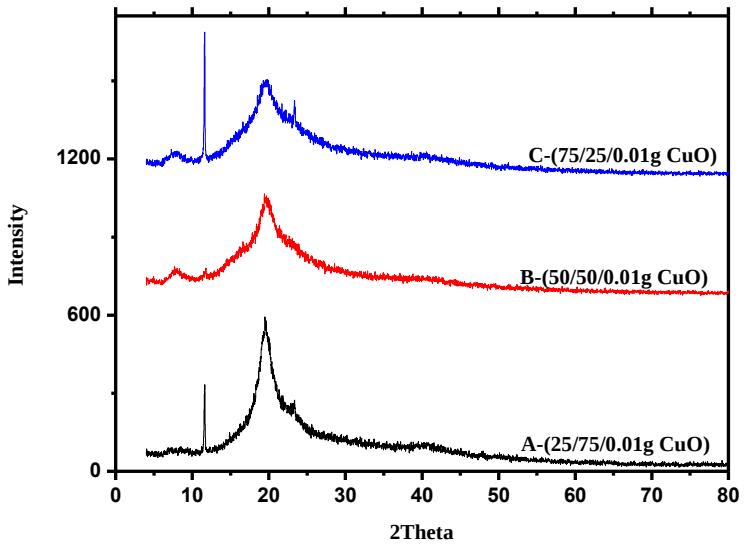


**Figure.3.53**. X-Ray diffraction of unirradiated nanocomposite film of (PVA/Gelatin/0. 01CuO).

### 3.6.4.2.3. X-ray diffraction of irradiated Nanocomposite films of (PVA/Gelatin /0.01CuO):

The effect of dose of gamma irradiation on studied nanocomposite films of (PVA/Gelatin/0.01CuO) of different ratios were also investigated using X-ray diffraction characterization.
The X-ray diffraction of irradiated nanocomposite film ratio (25/75/0.01CuO) of (PVA/Gelatin/0.01CuO) at 5KGy dose of gamma irradiation was investigated as in (Figure.3.54-A). One can see clearly that the obtained main peak of irradiated nanocomposite film ratio (25/75/0.01CuO) of (PVA/Gelatin/0.01CuO) at 5KGy becomes weaker and broader at (2θ) 19.38°, due to effect of the applied dose of gamma irradiation. Also, the broadening of the peaks indicates that the crystal size of CuO nanoparticles become small [172]. Peak of gelatin at 2 theta =12 becomed more intense in case of radition.

The observed peak shifted to lower intensity due to intercalation between CuO nanoparticles and PVA/Gelatin polymer matrix in the selected irradiated nanocomposite film ratio (25/75/0.01CuO) of (PVA/Gelatin/0.01CuO) [176].

(Figure.3.54-B). shows the X-ray diffraction of irradiated nanocomposite film (PVA/Gelatin/0.01CuO) for the selected ratio (50/50/0.01CuO) at irradiation doses (5KGy) of gamma irradiation. From these Figure; the peaks of 2θ and peak intensities decreases by applying the applied dose of gamma irradiation, also the observed peaks become more boarder than that presented in unirradiated case. The presented peaks 2θ were at 19.46°. This indicating the above results of decreasing peak 2θ, peak intensity and crystalline size by applying the dose of irradiation [172].

(Figure.3.54-C) shows the X-ray diffraction analysis pattern of nanocomposite film ratio (75/25/0.01CuO) of (PVA/Gelatin/0.01CuO) at irradiation dose 5KGy of gamma irradiation.

The yielding Figures observing the X-ray diffraction of irradiated nanocomposite film ratio (75/25/0.01CuO) of (PVA/Gelatin/0.01CuO) at (5KGy) dose of gamma irradiation. From these Figure the peak of 2θ become weaker and more boarder at (5KGy) equal 19.94°, . This it might be due to increasing of PVA ratio produced in crystalline phase in polymer matrix [176]. Peak of gelatin at 2 theta =12 become more broader, and less intense .

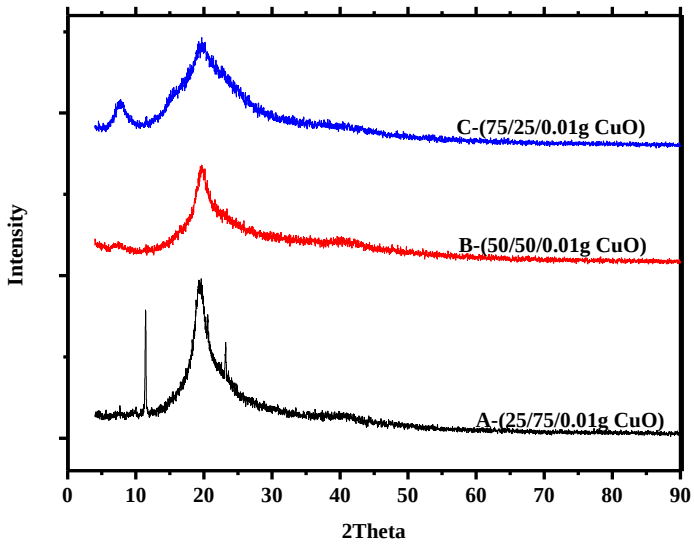


**Figure.3.54.** X-Ray diffraction of irradiated nanocomposite film of (PVA/Gelatin/0. 01CuO).

## 3.6.4.2.4.X-ray diffraction of unirradiated Nanocomposite films of (PVA/Gelatin /0.1CuO):

The X-ray diffraction technique of the produced unirradiated nanocomposite films ratios (25/75/0.1CuO), (50/50/0.1CuO) and

(75/25/0.1CuO) of (PVA/Gelatin/0.1CuO) were performed and illustrated in Figure.3.55.

(Figure.3.55-A) shows the X-ray diffraction of unirradiated nanocomposite films ratio (25/75/0.1CuO) of (PVA/Gelatin/0.1CuO). The diffraction patterns peak at about 2θ =20.08° represents the crystalline phase [171].

The presented peak of unirradiated nanocomposite films ratio (25/75/0.1CuO) of (PVA/Gelatin/0.1CuO) was weaker and broader at 2θ =20.08°. In other, words increasing of CuO nanoparticles in (PVA/Gelatin) matrix leading to decreasing of peak intensity. This is may be due to the interaction between PVA/Gelatin and CuO nanoparticles lead to the decreaseing of the intermolecular interaction between (PVA/Gelatin) chains and thus the crystalline degree [126].

(Figure.3.55-B) shows the XRD pattern of unirradiated nanocomposite film ratio (50/50/0.1CuO) of (PVA/Gelatin/0.1CuO). It can be seen clearly from these Figures, presence of broad peak illustrating splitting behavior into three peaks at about 2θ =11.58°, 25.08° and 20.62°. The peaks are corresponding to the (001) reflection for CuO nanoparticles, PVA and gelatin respectively. The broadening and splitting behavior increases and became more pronounced with increasing gelatin content. The presence of this behavior in unirradiated nanocomposite film ratio (50/50/0.1CuO) of (PVA/Gelatin/0.1CuO) suggested that the hybrid composites have low crystallinity with bi-dimensional structure as compared with above results composites [172].

(Figure.3.55-C) gives the XRD curves unirradiated nanocomposite film ratio (75/25/0.1CUO) of (PVA/Gelatin/0.1CuO).

The only crystalline phase was determined at the observed peak of 2θ =20.42° for unirradiated nanocomposite film ratio (75/25/0.1CUO) of (PVA/Gelatin/0.1CuO).

This crystallinity is a result of strong intermolecular and intra-molecular hydrogen bonding between the polymer molecular chains [173].

The XRD pattern of unirradiated nanocomposite film ratio (75/25/0.1CUO) of (PVA/Gelatin/0.1CuO) observed a weaker and boarder peak at 2θ=20.42°. However, the observed peak of 2θ decreases by additional of CuO nanoparticles to polymer matrix, of the studied ratio.

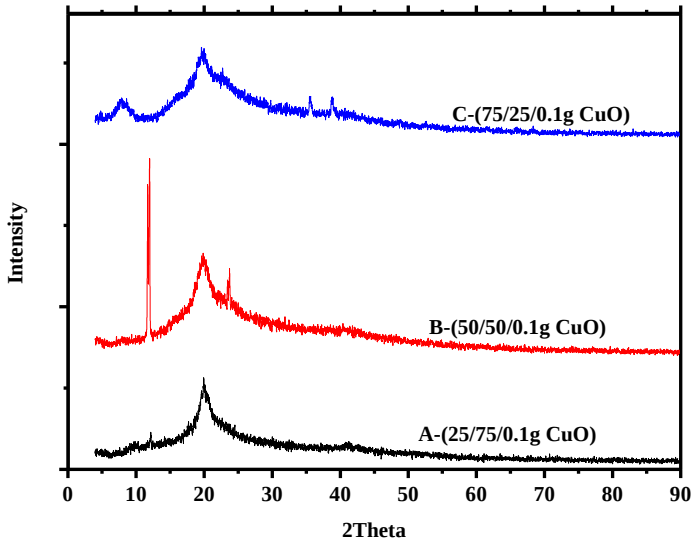


**Figure.3.55.** X-Ray diffraction of un irradiated nanocomposite film of (PVA/Gelatin/0. 1CuO).

**Table3.6.The strongest peaks observed in XRD Pattern of nanocomposite film of (PVA/Gelatin/0.01CuO) for different ratios.**

| Sample | case | 2θ(deg) | d (A°) | FWHM(deg) | Intensity (count) |
|---|---|---|---|---|---|

| | | | | | |
|---|---|---|---|---|---|
| **25/75/0.01CuO** | 0KGy | 20.00 | 4.56 | 0.00 | 66 |
| **25/75/0.01CuO** | 5KGy | 19.38 | 4.57 | 0.00 | 67 |
| **50/50/0.01CuO** | 0KGy | 20.25 | 4.53 | 2.76 | 95 |
| **50/50/0.01CuO** | 5KGy | 19.46 | 4.55 | 2.38 | 54 |
| **75/25/0.01CuO** | 0KGy | 20.50 | 4.57 | 1.88 | 119 |
| **75/25/0.01CuO** | 5KGy | 19.94 | 4.44 | 2.48 | 116 |

### 3.6.4.2.5. X-ray diffraction of irradiated Nanocomposite films of (PVA/Gelatin /0.1CuO):

The X-ray diffraction technique of the casted films was used to determine the variations in structure and crystallinity percent exists as a result of different treatments such as irradiation and CuO nanoparticles addition to the polymer.

Compositional determination of nanocomposite films ratios (25/75/0.1CuO), (50/50/0.1CuO) and (75/25/0.1CuO) of (PVA/Gelatin/0.1CuO) after exposed to dose gamma irradiation were characterized by wide angle X-ray diffraction analysis. The results of X-ray diffraction analysis were presented in Figure.3.56.

The X-ray diffraction patterns for irradiated nanocomposite films ratio (25/75/0.1CuO) of (PVA/Gelatin/0.1CuO) at radiation dose (5KGy) of gamma irradiation are given in (Figure.3.56-A)

The irradiated nanocomposite films ratio (25/75/0.1CuO) of (PVA/Gelatin/0.1CuO) at 5KGy shows peaks at $2\theta = 20.28^{\circ}$. Also, as a result of irradiation, the intensity of diffraction pattern at $2\theta$ decreases gradually by applying irradiation dose [126].

The XRD pattern of the of irradiated nanocomposite film ratio (50/50/0.1CuO) of (PVA/Gelatin/0.1CuO) at the applied dose of gamma irradiation was determined by X-ray diffraction analysis as shown in (Figure.3.56-B) The XRD pattern of irradiated nanocomposite film ratio (50/50/0.1CuO) of (PVA/Gelatin/0.1CuO) at the selected dose (5KGy) presented a broad peak illustrating splitting behavior into three peaks at about $2\theta = 11.58^{\circ}$, and $20.62^{\circ}$. The peaks are corresponding to the 001 reflection for CuO nanoparticles, PVA respectively. The broadening and splitting behavior increases and became more pronounced with increasing gelatin content, irradiation dose and CuO nanoparticles content. The presence of this behavior in irradiated nanocomposite film ratio (50/50/0.1CuO) of (PVA/Gelatin/0.1CuO) suggested that the hybrid composites have low crystallinity with bi-dimensional structure as compared with above results composites. The diffraction characteristic peak of the one dimensional stacking of the CuO nanoparticles is overlapped as a shoulder within the main broadened peak. Therefore, the presence of 001 reflection peak for CuO nanoparticles in the XRD pattern of the irradiated hybrid composites of (50/50/0.1CuO) of (PVA/Gelatin/0.1CuO) indicate a layered frame work due to showing that the lamellar structure of CuO nanoparticles is maintained. This similar to study **Zampronio et al., (2006)** [177] **(2005)** [178].

(Figure.3.56-C) presented the XRD pattern of irradiated nanocomposite film ratio (75/25/0.1CuO) of (PVA/Gelatin/0.1CuO) at (5KGy). From observed Figures view, the diffraction patterns of irradiated nanocomposite film ratio (75/25/0.1CuO) of (PVA/Gelatin/0.1CuO) at selected dose of gamma irradiation show presence of broad peak illustrating splitting behavior into tow peaks at $2\theta$

=11.47°, 21.22° . The peaks are corresponding to the 001 reflection for CuO nanoparticles, PVA and Gelatin respectively.

This indicating that the selected irradiated nanocomposite film ratio (75/25/0.1CuO) of (PVA/Gelatin/0.1CuO) have low crystallinty with a bi-dimensional structure as compared with the same ratio blend [177,178].

In general, the shifts of the characteristic peak in the patterns of nanocomposite film of (PVA/Gelatin/CuO) to lower 2θ values indicate that there is an increase in the interlayer spacing, which is consistent with the presence of the polymeric species in the matrix. Probably, the increase in d-spacing is an evidence of the replacement of the weakly bound inter lamellar water molecules with polymeric species. Although, this is an indication that the polymeric species lie in the interlayer region. In other words, the XRD data for CuO hybrid composites confirms the intercalation of organic polymers into the interlayer of CuO nanoparticles from the lower angle shifted (001) reflections upon intercalation [179,168].

The increase of d-spacing upon intercalation (interlayer expansion) is a consequence of removing one layer of water molecule from the inter lamellar domain [180].

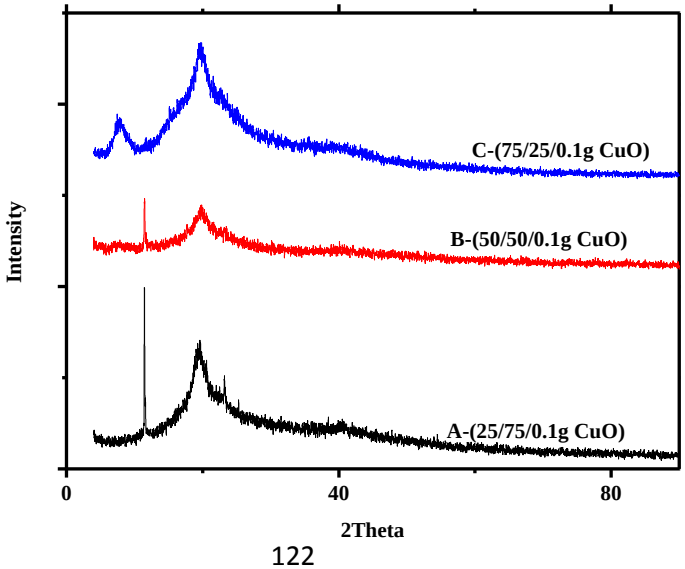

**Figure.3.56.** X-Ray diffraction of irradiated nanocomposite film of (PVA/Gelatin/0. 1CuO).

**Table 3.7.The strongest peaks observed in XRD Pattern of nanocomposite film of (PVA/Gelatin/0.1CuO) for different ratios.**

| **Sample** | **Case** | **2θ(deg)** | **d (A°)** | **FWHM( deg)** | **Intensity (count)** |
|---|---|---|---|---|---|
| **25/75/0.1CuO** | 0KGy | 20.08 | 4.64 | 0.00 | 26 |
| **25/75/0.1CuO** | 5KGy | 20.28 | 4.59 | 0.00 | 12 |
| **50/50/0.1CuO** | 0KGy | 20.62 | 7.63 | 0.13 | 142 |
| **50/50/0.1CuO** | 5KGy | 20.62 | 4.65 | 1.24 | 28 |
| **75/25/0.1CuO** | 0KGy | 20.42 | 4.56 | 0.00 | 24 |
| **75/25/0.1CuO** | 5KGy | 21.22 | 7.70 | 0.12 | 518 |

### 3.7. Removal of Eoisn Dye Using Polyme Blend and Nanocomposite:

### 3.7. 1. Polymer blend:

The behavior of unirradiated and irradiated Polymer blend ratios (25/75), (50/50), (75/25) of (PVA/Gelatin) at (5) kGy for removal Eosin Y were investigated as shown in Figure.3.57 and Figure.3.58.

From the obtained results it is obvious that, the removal percentages increase with increasing time and decrease in presence of irradiation. Also, results showed that, the polymer blend ratios (25/75),(50/50),(75/25) of (PVA/Gelatin) gives nearly equal the removal percentages. The values of removal percentages were (17%, 16%, 15%) and (15%, 14%, 13%) respectively.

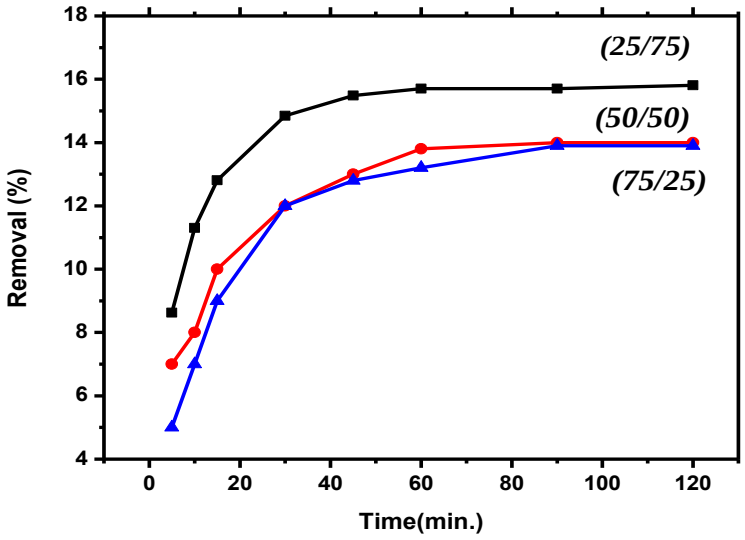


**Figure.3.57.** Effect of contact time for removal of Eosin Y dye by unirradiated polymer blend ratios (25/75), (50/50) and (75/25).

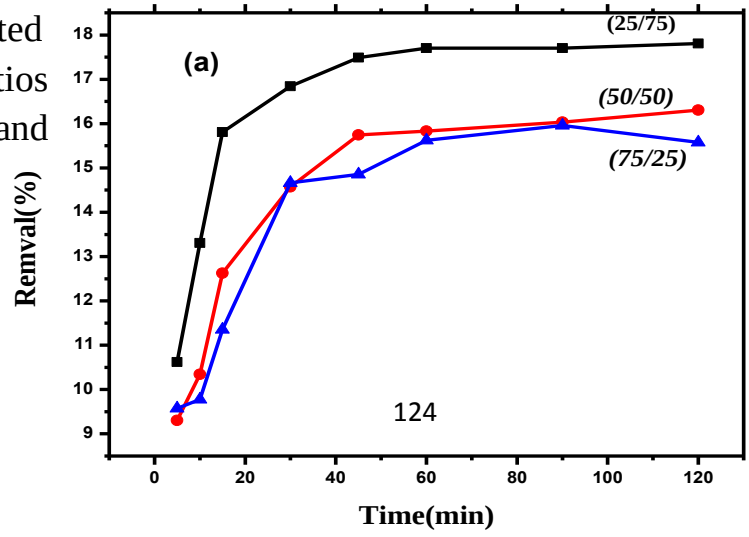

**Figure.3.58.** Effect of contact time for removal of Eosin Y dye by irradiated polymer blend ratios (25/75),(50/50) and (75/25) at 5KGy.

### 3.7. 2. Polymernanocomposite:

### 3.7. 2.1. Effect of time:

The investigation of adsorption rate of Eosin Y onto unirradiated Polymer nanocomposite ratios (25/75/0.01 CuO), (50/50/0.01 CuO), (75/25/0.01 CuO) and (25/75/0.1 CuO), (50/50/0.1 CuO), (75/25/0.1 CuO) at constant dose of selected Polymer nanocomposite ratios 0.2 g/L. The initial dye concentration was 5 mg/L at a pH of (4.0).

Samples were withdrawn at different time intervals at room temperature. From Figure.3.59 and Figure.3.60 it was shown that, the removal percentages (%) of Eosin Y were increases by increasing time.

Also, results showed that, the removal percentages (%) of Eosin Y had a sharp increase at the beginning of the reaction for all investigated Polymer nanocomposite ratios, followed by a continued slower removal rate and finally reached to the saturation.

The removal percentages (%) of Eosin Y onto unirradiated Polymer nanocomposite ratios (25/75/0.01 CuO), (50/50/0.01 CuO),(75/25/0.01 CuO) and (25/75/0.1 CuO),(50/50/0.1 CuO), (75/25/0.1 CuO) were (89%,82%,82%) and (80%, 78%, 79%) respectively.

This phenomenon can be due to the fact that at the beginning of the time, dye contact with the sorbent materials, the adsorption of Eosin Y was taken place probably via surface functional groups, there was plenty of binding sites available for dye adsorption onto the sorbent surface, so the dye molecules interacted easily in these sites. Until the binding sites were fully occupied, the dye molecules diffused into pores of the adsorbents for further adsorption [181].

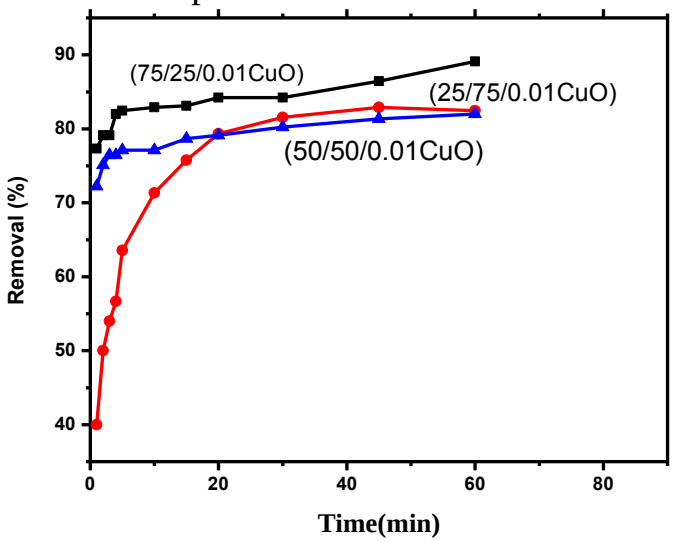


**Figure.3.59.** Effect of contact time for removal of Eosin Y dye by unirradiated polymer blend nanocomposite ratios (25/75/0.01 CuO),(50/50/0.01 CuO) and (75/25/0.01 CuO).

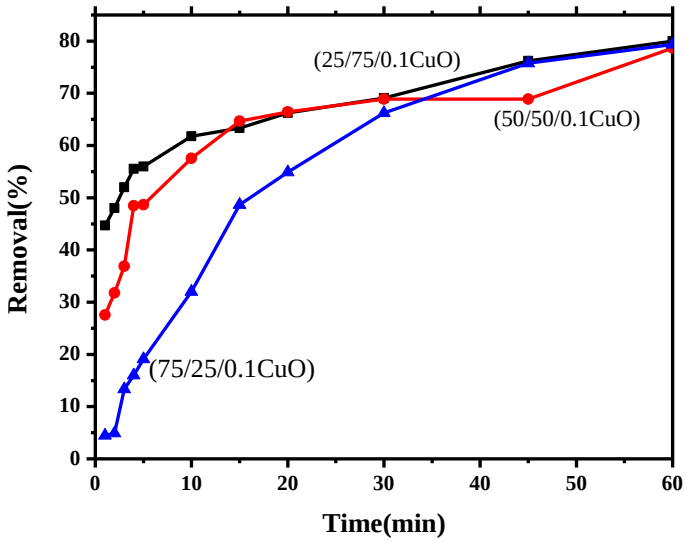

**Figure.3.60.** Effect of contact time for removal of Eosin Y dye by unirradiated polymer blend nanocomposite ratios (25/75/0. 1 CuO), (50/50/0. 1 CuO) and (75/25/0.1 CuO).

### 3.7. 2.2. Effect of PH:

The pH is an important parameter affecting the adsorption process. It affects the activities of functional groups on the surface of sorbents and also influences the availability of dye molecules. In order to examine the effect of initial pH value on removal of Eosin Y solution onto unirradiated Polymer nanocomposite ratios (25/75/0.01 CuO) ,(50/50/0.01 CuO),(75/25/0.01 CuO) and (25/75/0.1 CuO),(50/50/0.1 CuO), (75/25/0.1 CuO), dye adsorption experiments were done at pH range of 2 to 8 using initial dye concentration of 5 mg/L.

As it can be observed from Figure.3.61 and Figure.3.62, the dye removal percentage was decreasing by increasing pH value. It is found that the percentage removal of Eosin Y was higher when the pH is below 5. After pH 5, the adsorption rate decreased.

In acidic conditions, the surface of the adsorbent is positively charged due to high concentration of $H^+$, so electrostatic attraction between the adsorbent and the adsorbate (anionic dye) is enhanced. Lower adsorption of Eosin Y under alkaline conditions is due to the presence of hydroxyl ions on the surface of adsorbents competing with the adsorbate for adsorption sites [182].

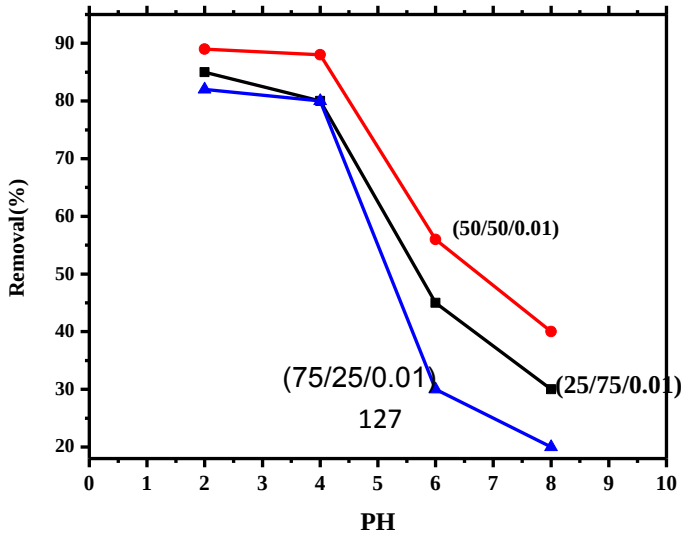

**Figure.3.61.** Effect of pH for removal of Eosin Y dye unirradiated polymer blend nanocomposite ratios (25/75/0.01 CuO),(50/50/0.01 CuO) and (75/25/0.01 CuO).

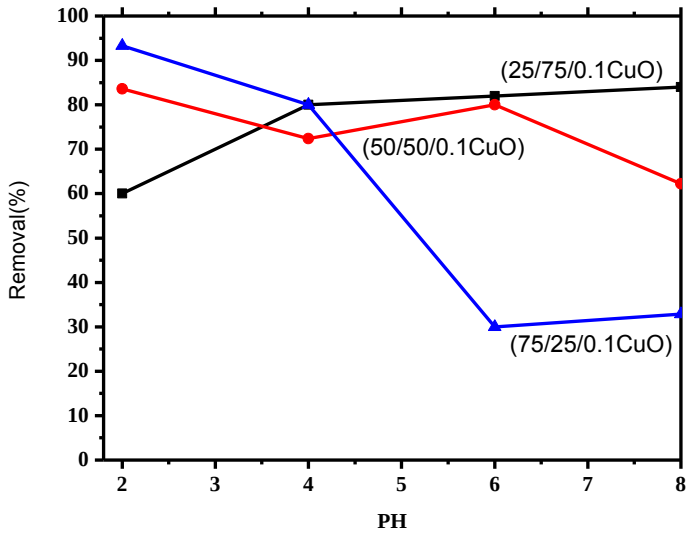


**Figure.3.62.** Effect of PH for removal of Eosin Y dye unirradiated polymer blend nanocomposite ratios (25/75/0. 1 CuO),(50/50/0. 1 CuO) and (75/25/0. 1 CuO).

### 3.7. 2.3. Effect of polymer nanocomposite dose:

Polymer nanocomposite doses are an important parameter which determines the capacity of Polymer nanocomposite for a given initial concentration of dye solution. The effect of Polymer nanocomposite doses was investigated by varying of unirradiated Polymer nanocomposite ratios (25/75/0.01 CuO) ,(50/50/0.01 CuO),(75/25/0.01 CuO) and (25/75/0.1 CuO),(50/50/0.1 CuO), (75/25/0.1 CuO) doses from 0.075 to 0.3 g/L at 5 mg/L dye concentration at PH 4.

Results in Figure.3.63 and Figure.3.64, revealed that by increasing of the unirradiated Polymer nanocomposite ratios (25/75/0.01 CuO),(50/50/0.01 CuO),(75/25/0.01 CuO) and (25/75/0.1 CuO),(50/50/0.1 CuO), (75/25/0.1 CuO) doses, the adsorption capacity (% color removal) increased significantly. With 0.2 g/L of studied polymer nanocomposite ratios, almost all dyes can be removed from the liquid. The increase in the polymer nanocomposite ratios dosage can be attributed to greater surface areas and the availability of more adsorption sites.

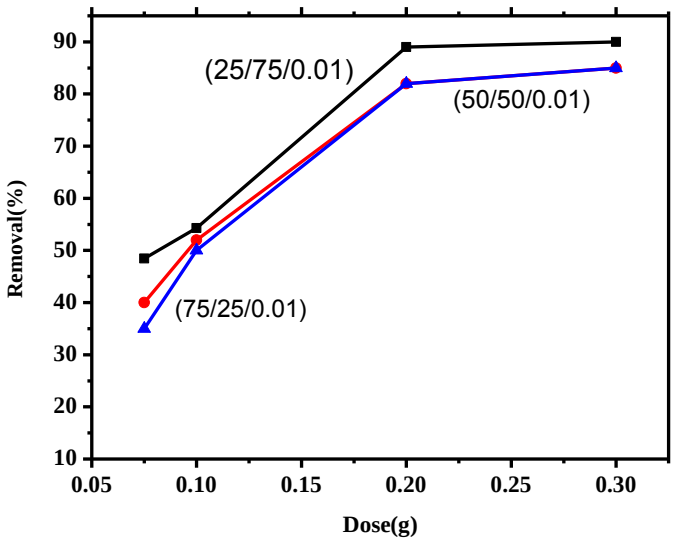


**Figure.3.63.** Effect of polyemer nanocomposite dose for removal of Eosin Y dye unirradiated polymer blend nanocomposite ratios (25/75/0.01 CuO),(50/50/0.01 CuO) and (75/25/0.01 CuO).

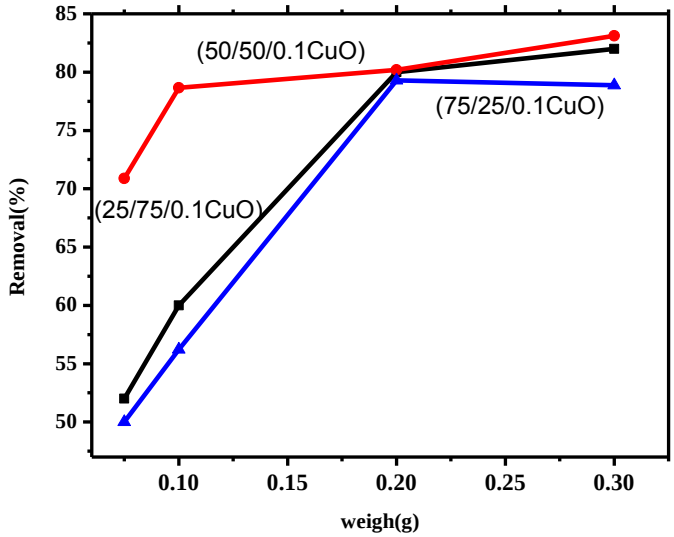


**Figure.3.64.** Effect of polyemer nanocomposite dose for removal of Eosin Y dye unirradiated polymer blend nanocomposite ratios (25/75/0. 1 CuO),(50/50/0. 1 CuO) and (75/25/0. 1 CuO).

### 3.7. 2.4. Effect of the dye concentration (ppm):

The effect of concentration on the removal of Eosin Y dye by unirradiated Polymer nanocomposite ratios (25/75/0.01 CuO),(50/50/0.01 CuO),(75/25/0.01 CuO) and (25/75/0.1 CuO),(50/50/0.1 CuO), (75/25/0.1 CuO) is shown in Figure.3.65 and Figure.3.66. The applied concentrations were (5 to 20 mg/L).

It is observed that, the percentages of removal increases with decreasing the concentration of dye. The amount of dye adsorption decreases from 80 % to 10% , while increasing the initial dye concentration from 5 to 20 mg/L. This proved the fact that the concentration gradient is an important driving force to overcome the mass transfer resistances between the liquid and solid phase.

This is due to at lower dye concentration, the ratio of solute connecting to the polymer nanocomposite sites is higher, which caused the increase in color removal efficiency, while at higher dye concentration, the lower adsorption percentage was caused by the saturation of adsorption sites[(216)].

.

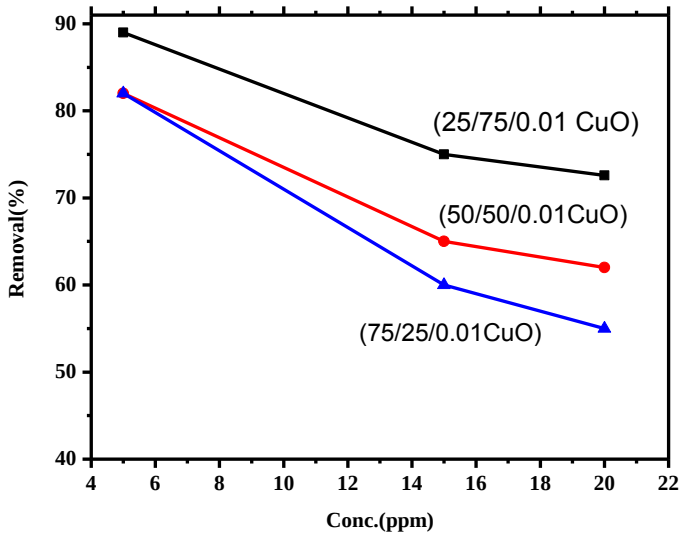


**Figure.3.65.** Effect of (Dye dose ppm) for removal of Eosin Y dye unirradiated polymer blend nanocomposite ratios (25/75/0.01 CuO),(50/50/0.01 CuO) and (75/25/0.01 CuO).

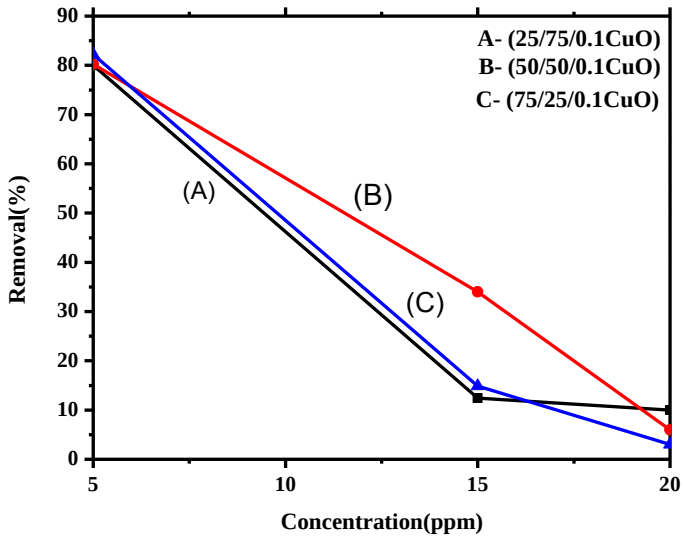


**Figure.3.66.** Effect of (Dye dose ppm) for removal of Eosin Y dye unirradiated polymer blend nanocomposite ratios (25/75/0. 1 CuO),(50/50/0. 1 CuO) and (75/25/0. 1 CuO).

### 3.7. 3. Irradiated polymer nanocomposite at optimum conditions:

The effect of selected radiation dose on the removal of Eosin Y dye onto irradiated Polymer nanocomposite ratios (25/75/0.01 CuO),(50/50/0.01 CuO),(75/25/0.01 CuO) and (25/75/0.1 CuO),(50/50/0.1 CuO), (75/25/0.1 CuO) at the optimum conditions (concentrations 5 mg/L , dose 0.2 mg/L , PH 4) is shown in Figure.3.67 and Figure.3.68.

The results, show that, removal percentages increase with increasing time and decrease in presence of irradiation. The values of removal percentages of irradiated Polymer nanocomposite ratios (25/75/0.01 CuO),(50/50/0.01 CuO),(75/25/0.01 CuO) and (25/75/0.1

CuO),(50/50/0.1 CuO), (75/25/0.1 CuO) were (80%,65%,50%) and (77%, 58%, 36%) respectively.

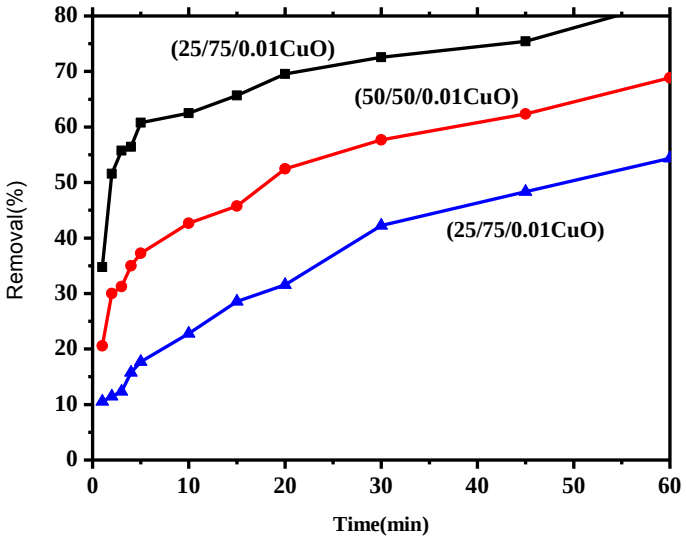


**Figure.3.67.** Effect of contact time on the removal of Eosin Y dye by irradiated(5KGy) polymer blend nanocomposite ratios (25/75/0. 01 CuO),(50/50/0.0 1 CuO) and (75/25/0.0 1 CuO).at optimum conditions.

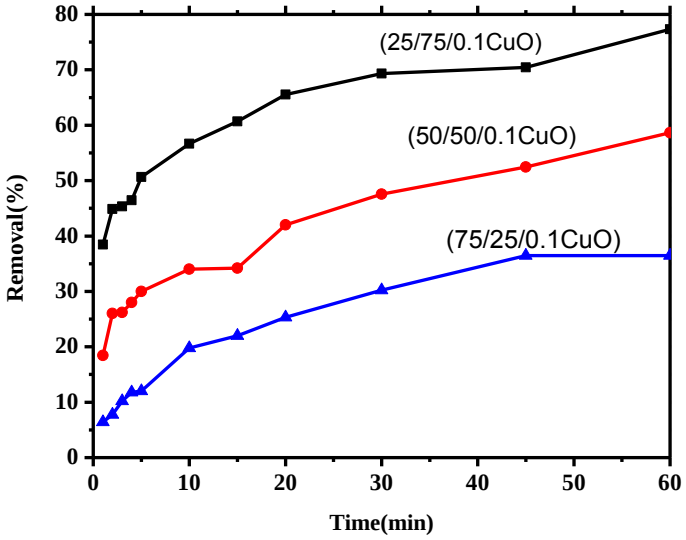


**Figure.3.68.** Effect of contact time on the removal of Eosin Y dye by irradiated (5KGy) polymer blend nanocomposite ratios (25/75/0. 1 CuO),(50/50/0. 1 CuO) and (75/25/0. 1 CuO).at optimum conditions

## 3.8 Conclusion:

The swelling degree percentages of unirradiated polymer blend of (PVA/Gelatin) film for different ratios in de-ionized water and with different solution of pH(4) and pH(10) were found to be increases gradually by increasing time until to reach saturation level.

It is found that the 24 hour is the specific time of saturation of studied un irradiated polymer blend ratios. The same behavior has been observed for the irradiated polymer blend ratios. Where the degradation process was absent for the studied irradiated polymer blend ratios of (PVA/Gelatin).

Infrared spectroscopy has been carried out for further characterization for composition of the as-prepared samples. It has also run to study the effect of dose of gamma radiation on the characteristic functional groups of the prepared polymer blends. A band centered at 3340.1 $cm^{-1}$ as the stretching vibration of hydroxyl group with strong hydrogen bonding as intra-and/or intertype. The band of N—H stretching obtained in the same region.

A weak band appeared at 2321.87 $cm^{-1}$ is the characteristic bands of symmetric C-H stretching. C, C triple bond band is appeared at 2132.88 $cm^{-1}$.

The stretching vibration bands of carboxylate anion $COO^{-}$ showed at 1708.62 $cm^{-1}$. A weak band is observed at 2136.74 $cm^{-1}$ and has been assigned to the combination frequency of (CH+CC). it is possible conclude that the produced film had an ester linkage and secondary alcoholic group. results suggest a complete esterification of the carboxylic acid of gelatin.

The polymer blend of (PVA/Gelatin) investigated using UV/Visible technique it is characterized by a strong band, in the range 300-320 nm. This can be attributed to II—II$^{*}$ transition which comes from unsaturated bands. Also another band was observed in the range 250-270 nm this band increased after radiation and becoming (293 nm).

In order to obtain information about the external shape and microstructure of polymer blend of (PVA/Gelatin) Scanning electron microscope (SEM) was performed. It is clear from images that the yield polymer blends films are homogeneous with regularity in the surface at high content of gelatin, homogeneity produced caused miscibility of polymer blend film of (PVA/Gelatin) through cross-linking. Homogeneity and smoothing increases by exposing the thin films to gamma irradiation (5KGy). In addition, cross-linking was increasing after irradiation due to presence the binder (citric acid) between the two miscible polymers in the surface of observing irradiation polymer blend different ratios.

For polymer blend thin films, three prominent peaks at $2\theta = 11°$, 17° and 35° for the blended films were observed. Also a characteristic peak at $2\theta = 7°$ to 8° has been obtained, intensity of this peak decreases by decreasing the amount of gelatin ratio in the polymer blend matrix, it is likely this peak refers to the presence of a small amount of triplehelical structure, characteristic of the rod-like triple helices of collagen which is small part of gelatin. In case of irradiated thin films polymer blend different ratios, the level of crystallinity percentage decreased after exposed to electron beam irradiation and with increasing the ratio of gelatin in the blend composition, this maybe refer to the increasing of the crosslinking induced in the polymer network

Swelling degree figured out for polymer blend nanocomposite unirradiated and irradiated, from the observed data, it is clear that the maximum values of swelling degree percentages of the studied unirradiated nanocomposite film ratios were appeared after 2hr of dipping in de-ionized water. The maximum values swelling degree percentages for the unirradiated nanocomposite film ratios (PVA/Gelatin/$CuO_{0.01\%,\ 0.1\%}$) reached after two hours, this percentage differ depends on gelatin ratio (more gelatin, less swelling degree). Then the swelling degree percentages start gradually to decrease till complete saturation occurs after 24hr.

In case of irradiated nanocomposite polymer blend (5KGy γ irradiation), swelling degree become less than for that unirradiated polymer blend nanocomposite, if we took un example the ratio (75/25/0.01 CuO), we found that swelling degree after two hours was (522%) and it decreased to(220%) at the same time(2 hours) after irradiation process.

FTIR studies shows no different between the polymer blend and prepared polymer nanocomposite, except a peak noticed at 868.92-708.71 $Cm^{-1}$ attributable to Cu—O—CU in plane vibration .

For polymer blend nancomposites, UV/VIS. Showed a strong broad band mentioned at range (300-340 nm), which corresponds to $II\text{-}II^{*}$ transition. This due to interaction of CuO Nannoparticles into the polymer matrix significantly as (red shift) on the appearing ratio. In UV data, the irradiation process and increasing of CuO nanoparticles content significantly affect the absorption bands of the investigated polymer blends nanocomposites, which give evidence of the stability of the prepared irradiated thin films.

SEM images of polymer nanocomposite films of (PVA/Gelatin/CuO) showed that the surface became smooth, continuous and in homogeneous case. Images show also regular small pores on the surface, it might be to the concentration of gelatin. Also, the CuO nanoparticles were distributed in the surface of polymer matrix.

In case of irradiated polymer nanocomposite films of (PVA/Gelatin/CuO) proved that smooth, homogeneity, disappearing of pores and distribution of CuO nanoparticles on the surface increases by applying of gamma irradiation. Also when the content of copper(ii) oxide increase, it start to accumulate in the surface of polymer blend thin films in different shapes.

The X-ray diffraction characterization of CuO nanoparticles, and nanocomposite films of (PVA/Gelatin/CuO) for the studied ratios obtained the following:

The shifts of the characteristic peak in the patterns of nanocomposite films of (PVA/Gelatin/CuO) to lower 2θ values indicate that there is an increase in the interlayer spacing polymer, which is consistent with the presence of the polymeric species in the matrix.

The behavior of unirradiated and irradiated Polymer blend ratios (25/75), (50/50), (75/25) of (PVA/Gelatin) at (5) kGy for removal Eosin Y were investigated. From the obtained results it is obvious that, the removal percentages increase with increasing time and decrease in presence of irradiation. Also, results showed that, the polymer blend ratios (25/75), (50/50), (75/25) of (PVA/Gelatin) gives nearly equal the removal percentages. The values of removal percentages were (17%, 16%, 15%) and (15%, 14%, 13%) respectively.

For polymer blend nanocomposite unirradiated, results show that the removal percentage increase with time, polymer blend nanocomposite dose (weight) .( With 0.2 g/L of studied polymer nanocomposite ratios, almost all dyes can be removed from the liquid. The increase in the polymer nanocomposite ratios dosage can be attributed to greater surface areas and the availability of more adsorption sites), and it is decreases with increasing of dye concentration (ppm) and pH value (removal of Eosin Y was higher when the pH is below 5. After pH 5, the adsorption rate decreased).

For Irradiated polymer nanocomposite, removal of dye studied at optimum conditions From the obtained results, it is illustrated that, the removal percentages increase with increasing time and decrease in presence of irradiation. The values of removal percentages of irradiated Polymer nanocomposite ratios (25/75/0.01 CuO),(50/50/0.01 CuO),(75/25/0.01 CuO) and (25/75/0.1 CuO),(50/50/0.1 CuO), (75/25/0.1 CuO) were (80%,65%,50%) and (77%, 58%, 36%) respectively.

## References:


1- Buzea, C., Pacheco, I.I. and Robbie, K., 2007. Nanomaterials and nanoparticles: Sources and toxicity. *Biointerphases*, *2*(4), pp.MR17-MR71.

2- Gruszczynski, L., 2012. The Reach Regulation and the TBT Agreement: the role of the TBT Committee in regulatory processes.

3- Kaplan, D.L., 1998. Introduction to biopolymers from renewable resources. In *Biopolymers from renewable resources* (pp. 1-29). Springer Berlin Heidelberg.

4- Gross, R.A. and Scholz, C. eds., 2001. *Biopolymers from polysaccharides and agroproteins*. American Chemical Society.

5- Matveev, Y.I., Grinberg, V.Y. and Tolstoguzov, V.B., 2000. The plasticizing effect of water on proteins, polysaccharides and their mixtures. Glassy state of biopolymers, food and seeds. *Food Hydrocolloids*, *14*(5), pp.425-437.

6- Walsh, D.J. and Rostami, S., 1985. The miscibility of high polymers: the role of specific interactions. In *Key Polymers Properties and Performance* (pp. 119-169). Springer, Berlin, Heidelberg.

7- Folkes, M.J. and Hope, P.S. eds., 1993. *Polymer blends and alloys*. London: Blackie Academic & Professional.

8- Kossoff , Mod. plast International vol. 17(11) **(1987)** 928.

9- Paul, D.R. and Newman, S., 1978. Polymer Blends, Academic. *New York*, *2*, p.319.

10- Gallat Y., and Nippler (eds) , ”Makromol Chem. Macromol symp”,16 **(1988)** 41.

11- Walsh, D.J. and Rostami, S., 1985. The miscibility of high polymers: the role of specific interactions. In *Key Polymers Properties and Performance* (pp. 119-169). Springer, Berlin, Heidelberg.

12- Olabisi, O., Robeson, L.M. and Shaw, M.T., 1979. Polymer-Polymer Miscibility Acad. *Press, NY*, p.126.

13- L.A. Utracki (Ed.), Polymer Blends Handbook, 1-122.2003 pages 12.

14- Manson J.A. and Spering L.H., Eds, "Polymer Blends and Composites", Plenum Press, New York and London, (1976).

15- Flory, P.J., 1970. Fifteenth Spiers memorial lecture. Thermodynamics of polymer solutions. *Discussions of the Faraday Society*, *49*, pp.7-29.

16- Utracki, L.A., Polymer Alloys and Blends: Thermodynamics and Rheology (Hanser, Munich, 1989).

17- Beerbower, A., Pattison, D.A. and G.D. Staflin, Am. Soc.Lubrication Eng. Trans. Vol. 6 (1983) 80.

18- Fayat, R., Jerome, R. and Teyssie, ph., J. Polymer. Sci., phys. Ed., vol. 19 (1981) 79.

19- Fayat, R., Jerome, R. and Teyssie, ph., J. Polymer. Sci., phys. Ed., vol. 20(1982) 2209.

20- Edenbaum, J., 1992. *Plastics additives and modifiers handbook*. Van Nostrand Reinhold Company.

21- Messersmith, P.B. and Giannelis, E.P., 1995. Synthesis and barrier properties of poly (ε-caprolactone)-layered silicate

nanocomposites. *Journal of Polymer Science Part A: Polymer Chemistry*, *33*(7), pp.1047-1057.

22- Wang, Z., Massam, J. and Pinnavaia, T.J., 2000. Epoxy-clay nanocomposites. *Polymer-clay nanocomposites*, *48*.

23- Camargo, P.H.C., Satyanarayana, K.G. and Wypych, F., 2009. Nanocomposites: synthesis, structure, properties and new application opportunities. *Materials Research*, *12*(1), pp.1-39.

24- Bailey, A.J. and Light, N.D., 1989. *Connective tissue in meat and meat products*. Elsevier Applied Science.

25- Ward, A.G., Courts, A. "The Sciences and Technology of Gelatin". New York: Academic press. ISBN0127350500, (1977).

26- Veis, A., 1964. The macromolecular chemistry of gelatin.

27- Pouradier, J. and VenetA. M. J. *Chim.,* 1961.*Phys.Chim.* boil.47 (11), pp 3914-58.

28- Achet, D. and He, X.W., 1995. Determination of the renaturation level in gelatin films. *Polymer*, *36*(4), pp.787-791.

29- Kim, S.J. and Ustunol, Z., 2001. Solubility and moisture sorption isotherms of whey-protein-based edible films as influenced by lipid and plasticizer incorporation. *Journal of agricultural and food chemistry*, *49*(9), pp.4388-4391.

30- Ou, S., Kwok, K.C. and Kang, Y., 2004. Changes in in vitro digestibility and available lysine of soy protein isolate after formation of film. *Journal of Food Engineering*, *64*(3), pp.301-305.

31- Rahman, M. and Brazel, C.S., 2004. The plasticizer market: an assessment of traditional plasticizers and research trends to meet new challenges. *Progress in Polymer Science*,*29*(12), pp.1223-1248.

32- Rodríguez, M., Oses, J., Ziani, K. and Mate, J.I., 2006. Combined effect of plasticizers and surfactants on the physical properties of starch based edible films. *Food Research International*, *39*(8), pp.840-846.

33- Sothornvit, R. and Krochta, J.M., 2001. Plasticizer effect on mechanical properties of β-lactoglobulin films. *Journal of Food Engineering*, *50*(3), pp.149-155.

34- Chen, C.H. and Lai, L.S., 2008. Mechanical and water vapor barrier properties of tapioca starch/decolorized hsian-tsao leaf gum films in the presence of plasticizer. *Food Hydrocolloids*, *22*(8), pp.1584-1595.

35- Paulo, J.D.A., dos Santos, J.S. and García, F.T., 2005. Effect of protein and plasticizer concentrations in film forming solutions on physical properties of edible films based on muscle proteins of a Thai Tilapia. *Journal of Food Engineering*, *70*(1), pp.93-100.

36- Jones, N.R., 1977. Uses of gelatin in edible products. *The science and technology of gelatin*, pp.366-392.

37- Krochta, J.M. and Mulder-Johnston, D.E., 1997. Edible and biodegradable polymer films: challenges and opportunities.*Food technology (USA)*.

38- Wood, P.D., 1977. *Technical and pharmaceutical uses of gelatin* (p. 424). Academic Press, London.

39- Bae, H.J., Park, H.J., Hong, S.I., Byun, Y.J., Darby, D.O., Kimmel, R.M. and Whiteside, W.S., 2009. Effect of clay content, homogenization RPM, pH, and ultrasonication on mechanical and barrier properties of fish gelatin/montmorillonite nanocomposite films. *LWT-Food Science and Technology*, *42*(6), pp.1179-1186.

40- Ozdemir, C., Yeni, F., Odaci, D. and Timur, S., 2010. Electrochemical glucose biosensing by pyranose oxidase immobilized in gold nanoparticle-polyaniline/AgCl/gelatin nanocomposite matrix. *Food Chemistry*, *119*(1), pp.380-385.

41- Brayner, R., Coradin, T., Vaulay, M.J., Mangeney, C., Livage, J. and Fiévet, F., 2005. Preparation and characterization of metal (Au)–and bimetallic alloys (AuNi)–gelatin nanocomposites. *Colloids and Surfaces A: Physicochemical and Engineering Aspects*, *256*(2), pp.191-197.

42- Zheng, J.P., Wang, C.Z., Wang, X.X., Wang, H.Y., Zhuang, H. and De Yao, K., 2007. Preparation of biomimetic three-dimensional gelatin/montmorillonite–chitosan scaffold for tissue engineering. *Reactive and Functional Polymers*, *67*(9), pp.780-788.

43- Smitha, S., Shajesh, P., Mukundan, P., Nair, T.D.R. and Warrier, K.G.K., 2007. Synthesis of biocompatible hydrophobic silica–gelatin nano-hybrid by sol–gel process.*Colloids and Surfaces B: Biointerfaces*, *55*(1), pp.38-43.

44- Gaihre, B., Aryal, S., Barakat, N.A. and Kim, H.Y., 2008. Gelatin stabilized iron oxide nanoparticles as a three dimensional template for the hydroxyapatite crystal nucleation

and growth. *Materials Science and Engineering: C*, *28*(8), pp.1297-1303.

45- Peppas, N.A. and Simmons, R.E.P., 2004. Mechanistic analysis of protein delivery from porous poly (vinyl alcohol) systems. *Journal of Drug Delivery Science and Technology*, *14*(4), pp.285-289.

46- Costa-Júnior, E.S., Barbosa-Stancioli, E.F., Mansur, A.A., Vasconcelos, W.L. and Mansur, H.S., 2009. Preparation and characterization of chitosan/poly (vinyl alcohol) chemically crosslinked blends for biomedical applications. *Carbohydrate Polymers*, *76*(3), pp.472-481.

47- Park, J.S., Park, J.W. and Ruckenstein, E., 2001. Thermal and dynamic mechanical analysis of PVA/MC blends hydrogels. *Polymer*, *42*(9), pp.4271-4280.

48- Matsumura, S., Tomizawa, N., Toki, A., Nishikawa, K. and Toshima, K., 1999. Novel poly (vinyl alcohol)-degrading enzyme and the degradation mechanism. *Macromolecules*, *32*(23), pp.7753-7761.

49- Lui, W.B. and Peng, J., 2005. Physical, mechanical, biodegradable properties and energy absorption behavior of corn grit-polyvinyl alcohol cushioning extrudates. *Journal of food engineering*, *71*(1), pp.73-84.

50- Saikia, D., Saikia, P.K., Gogoi, P.K., Das, M.R., Sengupta, P. and Shelke, M.V., 2011. Synthesis and characterization of CdS/PVA nanocomposite thin films from a complexing agent free system. *Materials Chemistry and Physics*, *131*(1), pp.223-229.

51- Fernandes, D.M., Hechenleitner, A.W., Lima, S.M., Andrade, L.H.C., Caires, A.R.L. and Pineda, E.G., 2011. Preparation, characterization, and photoluminescence study of PVA/ZnO nanocomposite films. *Materials Chemistry and Physics*,*128*(3), pp.371-376.

52- Yu, D.G., Lin, W.C., Lin, C.H., Chang, L.M. and Yang, M.C., 2007. An in situ reduction method for preparing silver/poly (vinyl alcohol) nanocomposite as surface-enhanced Raman scattering (SERS)-active substrates. *Materials chemistry and physics*, *101*(1), pp.93-98.

53- Yang, C.C., 2007. Synthesis and characterization of the cross-linked PVA/TiO 2 composite polymer membrane for alkaline DMFC. *Journal of Membrane Science*, *288*(1), pp.51-60.

54- Wang, H., Fang, P., Chen, Z. and Wang, S., 2007. Synthesis and characterization of CdS/PVA nanocomposite films.*Applied surface science*, *253*(20), pp.8495-8499.

55- Kundachira Subramani, N., 2015. Opto-electrical characteristics of poly (vinyl alcohol)/cesium zincate nanodielectrics. *The Journal of Physical Chemistry C*,*119*(35), pp.20244-20255.

56- Krklješ, A.N., Marinović-Cincović, M.T., Kacarevic-Popovic, Z.M. and Nedeljković, J.M., 2007. Radiolytic synthesis and characterization of Ag-PVA nanocomposites. *European Polymer Journal*, *43*(6), pp.2171-2176.

57- Yang, Y., Liu, C. and Wu, H., 2009. Preparation and properties of poly (vinyl alcohol)/exfoliated α-zirconium phosphate nanocomposite films. *Polymer Testing*, *28*(4), pp.371-377.

58- Kuljanin, J., Čomor, M.I., Djoković, V. and Nedeljković, J.M., 2006. Synthesis and characterization of nanocomposite of polyvinyl alcohol and lead sulfide nanoparticles. *Materials chemistry and physics*, *95*(1), pp.67-71.

59- Yao, K., Cai, J., Liu, M., Yu, Y., Xiong, H., Tang, S. and Ding, S., 2011. Structure and properties of starch/PVA/nano-SiO 2 hybrid films. *Carbohydrate polymers*, *86*(4), pp.1784-1789.

60- Yoon, S.D., Park, M.H. and Byun, H.S., 2012. Mechanical and water barrier properties of starch/PVA composite films by adding nano-sized poly (methyl methacrylate-co-acrylamide) particles. *Carbohydrate Polymers*, *87*(1), pp.676-686.

61- Bryaskova, R., Pencheva, D., Kale, G.M., Lad, U. and Kantardjiev, T., 2010. Synthesis, characterisation and antibacterial activity of PVA/TEOS/Ag-Np hybrid thin films.*Journal of colloid and interface science*, *349*(1), pp.77-85.

62- Mandal, M.K., Sant, S.B. and Bhattacharya, P.K., 2011. Dehydration of aqueous acetonitrile solution by pervaporation using PVA–iron oxide nanocomposite membrane. *Colloids and Surfaces A: Physicochemical and Engineering Aspects*,*373*(1), pp.11-21.

63- Ai, L.M., Feng, W., Chen, J., Liu, Y. and Cai, W.M., 2008. Evaluation of microstructure and photochromic behavior of

polyvinyl alcohol nanocomposite films containing polyoxometalates. *Materials Chemistry and Physics*, *109*(1), pp.131-136.

64- Karthikeyan, B., 2005. Spectroscopic studies on Ag–polyvinyl alcohol nanocomposite films. *Physica B: Condensed Matter*, *364*(1), pp.328-332.

65- Krklješ, A.N., Marinović-Cincović, M.T., Kačarević-Popović, Z.M. and Nedeljković, J.M., 2007. Dynamic thermogravimetric degradation of gamma radiolytically synthesized Ag–PVA nanocomposites. *Thermochimica Acta*, *460*(1), pp.28-34.

66- Eisa, W.H., Abdel-Moneam, Y.K., Shaaban, Y., Abdel-Fattah, A.A. and Zeid, A.M.A., 2011. Gamma-irradiation assisted seeded growth of Ag nanoparticles within PVA matrix.*Materials Chemistry and Physics*, *128*(1), pp.109-113.

67- Pattabi, M., Amma, B.S., Manzoor, K. and Sanjeev, G., 2007. Effect of 8MeV electron irradiation on the optical properties of PVP capped CdS nanoparticles in PVA matrix.*Solar energy materials and solar cells*, *91*(15), pp.1403-1407.

68- Taleb, M.F.A., El-Mohdy, H.A. and El-Rehim, H.A., 2009. Radiation preparation of PVA/CMC copolymers and their application in removal of dyes. *Journal of hazardous materials*, *168*(1), pp.68-75.

69- Yang, J.M., Chiang, C.Y., Wang, H.Z. and Yang, C.C., 2009. Two step modification of poly (vinyl alcohol) by UV radiation with 2-hydroxy ethyl methacrylate and sol–gel process

for the application of polymer electrolyte membrane. *Journal of Membrane Science*, *341*(1), pp.186-194.

70- Nablo, S.V. and Tripp, E.P., 1977. Low energy electron process applications. *Radiation Physics and Chemistry (1977)*, *9*(1-3), pp.325-352.

71- Frutiger, W.A. and Nablo, S.V., 1983. Performance characteristics of high power, multiple gun, electrocurtains®.*Radiation Physics and Chemistry (1977)*, *22*(3-5), pp.431-440.

72- Saunders, C.B., Lopata, V.J., Kremers, W., Chung, M., Singh, A. and Kerluke, D.R., 1995. Electron curing of fibre-reinforced composites: An industrial application for high-energy accelerators. *Radiation Physics and Chemistry*, *46*(4-6), pp.991-994.

73- Berejka, A.J. and Eberle, C., 2002. Electron beam curing of composites in North America. *Radiation Physics and Chemistry*, *63*(3), pp.551-556.

74- Cleland, M.R., 2006. Industrial applications of electron accelerators.

75- Fettes, E.M. ed., 1964. *Chemical reactions of polymers* (Vol. 19). Interscience Publishers.

76- Chapiro, A., 1977. Radiation induced grafting. *Radiation Physics and Chemistry (1977)*, *9*(1-3), pp.55-67.

77- Garnett, J.L., 1979. Grafting. *Radiation Physics and Chemistry (1977)*, *14*(1-2), pp.79-99.

78- Hu, F., Cheng, S. and Peng, P., 1992. Studies on hydrophilic functional polymer membranes prepared by radiation grafting of acrylonitrile.

79- Chapiro, A., 1983. A worldwide view of radiation sous Rayonnement. *Radiation Physics and Chemistry (1977)*, *22*(1-2), pp.7-10.

80- Hoffman, A.S., 1977. Applications of radiation processing in biomedical engineering—A review of the preparation and properties of novel biomaterials. *Radiation Physics and Chemistry (1977)*, *9*(1-3), pp.207-219.

81- Swallow, A.J., 1960. *Radiation Chemistry Of Organic Compounds. Vol. 2*. Pergamon Press; London.

82- Singh, A. and Silverman, J., 1992. Radiation processing of polymers.

83- Woods, R.J. and Pikaev, A.K., 1994. *Applied radiation chemistry: radiation processing*. John Wiley & Sons.

84- Clough, R.L., 2001. High-energy radiation and polymers: A review of commercial processes and emerging applications.*Nuclear Instruments and Methods in Physics Research Section B: Beam Interactions with Materials and Atoms*, *185*(1), pp.8-33.

85- Loan, L.D., 1977. Applications of radiation processing in the wire and cable field. *Radiation Physics and Chemistry (1977)*,*9*(1-3), pp.253-259.

86- Bennett, E.W., 1979. Applications of irradiation to industrial wires and cables. *Radiation Physics and Chemistry (1977)*,*14*(3-6), pp.947-951.

87- Goavec, P.G., 1979. Plastic materials and Acome's use of high energy electron processing in France. *Radiation Physics and Chemistry (1977)*, *14*(1-2), pp.61-67.

88- Ota, S., 1981. Current status of irradiated heat-shrinkable tubing in Japan. *Radiation Physics and Chemistry (1977)*,*18*(1-2), pp.81-87.

89- Baird, W.G. and Grace, W.R., 1977. Applications in plastic sheet and film. *Radiation Physics and Chemistry (1977)*, *9*(1-3), pp.225-233.

90- Bradley, R., 1984. *Radiation technology handbook*. M. Dekker.

91- Bly, J.H., 1988. *Electron beam processing*. International Information Associates.

92- Hunt, J.D. and Alliger, G., 1979. Rubber-application of radiation to tire manufacture. *Radiation Physics and Chemistry (1977)*, *14*(1-2), pp.39-53.

93- Trageser, D.A., 1977. Crosslinked polyethylene foam processes. *Radiation Physics and Chemistry (1977)*, *9*(1-3), pp.261-270.

94- Sagane, N. and Harayama, H., 1981. Plastic foam-Radiation crosslinked polyethylene foam. *Radiation Physics and Chemistry (1977)*, *18*(1-2), pp.99-108.

95- Cleland, M.R., 2006. Industrial applications of electron accelerators.

96- D Cleland, M.R., O'Neill, M.T. and Thompson, C.C., 1993. Sterilization with accelerated electrons. *Sterilization*

*Technology, A Practical Guide for Manufacturers and Users of Health Care Products*.

97- Herring, C.M. and Saylor, M.C., 1993. Sterilization with radioisotopes. *Sterilization Technology: A Practical Guide for Manufacturers and Users of Health Care Products, New York, NY: Van Nostrand Reinhold*.

98- Fairand, B.P., 2001. *Radiation sterilization for health care products: X-ray, gamma, and electron beam*. CRC Press.

99- Aikawa, Y., 2000. A new facility for X-ray irradiation and its application. *Radiation Physics and Chemistry*, *57*(3), pp.609-612

100- Watanabe, T., 2000. Best use of high-voltage, high-powered electron beams: a new approach to contract irradiation services. *Radiation Physics and Chemistry*, *57*(3), pp.635-639.

101- Sandle, T., 2013. *Sterility, sterilisation and sterility assurance for pharmaceuticals: technology, validation and current regulations*. Elsevier.

102- Andrews, L.S., Ahmedna, M., Grodner, R.M., Liuzzo, J.A., Murano, P.S., Murano, E.A., Rao, R.M., Shane, S. and Wilson, P.W., 1998. Food preservation using ionizing radiation. In *Reviews of environmental contamination and toxicology* (pp. 1-53). Springer New York.

103- ∪rbain, W.M., 1986. AFood Irradiation.@ Academic Press.*New York*, pp.52-57.

104- Madhavi, D.L., Deshpande, S.S. and Salunkhe, D.K., 1995.*Food antioxidants: Technological: Toxicological and health perspectives*. CRC Press.

105- Cleland, M.R., 2006. Industrial applications of electron accelerators.

106- Sivinski, H.D., 1975. Treatment of sewage sludge with combinations of heat and ionizing radiation (thermoradiation). In *Radiation for a clean environment*.

107- Ueda, N., Maeda, H., Hosono, H. and Kawazoe, H., 1998. Band-gap widening of CdO thin films. *Journal of applied Physics*, *84*(11), pp.6174-6177.

108- Ferreira, F.F., Tabacniks, M.H., Fantini, M.C.A., Faria, I.C. and Gorenstein, A., 1996. Electrochromic nickel oxide thin films deposited under different sputtering conditions. *Solid State Ionics*, *86*, pp.971-976.

109- Shaffiey, S.R., Shaffiey, S.F. and Ahmadi, M., 2015. Synthesis and evaluation of bactericidal properties of Ag2O nanoparticles against Aeromonas hydrophila. *International Journal of Nano Dimension*, *6*(3), p.263.

110- Condorelli, G.G., Costanzo, L.L., Fragalà, I.L., Giuffrida, S. and Ventimiglia, G., 2003. A single photochemical route for the formation of both copper nanoparticles and patterned nanostructured films. *Journal of Materials Chemistry*, *13*(10), pp.2409-2411.

111- Amin, M.T., Alazba, A.A. and Manzoor, U., 2014. A review of removal of pollutants from water/wastewater using different types of nanomaterials. *Advances in Materials Science and Engineering*, *2014*.

112- Enick, O.V. and Moore, M.M., 2007. Assessing the assessments: pharmaceuticals in the

environment.*Environmental Impact Assessment Review*, *27*(8), pp.707-729.

113- Jelić, A., Gros, M., Petrović, M., Ginebreda, A. and Barceló, D., 2012. Occurrence and elimination of pharmaceuticals during conventional wastewater treatment. In *Emerging and priority pollutants in rivers* (pp. 1-23). Springer Berlin Heidelberg.

114- Cherik, D., Benali, M. and Louhab, K., 2015. Occurrence, ecotoxicology, removal of diclofenac by adsorption on activated carbon and biodegradation and its effect on bacterial community: A review. *World Scientific News*, (10), pp.116-144.

115- Jelic, A., Gros, M., Ginebreda, A., Cespedes-Sánchez, R., Ventura, F., Petrovic, M. and Barcelo, D., 2011. Occurrence, partition and removal of pharmaceuticals in sewage water and sludge during wastewater treatment. *Water research*, *45*(3), pp.1165-1176.

116- Silva, G.G.D., Sobral, P.J.A., Carvalho, R.A., Bergo, P.V.A., Mendieta-Taboada, O. and Habitante, A.M.Q.B., 2008. Biodegradable films based on blends of gelatin and poly (vinyl alcohol): effect of PVA type or concentration on some physical properties of films. *Journal of Polymers and the Environment*, *16*(4), pp.276-285.

117- Vazquez-Roig, P., Segarra, R., Blasco, C., Andreu, V. and Picó, Y., 2010. Determination of pharmaceuticals in soils and sediments by pressurized liquid extraction and liquid chromatography tandem mass spectrometry. *Journal of Chromatography A*, *1217*(16), pp.2471-2483.

118- Bartelt-Hunt, S.L., Snow, D.D., Damon, T., Shockley, J. and Hoagland, K., 2009. The occurrence of illicit and therapeutic pharmaceuticals in wastewater effluent and surface waters in Nebraska. *Environmental Pollution*, *157*(3), pp.786-791.

119- Bahramifar, N., Tavasolli, M. and Younesi, H., 2015. Removal of eosin Y and eosin B dyes from polluted water through biosorption using Saccharomyces cerevisiae: Isotherm, kinetic and thermodynamic studies. *Journal of Applied Research in Water and Wastewater*, *2*(1), pp.108-114.

120- Ansari, R. and Mosayebzadeh, Z., 2010. Removal of Eosin Y, an anionic dye, from aqueous solutions using conducting electroactive polymers. *Iran Polym J*, *19*, pp.541-551.

121- Said, H.M., Alla, S.G.A. and El-Naggar, A.W.M., 2004. Synthesis and characterization of novel gels based on carboxymethyl cellulose/acrylic acid prepared by electron beam irradiation. *Reactive and Functional Polymers*, *61*(3), pp.397-404.

122- Nandi, S. and Winter, H.H., 2005. Swelling behavior of partially cross-linked polymers: a ternary system.*Macromolecules*, *38*(10), pp.4447-4455.

123- Yang, T., 2012. *Mechanical and swelling properties of hydrogels* (Doctoral dissertation, KTH Royal Institute of Technology).

124- Pal, K., Banthia, A.K. and Majumdar, D.K., 2007. Preparation and characterization of polyvinyl alcohol-gelatin hydrogel membranes for biomedical applications. *Aaps Pharmscitech*,*8*(1), pp.E142-E146.

125- Peppas, N.A. and Korsmeyer, R.W., 1987. Dynamically swelling hydrogels in controlled release applications.*Hydrogels in medicine and pharmacy*, *3*, pp.109-136.

126- Ali, Z.I., Ali, F.A. and Hosam, A.M., 2009. Effect of electron beam irradiation on the structural properties of PVA/V 2 O 5 xerogel. *Spectrochimica Acta Part A: Molecular and Biomolecular Spectroscopy*, *72*(4), pp.868-875.

127- Chiou, C.T., Freed, V.H., Schmedding, D.W. and Kohnert, R.L., 1977. Partition coefficient and bioaccumulation of selected organic chemicals. *Environmental Science & Technology*, *11*(5), pp.475-478.

128- Barry, B.W., 2001. Novel mechanisms and devices to enable successful transdermal drug delivery. *European journal of pharmaceutical sciences*, *14*(2), pp.101-114.

129- Shah, N.H., Carvajal, M.T., Patel, C.I., Infeld, M.H. and Malick, A.W., 1994. Self-emulsifying drug delivery systems (SEDDS) with polyglycolyzed glycerides for improving in vitro dissolution and oral absorption of lipophilic drugs. *International journal of pharmaceutics*, *106*(1), pp.15-23.

130- Peppas, N.A., 1997. Hydrogels and drug delivery. *Current opinion in colloid & interface science*, *2*(5), pp.531-537.

131- Thiebaud, S., Aburto, J., Alric, I., Borredon, E., Bikiaris, D., Prinos, J. and Panayiotou, C., 1997. Properties of fatty-acid esters of starch and their blends with LDPE. *Journal of Applied Polymer Science*, *65*(4), pp.705-721.

132- Krumova, M., Lopez, D., Benavente, R., Mijangos, C. and Perena, J.M., 2000. Effect of crosslinking on the mechanical

and thermal properties of poly (vinyl alcohol). *Polymer*, *41*(26), pp.9265-9272.

133- Shi, R., Zhang, Z., Liu, Q., Han, Y., Zhang, L., Chen, D. and Tian, W., 2007. Characterization of citric acid/glycerol co-plasticized thermoplastic starch prepared by melt blending.*Carbohydrate Polymers*, *69*(4), pp.748-755.

134- Yang, J., Webb, A.R. and Ameer, G.A., 2004. Novel citric acid-based biodegradable elastomers for tissue engineering.*Advanced Materials*, *16*(6), pp.511-516.

135- Yoon, S.D., Chough, S.H. and Park, H.R., 2006. Properties of starch-based blend films using citric acid as additive. II.*Journal of Applied Polymer Science*, *100*(3), pp.2554-2560.

136- Zou, G.X., Qu, J.P. and Zou, X.L., 2007. Optimization of water absorption of starch/PVA composites. *Polymer Composites*, *28*(5), pp.674-679.

137- El-Hefian, E.A., Nasef, M.M. and Yahaya, A.H., 2014. Chitosan-Based Polymer Blends: Current Status and Applications. *Journal of the Chemical Society of Pakistan*, *36*(1).

138- Raju, C.L., Rao, J.L., Reddy, B.C. and Veera Brahmam, K., 2007. Thermal and IR studies on copper doped polyvinyl alcohol. *Bulletin of Materials Science*, *30*(3), pp.215-218.

139- Shi, R., Bi, J., Zhang, Z., Zhu, A., Chen, D., Zhou, X., Zhang, L. and Tian, W., 2008. The effect of citric acid on the structural properties and cytotoxicity of the polyvinyl alcohol/starch films when molding at high temperature.*Carbohydrate Polymers*, *74*(4), pp.763-770.

140- Muyonga, J.H., Cole, C.G.B. and Duodu, K.G., 2004. Extraction and physico-chemical characterisation of Nile perch (Lates niloticus) skin and bone gelatin. *Food hydrocolloids*, *18*(4), pp.581-592.

141- Eberle, G., Schmidt, H. and Eisenmenger, W., 1996. Piezoelectric polymer electrets. *IEEE transactions on dielectrics and electrical insulation*, *3*(5), pp.624-646.

142- Yokoyama, Y. and Hall, H.K., 1982. Ring-opening polymerization of atom-bridged and bond-bridged bicyclic ethers, acetals and orthoesters. In *New Polymerization Reactions* (pp. 107-138). Springer, Berlin, Heidelberg.

143- Peppas, N.A., Bures, P., Leobandung, W. and Ichikawa, H., 2000. Hydrogels in pharmaceutical formulations. *European journal of pharmaceutics and biopharmaceutics*, *50*(1), pp.27-46.

144- Yin, R., Huang, Y., Huang, C., Tong, Y. and Tian, N., 2009. Preparation and characterization of novel gelatin/cerium (III) fiber with antibacterial activity. *Materials letters*, *63*(15), pp.1335-1337.

145- Jain, D., Carvalho, E., Banthia, A.K. and Banerjee, R., 2011. Development of polyvinyl alcohol–gelatin membranes for antibiotic delivery in the eye. *Drug development and industrial pharmacy*, *37*(2), pp.167-177.

146- Pal, K., Banthia, A.K. and Majumdar, D.K., 2006. Polyvinyl alcohol—gelatin patches of salicylic acid: preparation, characterization and drug release studies. *Journal of biomaterials applications*, *21*(1), pp.75-91.

147- Abd, I.J., Kader, K.A.M. and Abdel Hamied, S.F., 2002. Preparation ofpoly (vinyl alcohOl) films with promising physical properties in comparison with commercial polyethylene film. *J Ap-pl Polym Sci*, *86*(5), p.1219.

148- Elashmawi, I.S., Hakeem, N.A. and Selim, M.S., 2009. Optimization and spectroscopic studies of CdS/poly (vinyl alcohol) nanocomposites. *Materials chemistry and physics*,*115*(1), pp.132-135.

149- Abrusci, C., Martın-González, A., Del Amo, A., Catalina, F., Bosch, P. and Corrales, T., 2004. Chemiluminescence study of commercial type-B gelatines. *Journal of Photochemistry and photobiology A: Chemistry*, *163*(3), pp.537-546.

150- Bozzola, J.J. and Russell, L.D., 1999. *Electron microscopy: principles and techniques for biologists*. Jones & Bartlett Learning.

151- Tuhin, M.O., Rahman, N., Haque, M.E., Khan, R.A., Dafader, N.C., Islam, R., Nurnabi, M. and Tonny, W., 2012. Modification of mechanical and thermal property of chitosan–starch blends films. *Radiation Physics and Chemistry*, *81*(10), pp.1659-1668.

152- Vicentini, D.S., Smania, A. and Laranjeira, M.C., 2010. Chitosan/poly (vinyl alcohol) films containing ZnO nanoparticles and plasticizers. *Materials Science and Engineering: C*, *30*(4), pp.503-508.

153- PO-DA HONG, J.H.C. and WU, H.L., 1998. Solvent effect on structural change of poly (vinyl alcohol) physical gels. *Journal of applied polymer science*, *69*, pp.2477-2486.

154- Ali, Z.I. and Eisa, W.H., 2013. Characterization of Electron Beam Irradiated Poly Vinyl Alcohol/Poly Ethylene Glycol Blends. *Journal of Scientific Research*, *6*(1), pp.29-42.

155- Pawde, S.M., Deshmukh, K. and Parab, S., 2008. Preparation and characterization of poly (vinyl alcohol) and gelatin blend films. *Journal of applied polymer science*, *109*(2), pp.1328-1337.

156- Said, H.M., 2013. Development of films based on poly (vinyl alcohol)/gelatin blends cross linked by electron beam irradiation. *Arab J Nuc Sci Appl*, *46*(5), pp.70-78.

157- Rahman, M., Khan, M.A. and Tareq, S.M., 2010. Preparation and characterization of polyethylene oxide (PEO)/gelatin blend for biomedical application: Effect of gamma radiation.*Journal of Applied Polymer Science*, *117*(4), pp.2075-2082.

158- Wang, J.X., Sun, X.W., Yang, Y., Huang, H., Lee, Y.C., Tan, O.K. and Vayssieres, L., 2006. Hydrothermally grown oriented ZnO nanorod arrays for gas sensing applications.*Nanotechnology*, *17*(19), p.4995.

159- Angles, M.N. and Dufresne, A., 2000. Plasticized starch/tunicin whiskers nanocomposites. 1. Structural analysis. *Macromolecules*, *33*(22), pp.8344-8353.

160- Mathew, S., Brahmakumar, M. and Abraham, T.E., 2006. Microstructural imaging and characterization of the mechanical, chemical, thermal, and swelling properties of starch–chitosan blend films. *Biopolymers*, *82*(2), pp.176-187.

161- Oliveira, H.P., Graeff, C.F.O. and Rosolen, J.M., 1999. Synthesis and structural characterization of tetrakis (n-methyl-4-pyridyl) porphyrin copper into v 2 o 5 xerogel.*Materials research bulletin*, *34*(12), pp.1891-1903.

162- de Bastos Couto, D.M.M., 2015. *Biological effects of polyacrylic acid-coated and non-coated superparamagnetic iron oxide nanoparticles in in vitro and in vivo experimental models* (Doctoral dissertation, Universidade do Porto (Portugal)).

163- Yoshii, F., Zhanshan, Y., Isobe, K., Shinozaki, K. and Makuuchi, K., 1999. Electron beam crosslinked PEO and PEO/PVA hydrogels for wound dressing. *Radiation Physics and Chemistry*, *55*(2), pp.133-138.

164- Kooti, M. and Matouri, L., 2010. Fabrication of nanosized cuprous oxide using fehling's solution. *Scientia Iranica*, *17*(1), pp.73-78.

165- Lou, X.W.D., Archer, L.A. and Yang, Z., 2008. Hollow micro-/nanostructures: Synthesis and applications. *Advanced Materials*, *20*(21), pp.3987-4019.

166- Coates, J., 2000. Interpretation of infrared spectra, a practical approach. *Encyclopedia of analytical chemistry*.

167- Yue, Y. and Liang, H., 2017. Micro-and Nano-Structured Vanadium Pentoxide (V2O5) for Electrodes of Lithium-Ion Batteries. *Advanced Energy Materials*.

168- Guerra, E.M., Ciuffi, K.J. and Oliveira, H.P., 2006. V 2 O 5 xerogel–poly (ethylene oxide) hybrid material: synthesis,

characterization, and electrochemical properties. *Journal of Solid State Chemistry*, *179*(12), pp.3814-3823.

169- Eisa, W.H., Abdel-Moneam, Y.K., Shabaka, A.A.M. and Hosam, A.E.M., 2012. In situ approach induced growth of highly monodispersed Ag nanoparticles within free standing PVA/PVP films. *Spectrochimica Acta Part A: Molecular and Biomolecular Spectroscopy*, *95*, pp.341-346.

170- Vijayakumar, G.N.S., Rathnakumari, M. and Sureshkumar, P., 2011. Synthesis, dielectric, AC conductivity and non-linear optical studies of electrospun copper oxide nanofibers.*Archives of applied science research*, *3*(5), pp.514-525.

171- Swarthmore, P.A., 1991. Joint Committee on Powder Diffraction Standards Diffraction data file. *JCPDS International Center for Diffraction Data*.

172- Wu, H.Q., Wei, X.W., Shao, M.W., Gu, J.S. and Qu, M.Z., 2002. Synthesis of copper oxide nanoparticles using carbon nanotubes as templates. *Chemical physics letters*, *364*(1), pp.152-156.

173- Gautam, A. and Ram, S., 2009. Synthesis, mechanical and I–V characteristics of Ag–PVA nanocomposite films. *physica status solidi (a)*, *206*(7), pp.1471-1477.

174- Cheng, Q., Pan, F., Chen, B. and Jiang, Z., 2010. Preparation and dehumidification performance of composite membrane with PVA/gelatin–silica hybrid skin layer. *Journal of Membrane Science*, *363*(1), pp.316-325.

175- Jayasekara, R., Harding, I., Bowater, I., Christie, G.B.Y. and Lonergan, G.T., 2004. Preparation, surface modification and

characterisation of solution cast starch PVA blended films.*Polymer testing*, *23*(1), pp.17-27.

176- Samar Mohamed Fathi."Effect of Ionizing Radiation on synthetic metal polymer composite", Master thesis, **(2011),** Women college, Ain Shams university, Cairo.

177- El-Hefian, E.A., Nasef, M.M. and Yahaya, A.H., 2010. The preparation and characterization of chitosan/poly (vinyl alcohol) blended films. *Journal of Chemistry*, *7*(4), pp.1212-1219.

178- Zampronio, E.C., Greggio, D.N. and Oliveira, H.P., 2003. Preparation, characterization and properties of PVC/V 2 O 5 hybrid organic–inorganic material. *Journal of non-crystalline solids*, *332*(1), pp.249-254.

179- Park, N.G., Ryu, K.S., Park, Y.J., Kang, M.G., Kim, D.K., Kang, S.G., Kim, K.M. and Chang, S.H., 2002. Synthesis and electrochemical properties of $V_2O_5$ intercalated with binary polymers. *Journal of power sources*, *103*(2), pp.273-279.

180- Barbosa, G.N., Brunello, C.A., Graeff, C.F. and Oliveira, H.P., 2004. Preparation and properties of homogeneous V 2 O 5–SiO 2 xerogel composite based on interpenetrating polymer network. *Journal of Solid State Chemistry*, *177*(3), pp.960-965.

181- HUI, G., 2015. *Adsorptive removal of Rhodamine B from aqueous solution using brewer's spent grains: batch and column study* (Doctoral dissertation).

182- Mahmoud, A.A., Osman, O., Eid, K., Ashkar, E., Okasha, A., Atta, D., Eid, M., Aziz, Z.A. and Fakhry, A., 2014. FTIR spectroscopy of natural bio-polymers blends. *Middle East Journal of Applied Sciences*, *4*(4), pp.816-824.